INVESTIGATION OF NOVEL GAS DIFFUSION MEDIA FOR APPLICATION IN PEM FUEL CELL RIBBON ASSEMBLIES

Joshua David Sole

Thesis Submitted to the Faculty of
Virginia Polytechnic Institute and State University
in partial fulfillment of the requirements for the degree of:

MASTER OF SCIENCE
in
Mechanical Engineering

Committee Members:

Dr. Michael W. Ellis, Chair
Dr. David A. Dillard
Dr. Douglas J. Nelson

December 12, 2005
Blacksburg, Virginia

Keywords: diffusion media, GDL, PEM, ribbon, strip

INVESTIGATION OF NOVEL GAS DIFFUSION MEDIA FOR APPLICATION IN PEM FUEL CELL RIBBON ASSEMBLIES

Joshua David Sole

ABSTRACT

A new type of fuel cell architecture, the fuel cell ribbon, is presented. The fuel cell ribbon architecture relies on the gas diffusion layer (GDL) to conduct electrical current in-plane to adjacent cells or collector terminals. The potential advantages of the fuel cell ribbon architecture with respect to conventional fuel cell stacks include reduced manufacturing costs, reduced weight, reduced volume, and reduced component cost. The critical component of fuel cell ribbon assemblies, the gas diffusion media, is investigated herein. Analytical models which focus on the electrical loses within the gas diffusion media of the novel architecture are developed. The materials and treatments necessary to fabricate novel gas diffusion media for fuel cell ribbon assemblies are presented. Experimental results for the novel gas diffusion media of are also presented.

One dimensional and two dimensional analytical models were developed for the fuel cell ribbon. The models presented in this work focus on the losses associated with the transport of the electrons in fuel cell ribbon assemblies, rather than the complex system of equations that governs the rate of electron production. The 1-D model indicated that the GDL used in ribbon cells must exhibit an in-plane resistance which is approximately an order of magnitude lower than the resistance of gas diffusion media typically used in conventional fuel cells. A 2-D model was developed with which a parametric study of GDL properties and ribbon cell dimensions was performed. The parametric study indicated that ribbon cells of useful size can be constructed using novel diffusion media that offer reduced resistivity, and that the ribbon cells can produce as much as 80-85% of the power density produced in a conventional fuel cell.

Novel gas diffusion media for fuel cell ribbons that have the necessary characteristics suggested by the analytical study were developed.. Properties and performance for a commercially available gas diffusion media, ELAT, were measured as a reference for the novel media developed. The increased thickness PAN (ITPN) series

diffusion media was constructed of PAN based fibers exhibiting similar resistive properties to the fibers used in ELAT. The ITPN series of materials were woven in a manner which made them approximately twice the thickness of ELAT, effectively reducing their in-plane resistance to half the resistance exhibited by ELAT. The coarsely woven pitch (CWPT) series of materials were constructed in a manner which yielded a similar number of fibers in the plane of the material to ELAT and a similar material thickness to ELAT, but the fibers used were mesophase pitch based fibers which exhibit a resistivity of approximately one-tenth the resistivity of the fibers used to make the ELAT and ITPN materials. The reduction in fiber resistivity led to the CWPT material having an in-plane resistance an order of magnitude lower than ELAT. The widely used ELAT material exhibited an in-plane resistance of 0.39 Ω/sq., a through-plane area specific resistance of 0.007 Ω-cm^2, and a Darcy permeability coefficient of 8.1 Darcys. The novel diffusion materials exhibited in-plane resistances in the range of 0.18-0.036 Ω/sq., through-plane area specific resistances in the range of 0.017-0.013 Ω-cm^2, and Darcy permeability coefficients in the range of 30-150 Darcys.

Experiments were performed to validate the analytical model and to prove the feasibility of fuel cell ribbon concept. When the novel gas diffusers were adhered to a catalyzed membrane and tested in a ribbon test assembly utilizing serpentine flow channels and in-plane current collection, a range of performance was achieved between 0.28-0.4 A/cm^2 at a cell output potential of 0.5 V. In contrast, when ELAT was adhered to a catalyzed membrane and tested in the fixture requiring in-plane conduction, a current density of 0.21 A/cm^2 was achieved at 0.5 V. Additionally, the 2-D finite element model was used to predict the performance of a ribbon cell based on the cells performance when a conventional method of through-plane conduction was utilized. The agreement between the experimental data and the model predictions was very good for the ELAT and ITPN materials, whereas the predictions for the CWPT materials showed more significant deviation which was likely due to mass transport and contact resistance effects.

ACKNOWLEDGEMENTS

I am very thankful for the help of my committee members for their input throughout this process. I am especially thankful for the help of my committee chair, Dr. Mike Ellis, for all of the scheduled and unscheduled meetings he made time for over the past couple years. The advice and guidance I received during those meetings was absolutely vital to the completion of this work.

I would also like to thank all of those who I have worked with and learned from along the way: Dr. Nate Siegel for all of the questions he answered for me early on in my graduate studies, Ashley Abbott for forcing me to work less, Ken Henderson for his constant willingness to help, Mike Christopher for sacrificing his time to make up for my ignorance of LabView®, Ritesh Agarwal for teaching the lab members a variety of Hindi phrases that kept us all entertained, and Dr. Mike Hickner for the time he spent teaching me at Sandia and for making the arrangements necessary to make my visit possible.

In addition, I would like to thank Mandy O'Neal for giving me the motivation I needed to spend many sleep deprived nights trying to finish my thesis, and for helping me to stay awake during those long nights.

Finally, I would like to thank my parents to whom this work is dedicated, and my brothers for always being sources of whatever I needed at any given time, whether it was motivation, encouragement, guidance, or simply a distraction.

DEDICATION

To Howard B. and Susan L. Sole for their continuous love and support throughout my educational endeavors.....but I’m not done yet, so please send money.

PREFACE

This work was completed at Virginia Polytechnic Institute and State University and was funded in part by Ecolectrix LLC, the National Science Foundation Integrative Graduate Education and Research Traineeship (IGERT) fellowship program, and the United States Department of Energy Graduate Automotive Technology Education (GATE) program.

TABLE OF CONTENTS

LIST OF FIGURES

[#] Reprinted from referenced publication with permission from Elsevier

[#] Reprinted from referenced publication with permission from Elsevier

LIST OF TABLES

NOMENCLATURE

English Notation

A	cross-sectional area, m^2
BP_a	anode back pressure, kPa-ga.
BP_c	cathode back pressure, kPa-ga.
d	operating thickness of GDL, cm
D_{fiber}	diameter of a carbon fiber, cm
d_o	uncompressed thickness of GDL, cm
I	electrical current flow in resistance fixture, A
$i_{cc,avg}$	average current flux at ribbon collector plate, A/cm^2
i_x	local current flux in x-direction, A/cm^2
$\hat{i}_x$	dimensionless current flux in x-direction
i_y	local current flux in y-direction, A/cm^2
$\hat{i}_y$	dimensionless current flux in y-direction
j_{uni}	average uniform current density, A/cm^2
j	average current density presented in figures, A/cm^2
$\hat{j}_{avg}$	ratio of average ribbon current density to average conventional cell current density
$\hat{j}_{\exp}$	experimentally determined ratio of average ribbon cell current density to average conventional cell current density
j_{MEA}	local current density exiting the MEA, A/cm^2
$\hat{j}_{model}$	analytically determined ratio of average ribbon cell current density to average conventional cell current density
j_{ref}	reference value of average current density from conventional data, A/cm^2
k_d	Darcy permeability coefficient, m^2
L_d	flow length through porous media, m
L	ribbon cell length, cm
L_{fiber}	length of a carbon fiber, cm
L_V	length between voltage contacts for in-plane resistance fixture, cm

L_1	length between current contacts for in-plane resistance fixture, cm
n_{fibers}	number of fibers in a carbon fiber tow
ΔP	pressure differential across porous media, Pa
Q	volumetric flow rate through porous media, m^3/s
Q_{H2}	volumetric flow rate of hydrogen into fuel cell fixture, sccm (cm^3/min)
Q_{AIR}	volumetric flow rate of air into fuel cell fixture, sccm (cm^3/min)
R	measured bulk resistance in resistance fixtures, Ω
R_A	through-plane area specific resistance, Ω-cm^2
R_{fiber}	resistance of a single carbon fiber, Ω
R_{IP}	thickness normalized in-plane resistance, Ω/sq.
R_{tow}	resistance of a carbon fiber tow, Ω
Re	Reynolds number
RH_a	anode inlet gas relative humidity, %
RH_c	cathode inlet gas relative humidity, %
t	GDL thickness, cm
t	time, hours
T_{cell}	cell temperature, °C
u_{RA}	experimental uncertainty of area specific resistance values, Ω-cm^2
u_{RIP}	experimental uncertainty of in-plane resistance values, Ω/square
V_{cell}	output electrical potential of a fuel cell, V
V_{cell}	output electrical potential of a fuel cell used in figures, V
V_A	local anode electrical potential, V
V_C	local cathode electrical potential, V
$\widehat{V}_C$	dimensionless cathode GDL potential
ΔV	voltage drop across sample in resistance fixtures, V
w_1	first width of sample in through-plane resistance fixture, cm
w_2	second width of sample in through-plane resistance fixture, cm
w	fuel cell ribbon width, cm
x	horizontal axis label
$\widehat{x}$	dimensionless horizontal dimension
Δx	size of differential element in the horizontal direction, cm

y	vertical axis label
$\hat{y}$	dimensionless vertical direction

Greek Notation

ε	porosity, volume fraction
μ	dynamic viscosity, kg/m-s
Π_1	dimensionless group of parameters number 1
Π_2	dimensionless group of parameters number 2
ρ	fluid density, kg/m^3
$\rho_{b,o}$	bulk density, g/cm^3
ρ_{fiber}	resistivity of a carbon fiber, Ω-cm
ρ_I	in-plane resistivity, Ω-cm
ρ_T	through-plane resistivity, Ω-cm
ρ_r	solid (real) phase density, g/cm^3
$\boldsymbol{\sigma}$	orthotropic conductivity tensor, S/cm
φ	electrical potential, V
$\Delta\varphi_{anode}$	potential loss in anode GDL, V
$\Delta\varphi_{cell}$	overall cell potential loss, V
Ω	unit of resistance, Ohms

1 INTRODUCTION

In the past ten years significant emphasis has been placed on the development of cleaner sources of energy in the United States and around the world. More specifically, large investments have been made in the research and development of hydrogen fuel cells. The capabilities of fuel cell technology have been demonstrated in numerous ways in recent years, yet the efforts to introduce mass produced fuel cells at the consumer level are still ongoing. The hope among scientists and engineers is that proton exchange membrane fuel cells (PEMFCs) will be a viable technology for power production in commercial applications, residential housing, transportation, and portable electronics; effectively replacing a broad range of power sources spanning from the internal combustion engine to the alkaline battery. This chapter will first discuss the chemistry behind the operation of PEMFCs, the components that make up a single PEMFC, and the manner in which PEMFCs are typically attached together to form a stack capable of delivering much greater power than a single cell is capable of producing. The final two sections of this chapter will discuss an alternative to the conventional method of configuring cells into a stack, and will address the objectives of the current work.

1.1 PROTON EXCHANGE MEMBRANE (PEM) FUEL CELL OPERATION

This section will detail the basic electrochemistry which occurs within proton exchange membrane fuel cells, focusing exclusively on the electrodes and the membrane. The fuel cells of interest in this work are referred to as proton exchange membrane (PEM) fuel cells because the membrane separating the electrode does just that, it facilitates the exchange of protons from the anode to the cathode due to its acidic nature.

At the anode, hydrogen is transported to the catalyst sites where it reacts to yield protons and electrons. Active catalyst sites must be in contact with the reactant gas, an electron conductor (typically carbon black) and a proton conductor (electrolyte) for the reaction to take place. The electrons produced travel into the electron conductor and through an external circuit which terminates at the cathode. The protons produced when

the hydrogen molecules are split travel into the proton conductor, through the electrolyte membrane, and to an active catalyst site in the cathode. The anode reaction can be seen in equation 1.1 below and in Figure 1.1 on the next page.

$$2H_2 \rightarrow 4H^+ + 4e^- \quad (1.1)$$

The reactive chemical component at the cathode of a PEM fuel cell is oxygen. At the cathode, diatomic oxygen is reduced on the catalyst surface where it combines with the electrons that have departed the anode and traveled the external circuit and with the protons which have departed the anode and traveled through the polymer electrolyte membrane. Diatomic oxygen molecules are required for this reaction at half the rate at which the diatomic hydrogen molecules are split into protons, and electrons, and the resulting product is water. The cathode reaction is detailed in Equation 1.2.

$$O_2 + 4H^+ + 4e^- \rightarrow 2H_2O \quad (1.2)$$

Overall, PEM fuel cells yield the following reaction:

$$2H_2 + O_2 \rightarrow 2H_2O \quad (1.3)$$

The electrode reactions and a schematic of the electrochemistry are summarized in Figure 1.1.

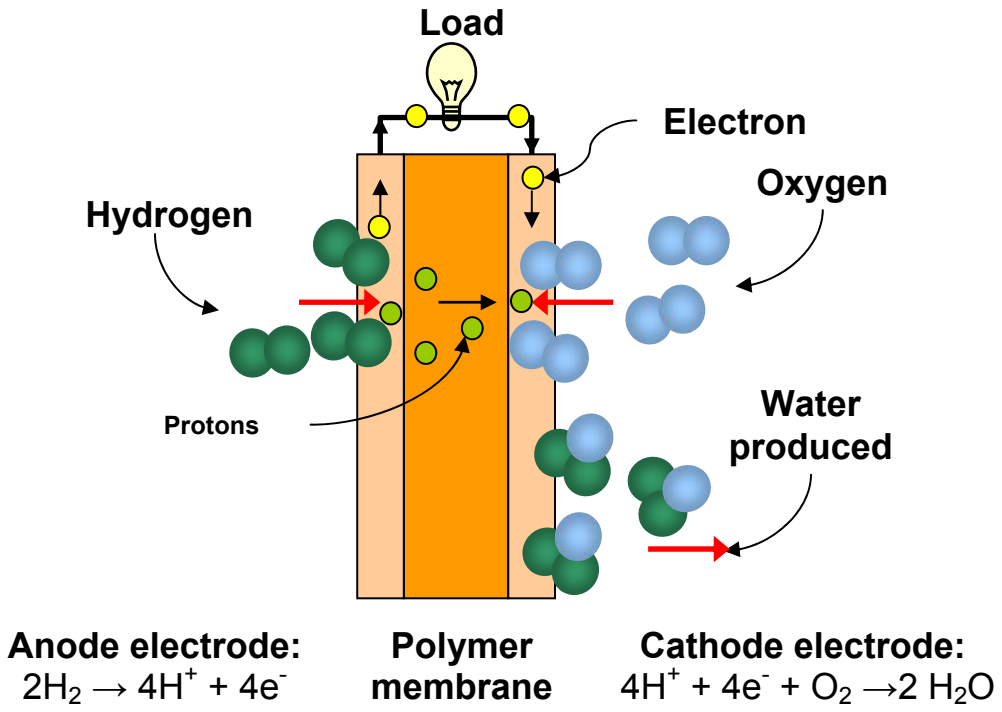

Figure 1.1 – Schematic of PEM fuel cell electrode reactions.

1.2 PEM FUEL CELL COMPONENTS

There are relatively few components that make up a single PEM fuel cell. Each of the following components - the catalyst layers, the polymer membrane, the gas diffusion layer, and the collector plates, are discussed briefly in this section.

Figure 1.2 illustrates the assembly of a single PEM fuel cell. Starting from the center and working outward, the polymer membrane separates the reactants in the PEM fuel cell. The proton exchange membrane (PEM) is relatively impermeable to electrons, but an excellent conductor of protons, thus forcing electrons through the external circuit, while allowing the travel of protons to the cathode.

The catalyst layers used in PEM fuel cells are typically a mixture of platinum particles (dia.~7 nm) supported on carbon particles (dia.~30 nm), mixed in a ratio of approximately 2:1 with a proton conducting polymer electrolyte, typically Nafion® by DuPont. This mixture can be applied to the gas diffusion layer (to be discussed later) and then hot pressed to the membrane. Alternatively, the catalyst mixture can be applied

directly to the membrane by a variety of methods such as, painting, spraying, or hot pressing. In this work, the membrane with catalyst layers on each side is referred to as the membrane electrode assembly (MEA). It is important to note that in other works, MEA is sometimes used to mean the entirety of the membrane, catalyst layers, and gas diffusion layers.

The gas diffusion layer (GDL) in a PEM fuel cell serves a variety of purposes. This layer must be porous to allow the hydrogen or oxygen to diffuse to the catalyst layers. Additionally, the GDL must be well suited to transport the water produced at the cathode reactions sites outward from the reaction sites to avoid what is called electrode flooding. Flooding simply refers to the fact that if too much water is surrounding the catalyst site, then it is more difficult for gases to diffuse to the catalyst site due to the presence of the water. The GDL must also be electrically conductive since the electrons produced at the anode must travel through the GDL to the external circuit and around to the cathode to complete the reaction. Resistance to corrosion is also an issue of concern since the GDL resides in a moist and acidic environment. Due to the requirements of permeability, electrical conductivity, and corrosion resistance, the GDL is typically constructed of flexible carbon fiber based woven fabric, or stiff carbon fiber based paper.

The final components required for a single PEM fuel cell are the collector plates. The collector plates are typically pressed against the gas diffusion layer to collect electrons from the anode GDL and transport them into the external circuit, or to conduct electrons from the external circuit into the cathode GDL to complete the circuit. Additionally, the collector plates typically have a flow field machined into them to evenly distribute the reactant gas uniformly over the surface of the GDL.

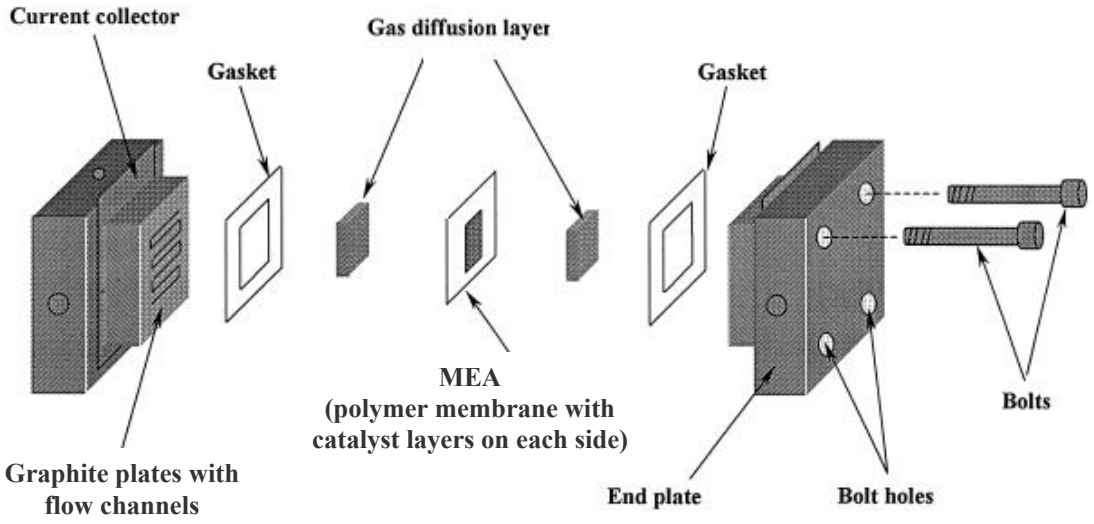

Figure 1.2 – Single PEM fuel cell components and assembly [1].

1.3 CONVENTIONAL PEMFC STACK ARCHITECTURE

The most widespread means of combining the power of many fuel cells is by connecting the cells electrically in series to form a stack as depicted in Figure 1.3. It can be seen in the diagram that each individual cell is sandwiched between two bipolar plates. The bipolar plates serve the purpose of transferring electrons from each cell to the adjacent cell. The bipolar plates also include gas flow channels to distribute the gases to each cell. Each plate has a flow channel for hydrogen on one side and a flow channel for oxygen or air on the other side. Following assembly of the stack, the endplates will be connected using tie rods to apply pressure to the entire stack. This type of fuel cell stack will be referred to often in this work as a *conventional* fuel cell stack architecture due to its widespread adoption among PEM fuel cell designers and researchers. Although this style of fuel cell stack is very common there are two major challenges with the conventional fuel cell stack architecture.

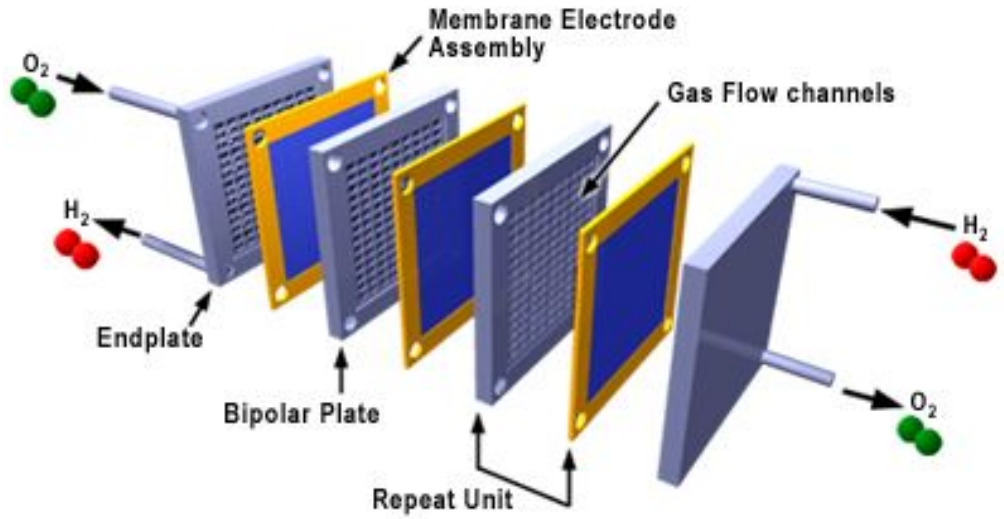

Figure 1.3 – Conventional fuel cell stack architecture [2].

The first major challenge with the conventional fuel cell stack architecture is the need for extensive gas manifolds. Figure 1.4 is a cross section of the conventional architecture consisting of a three cell stack. The figure shows the need for each bipolar plate to have hydrogen flowing in the gas channels on one side of the bipolar plate and air or oxygen flowing in the gas channels on the opposite side. Therefore, the conventional stack configuration requires a number of flow fields equal to two times the number of cells. In many cases, a conventional stack will consist of over one hundred individual cells, thus requiring two hundred individual flow fields. Each flow field is comprised of numerous flow channels. Thus, the number of channels that must be formed to distribute reactant gas is enormous. The channels cannot be easily consolidated into larger flow channels because the shoulders between the channels are needed to maintain uniform pressure and good electrical contact over the GDL surface.

In addition to the difficulty of distributing gases effectively to hundreds of flow fields, the possibility of gases leaking and reaching the wrong electrode is a very prominent problem. If gases were to mix on an electrode of one cell, that cell would be unable to produce any significant current. Additionally, since the conventional stack architecture connects all cells electrically in series, if one cell fails the entire stack fails. The series only electrical connection scheme lends itself to serious reliability concerns of which fuel or oxidant leakage is a significant contributor.

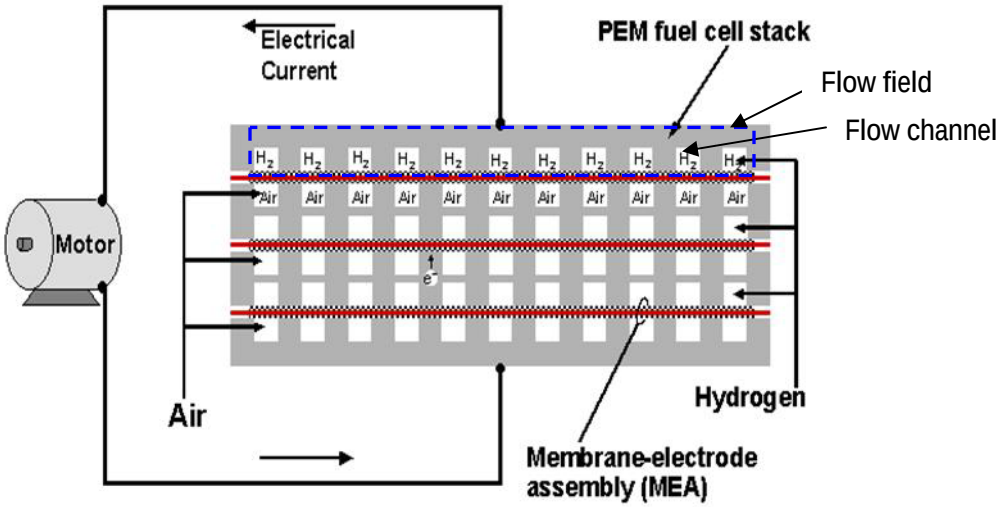

Figure 1.4 – Depiction of a 3 cell stack, showing two flow fields per cell [3].

The second major challenge associated with the conventional fuel cell stack architecture is related to cost. The two most significant costs in a PEM fuel cell stack are the precious metal catalyst and the bipolar plates [11]. The elimination of the precious metal catalyst is unlikely if not impossible; therefore this cost concern can only be addressed by attempting to reduce the quantity required in each cell. The catalyst loadings required in PEM fuel cells have decreased over thirty fold in the past ten years while performance has increased significantly over the same time period. This trend seems to indicate that the technology of reducing catalyst material in PEM fuel cells has nearly reached its maturity, making catalyst reduction an unlikely candidate for cost reduction. Therefore, the focus in this work will be aimed at attacking the high cost of the bipolar plates utilized in conventional PEM fuel cell stacks. The bipolar plates currently make up approximately 25-30% of the cost associated with a conventional fuel cell stack [11]. This percentage corresponds to a cost of $20/kW for the bipolar plates used in a stack. In contrast, the internal combustion engine has a cost of approximately $30/kW [12]. In addition to the exorbitant final cost of bipolar plates, approximately 58-72% of the cost is associated with the raw materials required to manufacture the plates, which typically consist of some combination of carbon black, carbon fibers, and an epoxy resin [11]. Therefore, it seems unlikely that bipolar plates will drop significantly in cost since

the materials used to manufacture the plates already enjoy widespread use in other industrial applications.

This research focuses on a new style of fuel cell stack architecture that reduces the challenges associated with complex flow fields, a purely series connection, and the cost issues related to the bipolar plates. The new fuel cell ribbon stack architecture will be discussed briefly in the next section. A more detailed discussion of the ribbon architecture is provided in Section 2.1.

1.4 PEM FUEL CELL RIBBON STACK ARCHITECTURE

This work proposes the design and development of the fuel cell ribbon stack architecture which relies on the gas diffusion layer, not the bipolar plates, to transport electrons to the next cell in the stack. The ribbon architecture addresses the challenges associated with a conventional architecture by first configuring the cells in a manner which allows for fewer flow fields due to the anodes and cathodes of each cell being aligned as seen in Figures 1.5. Moreover, the flow field design can be more flexible because the ribbon design does not rely on the gas channel shoulders to compress the GDL and provide electrical contact at the GDL. Additionally, the ribbon architecture addresses the cost issue related to the bipolar plates by complete elimination of the bipolar plates from the design. Initially the ribbon architecture will only utilize an electrically series connection among cells, but due to the planar and potentially flexible nature of the ribbon stacks, there is significant potential for a variety of series and parallel electrical connection schemes which could greatly increase stack reliability compared to a conventional fuel cell stack. A diagram of the fuel cell ribbon architecture showing the key components of the design is displayed in Figure 1.5.

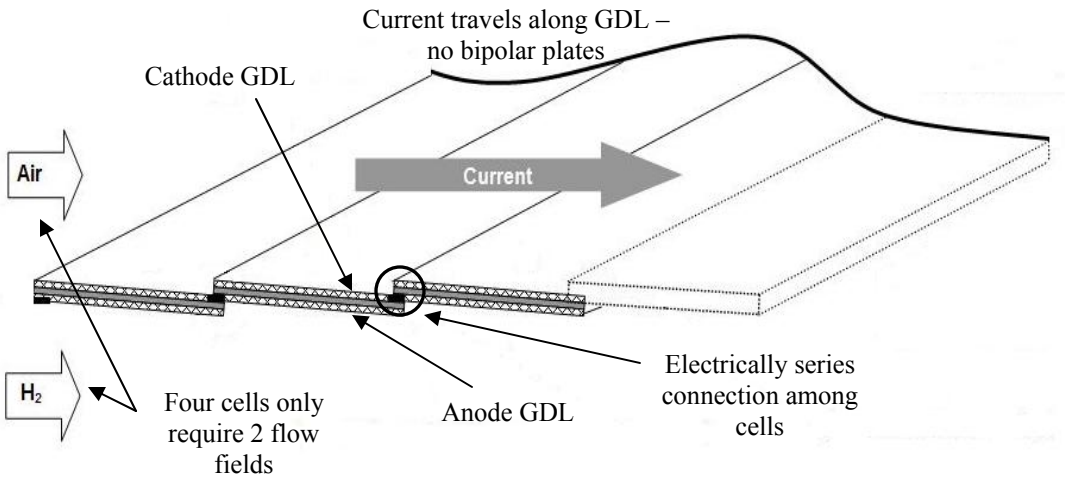

Figure 1.5 – Diagram of the proposed fuel cell ribbon stack architecture [4].

The focus of this work will be the development of a single ribbon fuel cell from which a variety of fuel cell ribbon designs can be developed. The following section will detail the objectives which must be achieved to develop the single ribbon cell technology.

1.5 RESEARCH OBJECTIVES

The core technology which will enable the fuel cell ribbon stack concept to be realized is the high conductivity gas diffusion media which is required to conduct electrons in the plane of the fuel cell ribbon to the adjacent ribbon in the stack. The following objectives all have the central focus of demonstrating fuel cell ribbon feasibility and assuring that the early stages of the fuel cell ribbon development provide a sound foundation for future development. The objectives of this work are to:

- Identify suitable diffusion media which exhibits sufficiently low electrical resistance for use as a current carrier and gas diffuser in a fuel cell ribbon
- Identify or develop treatments (hydrophobic treatment, carbon infill, etc.) for the diffusion media which will enable acceptable performance in a fuel cell environment

- Apply the treated diffusion media to a catalyzed proton exchange membrane and demonstrate performance exceeding the performance of similar stack concepts observed in the existing literature
- Develop an analytical model which will aid in the identification of suitable resistive properties of the diffusion media
- Develop a numerical finite element model capable of predicting the performance of a PEMFC using the diffusion media in a fuel cell ribbon configuration, and to validate the predictions experimentally
- Develop experimental equipment and procedures to characterize the diffusion media

The following chapter, Chapter 2, will discuss the literature related to the fuel cell ribbon concept and common diffusion media treatments. Next, Chapter 3 will detail the analytical efforts undertaken in this work, while Chapter 4 will detail the experimental efforts. Chapter 5 will present the results of the analytical and experimental efforts, while Chapter 6 will conclude this work with some observations and recommendations for future work in the development of the fuel cell ribbon concept.

2 LITERATURE SURVEY

This work will focus on the development of advanced diffusion media to enable the utilization of alternative fuel cell stack architectures, particularly architectures which do not depend on bipolar plates, but rather utilize the gas diffusion layer (GDL) as a current collector and conductor. More specifically, this work focuses on what has been coined a "fuel cell ribbon stack architecture" [4]. The following chapter will first introduce the ribbon stack architecture. Section 2.2 will discuss the existing literature pertaining to stacks which share similar in-plane electrical current transport schemes as the ribbon stack architecture. Additionally, this chapter will review the existing literature regarding materials used for GDL fabrication, surface treatments applied to GDL substrates to enhance the interfacial properties of the GDL, and a variety of important characteristics of GDLs and how these characteristics are measured. Finally, the impact this work will have on ribbon stack research will be discussed in the last section of this chapter.

2.1 STATUS OF RIBBON STACK DEVELOPMENT

Although the ribbon fuel cell offers distinct advantages over a conventional PEMFC stack in terms of size, weight, and ease of manufacture, the ribbon concept also introduces new challenges to the design process. This section will introduce the fuel cell ribbon architecture, describe the performance and applications of similar architectures seen in the literature, and discuss the technical challenges associated with the fuel cell ribbon architecture.

2.1.1 Description

The most significant difference between the ribbon stack architecture and the conventional PEMFC stack architecture is the absence of the interconnecting bipolar plates, and the reduced complexity of the fuel and oxidant supply system.

As discussed in Section 1.3 the bipolar plates in a conventional fuel cell stack assembly account for approximately 25-30% of the stack cost, making the bipolar plates a significant barrier to PEMFC stack cost reduction. The ribbon stack architecture utilizes the conductivity of the GDL to carry current laterally to the adjacent cell, rather than relying on a bipolar plate to conduct current in a direction perpendicular to the MEA to an adjacent cell. The elimination of bipolar plates from the PEMFC stack architecture also contributes to a greatly simplified means of manufacture. The brittleness of graphite bipolar plates make them very sensitive to handling and assembly, slowing the assembly process and requiring assembly by hand or precision machinery. Conversely, the fuel cell ribbon stack lends itself to a streamlined method of manufacture using equipment resembling modern laminating equipment.

In a conventional PEMFC stack, both fuel and oxidant must be delivered to each cell individually through a complex manifold, thus requiring a number of flow fields equal to twice the number of cells in the stack. Yet, in a ribbon stack multiple cells could share a common fuel flow field, and a common oxidant flow field, thus significantly reducing the complexity of the supply of fuel and oxidant to the cells. An example of flow field sharing among cells made possible by the adjacent nature of the cell connections can be seen in Figure 2.1.

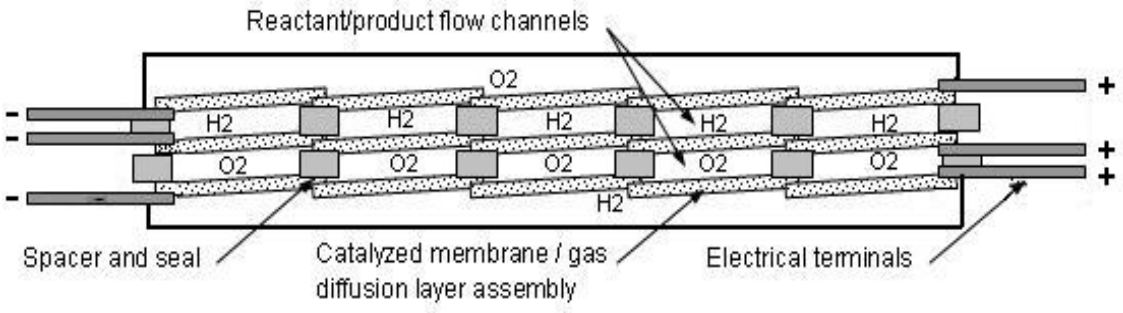

Figure 2.1 – Fifteen ribbon cell series/parallel stack requiring 4 flow fields [4].

In order for the fuel cell ribbon stack architecture to be realized a variety of advancements must be made, including:

- Development of a high conductivity GDL to counteract the increased distance of electron travel in the plane of the GDL versus through the plane of the GDL;
- Development of methods for adhering the high conductivity GDL to the catalyzed membrane;
- Development of suitable means for connecting adjacent cells;
- Development of flow fields to effectively supply fuel, supply oxidant, and remove product water;
- Development of techniques for removal of waste heat generated by the chemical reactions

Each of these advancements presents challenges which will be discussed further in the following section.

A diagram of a fuel cell ribbon stack along with some of the associated developmental needs can be seen in Figure 2.2. The figure also describes the adaptability of a fuel cell ribbon to a variety of power requirements. The number of cells can be increased to increase voltage, while the length of each ribbon can be increased to increase the total current being produced.

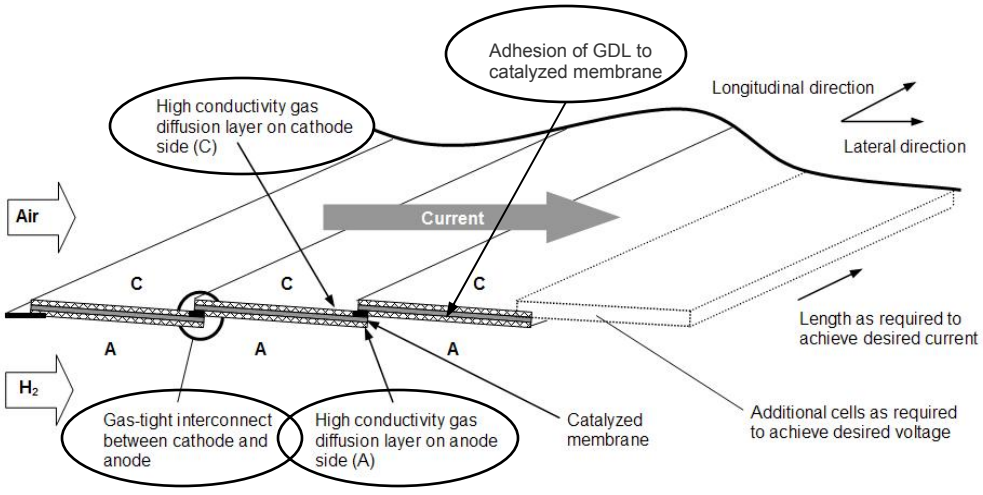

Figure 2.2 – Diagram illustrating challenges (circled) associated with a ribbon stack.

2.1.2 Technical challenges

Perhaps the greatest challenge associated with the ribbon stack architecture is the need for a high conductivity GDL. Currently available commercial gas diffusion media exhibits conductivities suitable for current travel through their thickness, but not for current travel along their length. The resistive losses associated with the flow of current in the plane of commercially available GDLs would significantly reduce cell performance. Reducing the resistance of the GDL can be achieved by either increasing the thickness to provide a greater cross section for current flow, or by modifying the materials to decrease the bulk resistivity of the diffusion media. Taking either of these options to an extreme would be detrimental to the fuel cell stack by increasing the diffusive path length of the gases, or by increasing the material cost.

An additional challenge associated with the ribbon design is that in the absence of stack compression the GDL must be adhered to the catalyzed membrane. This challenge is not expected to be a significant roadblock in the development of the fuel cell ribbon stack due to the available literature discussing methods of electrode adhesion to the polymer membrane [13, 14, 15, 16]. Additionally, it will be shown that the literature supports the application of a microporous layer (MPL) on the surface of the GDL to aid in water transport and contact between the GDL and the catalyst layer. The addition of the MPL will also aid in the adhesion of the GDL to the catalyzed membrane. The available literature discussing the effects of a MPL will be discussed further in a later section.

The connection between adjacent cells is another significant concern in the development of fuel cell ribbon stacks. The interconnect must provide excellent contact between adjacent cells, have very low electrical resistance, and be impermeable to gases to avoid fuel or oxidant crossover. The interconnect must also be stable in a warm and moist acidic environment. The present research will focus on the application of the necessary treatments to the diffusion media, reducing the resistance of the diffusion media, and adhering the diffusion media to an MEA for use as a gas diffusion layer and electrical current carrier in a single fuel cell ribbon.

2.1.3 Alternative PEMFC stacks and applications

Proton exchange membrane fuel cells are considered to be the prime alternative energy technology for a broad spectrum of power levels ranging from milliwatts to megawatts. Currently, many researchers believe that alternative PEM fuel cell stack architectures, such as the ribbon assembly, are most suitable for portable or low power applications due to the challenges associated with drastically reducing the resistance of the gas diffusion media.

In 1998 Heinzel et al. [6] published a paper presenting a banded fuel cell structure. This structure utilized lateral current conduction, much like the ribbon arrangement presented herein. Furthermore, they proposed that a banded structure consisting of 4 laterally connected cells be placed between electrically insulated plates with electrical conductors attached to the final cells. This method of connection could be utilized to connect any number of banded structures to increase the stack power. Heinzel et al. tested a 2 layer, 4-cell per banded layer, fuel cell stack running at room temperature. The current density obtained at 0.5 Volts per cell was 0.23 A/cm^2 when operating on air, and 0.34 A/cm^2 when operating on oxygen. Conventional PEM fuel cells operating on air typically achieve current densities between 0.5 – 1 A/cm^2 at 0.5 V. A diagram of a banded structure can be seen in Figure 2.3, and a diagram of the dual layer banded structure can be seen in Figure 2.4.

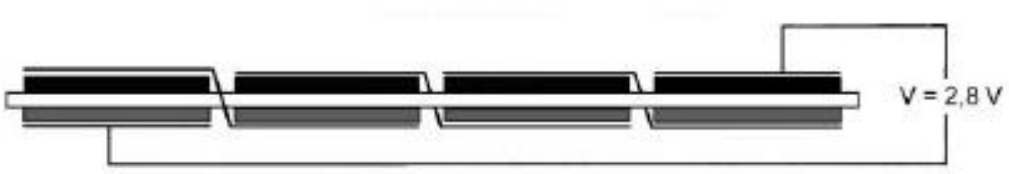

Figure 2.3 – Banded structure presented by Heinzel [5].

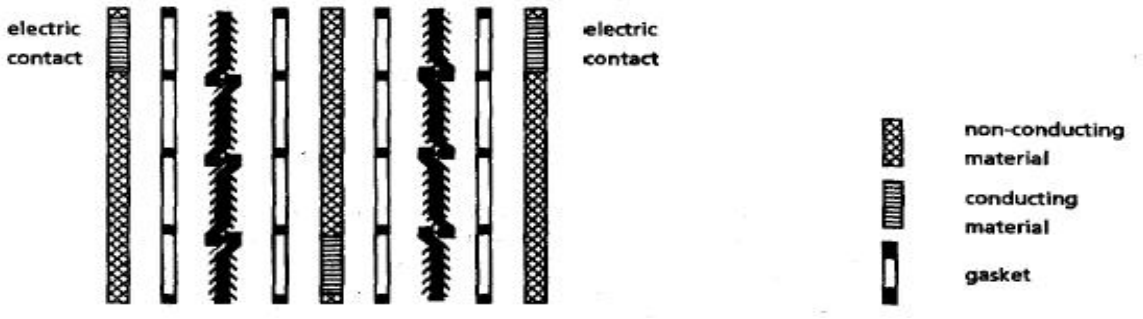

Figure 2.4 – Multiple band stack presented by Heinzel [6].

Heinzel et al. [5] support the use of alternative stacks for portable electronics. Heinzel et al. use what they have called a combination banded structure where three cells are linked in a conventional configuration, then the small conventional stacks are compressed together using bipolar plates consisting of gaps through which an interconnect can be passed to the adjacent conventional stack and proper insulation to avoid short circuits. A diagram of the combination bipolar plate and banded structure PEMFC stack can be seen in Figure 2.5. A prototype of the combination configuration was built to produce between 15-20 Watts of power, which is sufficient to power a laptop computer. The active area of the cells was not reported making it impossible to determine the quality of performance achieved by the prototype. Heinzel also acknowledged the need to increase the conductivity of the GDL for a PEMFC stack utilizing lateral electrical conduction. In order to increase the conductivity of commercially available diffusion media, Heinzel et al. partially filled the pores of the GDL with carbon black to lower the through-plane resistance by 20%. This method of increasing conductivity was also utilized in the work presented in this thesis.

Figure 2.5 – Combination banded fuel cell stack by Heinzel [5].

Green et al. [17] proposed a tubular design for PEMFC stacks for use in ambient air. The cells are connected laterally using perforated nickel foil to conduct the electricity from the cathode GDL to the adjacent anode GDL. The anode of each cell is in contact with a perforated plastic tube which is filled with hydrogen, while a perforated tubular stainless steel sleeve is placed around cathodes of the cells and tightened to provide adequate compression. Appropriate gasketing was used between the cathode GDLs and the stainless steel sleeve to avoid short circuits. Polarization curves are presented and exhibit current densities of approximately 0.3 A/cm^2 at a cell potential of 0.5 V. Significant degradation of performance was observed over time, likely due to corrosion of the nickel foil cell interconnects. A performance drop of up to 50% was observed in less than a 1 hour window of time.

Chu et al. [7, 18, 19] have done significant work on what is termed a monopolar strip stack. Their configuration is called monopolar due to all of the like poles being aligned laterally. The monopolar strip stack arrangement is the most similar arrangement to the proposed ribbon architecture found in the literature. Chu et al. do not discuss details of the material used, but do present polarization data and a diagram of the monopolar strip stack. Two different strip stacks were tested, one consisting of five laterally connected cells, and another consisting of ten laterally connected cells. In both cases the stacks were tested under varying temperature and relative humidity. The best performance was obtained using a relative humidity of 100% and a cell temperature of 50°C. At these operating conditions the 5-cell and 10-cell strip stacks both exhibited a current density of 0.11 A/cm^2. A diagram of the strip stack proposed by Chu can be seen in Figure 2.6.

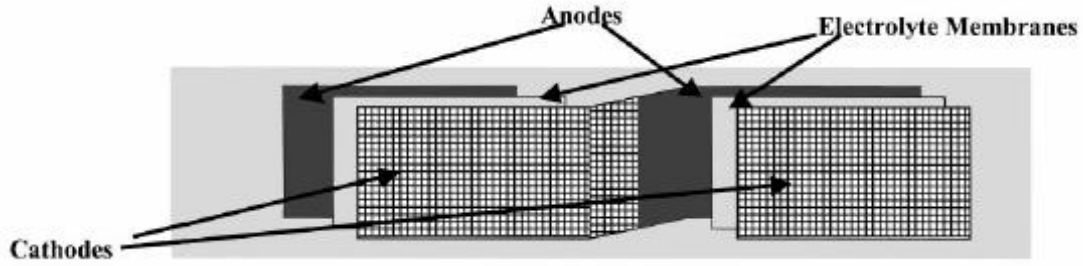

Figure 2.6 – Monopolar strip stack presented by Chu [7].

Lee et al. [8] discuss work on a PEMFC stack termed a flip-flop configuration which utilizes lateral current conduction. The flip-flop configuration does not require the current collector to pass through a common membrane as is required in the banded and strip arrangements by Chu and Heinzel. Instead, the flip flop design would have four or more electrodes on each side of the same membrane, where half of the electrodes on the top are anodes, and the other half are cathodes. The current carrying media connects two electrodes on the top, and then a separate current carrier would connect two electrodes on the bottom to form a series electrical connection between the cells. Figure 2.7 greatly clarifies the design. The performance achieved in this configuration is similar to the performance achieved by Chu et al. The achieved performance for a 4 cell assembly at room temperature with 1 atm of backpressure on both the anode and the cathode resulted in a current density of 0.14 A/cm^2 at a single cell potential of 0.5 Volts. The flip-flop design did utilize compression and separate flow fields for each cell, but relied on the current carrying cross members to carry the current laterally to the adjacent electrode.

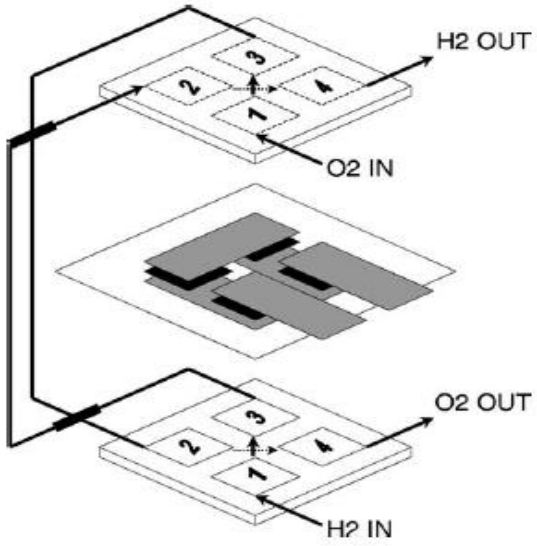

Figure 2.7 – Flip-flop design proposed by Lee [8].

Table 2.1 provides a performance comparison of the alternative fuel cell stacks discussed above. It clearly shows that the cells utilizing compression yielded greater results.

Table 2.1 – Alternative stack performance comparison when operated on air.

Reference	Operating condtions	Peak current density (A/cm^2) at 0.5 Volts	Compression used
Heinzel [6]	T_{cell} = ambient, RH_c = ambient, RH_a = unknown	0.23	YES
Green [17]	T_{cell} = ambient, RH_c = ambient, RH_a = none	0.3*	YES
Chu [7]	T_{cell} = 50°C, RH_c = 100%, RH_a = 100%	0.11	NO
Lee [8]	T_{cell} = ambient, RH_c = unknown, RH_a = unknown	0.14	YES

* sustained for only 1 hour before cell degraded

2.2 GAS DIFFUSION LAYER MATERIALS AND FABRICATION

In a proton exchange membrane fuel cell (PEMFC) stack, the gas diffusion media is sandwiched between the bipolar plate and the catalyst layer to form the gas diffusion layer (GDL). The catalyst layer requires reactant gases and moisture to keep the membrane hydrated, while the reactions in the catalyst layer cause the generation of water, heat, and electricity. Therefore, the diffusion media must allow gases to reach the catalyst, while allowing heat, water, and electricity to leave the catalyst sites. The transport of water from the catalyst sites, through the diffusion media, and into the gas channel, is critical because the formation of water can clog the pores and limit the reaction rate. Mathias et al. [20] provide a detailed list of specific functions the gas diffusion media must perform which is presented here:

- Reactant permeability: provide reactant gas access from flow-field channels to catalyst layers including in-plane permeability to regions adjacent to lands
- Product permeability: provide passage for removal of product water from catalyst layer area to flow channels

- Electronic conductivity: provide electronic conductivity from bipolar plates to catalyst layers including in-plane conductivity to regions adjacent to channels
- Heat conduction: provide for efficient heat removal from the membrane electrode assembly (MEA) to the bipolar plates where coolant channels are located
- Mechanical strength: provide mechanical support to the MEA in the case of different reactant gas pressures at the cathode and anode

In addition to the functions specified by Mathias et al., the diffusion media must also be resistant to corrosion. The environment inside a PEMFC is typically very moist, acidic, and has high concentrations of hydrogen at the anode. Most materials, particularly metal, are prone to corrosion in this type of environment. The requirements identified by Mathias, along with the need for stability in a corrosive environment, limit the options for materials which can be used as diffusion media in PEM fuel cells. The most commonly used materials that meet these requirements are porous carbon based papers or cloths.

This section will discuss the different types of cloth and paper materials used for gas diffusion media in PEM fuel cells and the treatments typically performed on the base material (substrate) prior to its use in a PEM fuel cell.

2.2.1 Materials

Care must be taken when selecting material for use in a PEM fuel cell due to the corrosive environment within the cell. This section will discuss the materials suitable for the construction of gas diffusion layers in PEMFCs; the properties of the suitable materials; and the processes for fabricating gas diffusion media out of the base materials discussed herein.

Carbon fibers are the predominant materials used for the construction of diffusion media due to their resistance to corrosion and high electrical conductivity. Mathias et al. [20] provide a discussion of different types of carbon fibers currently available, and also the different types of carbon fiber products used for gas diffusion media. Two types of carbon fibers which have drastically different properties and are suitable for application

in PEM fuel cells are discussed by Mathias. The physical properties of both coal tar pitch and polyacrylonitrile (PAN) based carbon fibers will be discussed.

Mathias et al. describe the three types of carbon fiber that make up the carbon fiber industry: polyacrylonitrile (PAN) based fibers, isotropic pitch based fibers, and mesophase pitch based fibers. Fibers which use PAN as a precursor make up 90% of the world's carbon fiber market, making this type of fiber the most readily available and predominantly used in PEM fuel cell diffusion media. Mesophase and isotropic pitch based fibers are derived from heavy fractions of petroleum or coal. The isotropic version is of low quality and its properties, both electrical and mechanical, are substandard compared to PAN based fibers, while the properties of the mesophase pitch are in some cases far superior to that of the PAN based fibers.

Cytec [21] has published a detailed list of properties for a variety of carbon fibers which they produce. The list includes PAN based carbon fibers, as well as mesophase pitch based carbon fibers. The properties of the two different fiber types will be compared. Mechanically, the mesophase pitch fibers exhibit longitudinal tensile strengths of the same order as the PAN based fibers, while the longitudinal compressive strength of the pitch fibers is only one eighth of the strength of the PAN based fibers. When the energy transfer abilities of the PAN and mesophase pitch based fibers are compared, the mesophase pitch fibers clearly dominate. The mesophase pitch based fibers exhibit electrical conductivities 10-15 times greater than that of PAN based fibers, while the thermal conductivity of the mesophase pitch fibers can be as great as 100 times that of the PAN based fibers.

Due to the differences in physical properties for mesophase pitch and PAN based carbon fibers; different processes must be followed to successfully produce woven carbon cloths from each type of fiber. The general process for producing carbon fiber cloth is as follows: 1) produce precursor fiber tows by drawing coal tar pitch or PAN polymer through a 200-12,000 fiber die; 2) stabilize the tows at moderate temperature in an oxidizing environment to prepare them for weaving; 3) twist tows into yarns if possible; 4) weave the stabilized tows or yarns; 5) subject woven cloth to appropriate heat treatments (graphitization) to yield a high conductivity carbon cloth. Due to the strength difference of the precursor (pre graphitized) tows, much larger tow sizes are required in

order to successfully weave pitch precursor tows. The low compressive and shear strength of the pitch precursor tows also make it difficult to twist the pitch tows into yarns prior to weaving. Therefore, cloths made from PAN based carbon fibers typically consist of tow sizes of 200-400 fibers which are twisted into 2, 4, or 6 ply yarns prior to weaving and graphitization. Conversely, pitch based carbon cloths are typically produced from tows which are 2,000-12,000 fibers, where the woven structure is comprised of untwisted tows rather than yarns due to the fragility of the pitch fibers.

Mathias et al. describe carbon fiber based materials as good candidates for diffusion media due to their corrosion resistance, high electrical conductivity, and high porosity (typically $\geq 70\%$). There are two types of carbon fiber based materials which are typically used for PEMFC gas diffusion media; carbon paper, and carbon cloth. Carbon paper is less expensive to manufacture due to the acceptance of chopped fiber, random orientation, and existing large scale paper making equipment. Carbon cloth is a more costly manufacturing process requiring tow or yarn formation of the precursor filaments, weaving of the tows or yarns, followed by carbonization. Two types of weave patterns are common for the carbon cloths; plain weaves and satin weaves. A plain weave consists of the fill yarns alternating over and under the warp yarns (machine direction). This configuration creates a very tight, dimensionally stable, and isotropic fabric. Plain weaves are the most common weaves seen in carbon cloth gas diffusion media for PEM fuel cells. A satin weave is denoted by the interval at which the fill yarns go under a single warp yarn. For example, in an 8 harness satin weave, each fill yarn will go over seven consecutive warp yarns, and then under the eighth warp yarn, and then the sequence is repeated. Figure 2.8 is a graphical representation of a plain and a 5 harness satin weave.

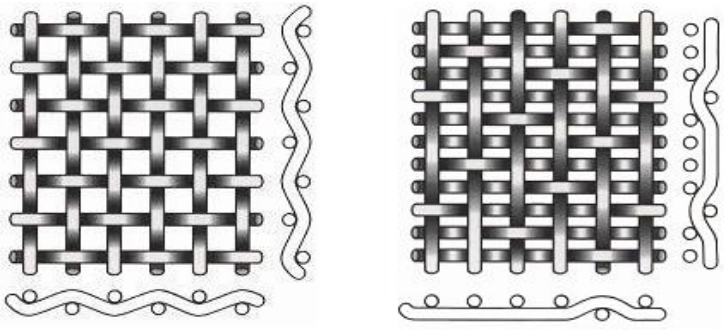

Figure 2.8 - Example of a plain (left) and a 5 harness satin (right) weave.

2.2.2 Hydrophobic polymer content

Water transport and electrode flooding within PEM fuel cells are poorly understood phenomena. Therefore, many of the treatments performed on gas diffusion media are based on empiricism rather than the governing physics. Mathias et al. [20] provides an overview of the predominant techniques, while others will be cited with more specific details of the effect of the hydrophobic polymer content in the gas diffusion media.

Mathias et al. [20] claim that it is necessary to apply a hydrophobic polymer such as PTFE to the diffusion media on the cathode to aid in water transport since water is produced there, and also on the anode to aid in the prevention of flooding during cold start up (i.e. warm humid stream of hydrogen, and a cold cell causes water to condense). Additionally, Mathias has observed that the available literature indicates a range of PTFE content between 5-30 wt%. The PTFE is most commonly applied by repeatedly dipping the diffusion media into an aqueous suspension of PTFE particles, followed by drying, until the appropriate mass has been added to the diffusion media. The amount of PTFE added to the diffusion media can be controlled by the length of soak time, and by the concentration of the aqueous suspension. Once the desired mass has been added, the diffusion media is heated to 350°C in order to sinter the PTFE particles together and fix the PTFE to the diffusion media substrate.

Wang et al. [22] performed tests where fluorinated ethylene propylene (FEP) was used to provide a hydrophobic treatment to gas diffusion media. In this work, PEM fuel cells were tested over a range of temperature and relative humidity. Contact angle was compared for carbon paper diffusion media at different loadings of FEP content: 10, 20, 30 and 40 wt%. It was found that the change in FEP content caused no appreciable change in the contact angle of the meniscus rise when the material was partially suspended in water, thus indicating that the effectiveness of the FEP on the surface of the diffusion media remained the same over all loadings. Wang et al. also collected polarization data for cells utilizing diffusion media containing 10 and 30 wt% FEP. It was observed that the diffusion media consisting of 10 wt% FEP performed significantly better in the mass transport limited region of the polarization data. It was initially

believed that higher FEP loading led to decreased bulk porosity, and therefore increased mass diffusion resistance. But, when the porosity (pore volume/total volume) of both media was estimated, a difference of only 0.07 was calculated. Additionally, SEM images of the surface morphology were taken for the diffusion media containing 10 and 30 wt% FEP. It was observed that the carbon paper containing 30 wt% FEP exhibited significant pore blockage at the surface. Therefore, the higher performance of the carbon paper impregnated with 10 wt% FEP was attributed to the decreased surface pore blockage (not reduced bulk porosity) of the diffusion media at the lower FEP concentrations, which results in a lower resistance to gas species flow.

Prasanna et al. [23] investigated how the hydrophobic polymer content in carbon paper diffusion media influenced the ex-situ measured bulk properties of the material, along with the performance in a PEM fuel cell. Teflon™ (PTFE) was used to provide the hydrophobic characteristics to the diffusion media. Experiments were performed for four different levels of PTFE content: 10, 20, 30, and 40 wt%. When the bulk area specific resistances of the four different diffusion media were measured, the results showed that the 10 wt% PTFE diffusion media exhibited the lowest area specific resistance, while the 40 wt% PTFE diffusion layer exhibited the greatest area specific resistance. Accordingly, the carbon papers containing 20 and 30 wt% exhibited resistances in between the two extremes. Each impregnated carbon paper was also subjected to a gas permeability test. The carbon paper with 10 wt% PTFE exhibited the highest rate of gas permeation, 30.4 mL/min-cm^2-Pa. This value decreased slightly for the carbon paper containing 20 wt% PTFE, but dropped to a value of 9.9 mL/min-cm^2-Pa for the paper containing 40 wt% PTFE. When the varying carbon papers were used as diffusion media in a PEM fuel cell, the paper containing 20wt% PTFE exhibited the best polarization data, while the paper containing 10 wt% PTFE performed very similarly. The performance of the 40 wt% PTFE carbon paper was significantly lower than the others tested. AC impedance spectra were also taken when the cells were running at a constant voltage of 0.85 Volts. At this voltage, there is expected to be very little water production, resulting in the difference in imaginary impedances observed to be attributed to decreased diffusion layer permeability. Again, the 10 and 20 wt% PTFE curves fell very close to each other, while the 30 wt%

curve was slightly worse, and the 40 wt% curve exhibited significantly higher imaginary impedance.

Park et al. [24] investigated the effects of PTFE content in two different carbon papers, a 190 μm and a 250 μm version manufactured by Toray. PTFE was added to each paper to achieve weight percentages of PTFE content in the diffusion media of: 0, 5, 15, 25, 35, and 45 wt%. Porosity and polarization performance were recorded for each treated diffusion media. When the PTFE content was increased from 0 to 35 wt% in the 190 μm sample the porosity only decreased by 8%, but when the PFTE content was raised from 0 to 45 wt% the porosity decreased by 15%. For the samples containing 5, 15, or 25 wt% PTFE the porosity decreased incrementally as expected. Similar decreases in porosity were observed with the addition of PTFE to the 250μm carbon paper substrate. For the polarization data collection, the hydrogen was humidified to saturated conditions, while the relative humidity of the air was varied anywhere from 20% up to saturated conditions. In the low current density region of the polarization curve, very little difference was observed between varying GDL PTFE content. In the higher current density regions, the GDLs with greater PTFE content exhibited a drop in performance, likely due to the decreased permeability. The mass transport effects became greater with increasing air stream relative humidity, also indicating an electrode flooding effect. This paper also addresses the application of a microporous layer (MPL) to the diffusion media. Park et al. find that the MPL seems to equalize effects that relative humidity can have on performance. This behavior is attributed to the small pore structure of the MPL acting as a buffer zone to prevent serious changes in saturation in the catalyst structure, thus reducing the likelihood of flooding or drying of the electrode. The composition and effects of the MPL will be discussed further in the next section of this work.

Table 2.2 summarizes the recommended level of hydrophobic polymer observed in the sources discussed in this section.

Table 2.2 – Hydrophobic polymer content summary from references.

Reference	Polymer Used	Optimal hydrophobic polymer loading
Mathias [20]	not specified	5 - 30%
Wang [22]	FEP	10%
Prasanna [23]	PTFE	10 - 20%
Park [24]	PTFE	0 - 15%

2.2.3 Microporous layer (MPL) composition

The microporous layer is a layer which is added to the carbon based cloth or paper for a variety of reasons. The three main reasons given for the use of this layer are to support the deposition of the catalyst [9, 13, 22, 25], enhance the ability of the GDL to transport water away from the catalyst sites [9, 13, 22, 25, 26, 27], and to reduce electrical contact resistance between the GDL and the catalyst layer [22]. In addition, the MPL could be useful to aid in adhesion between the GDL and the catalyst layer in a fuel cell ribbon. An extensive discussion of the functions, composition, loading, and application of the MPL to diffusion media was presented recently by Henderson [28]. Figure 2.9 displays the location of the MPL within a PEMFC.

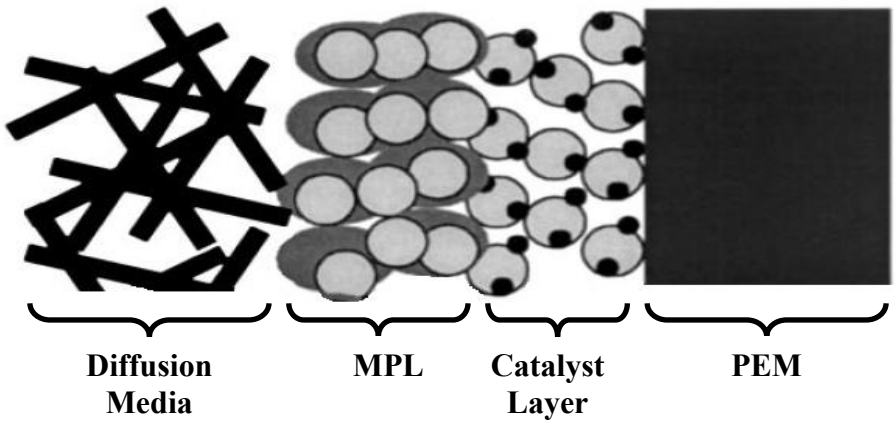

Figure 2.9 – Typical configuration of MPL within a PEMFC [9].

Some of the earliest work published pertaining to the use of a microporous layer was done by Paganin et al. in 1996 [29]. Paganin utilized a carbon cloth as a diffusion layer and deposited a MPL onto the cloth by a vacuum filtering process. The MPL was made from a homogeneous water based suspension of Teflon-30 emulsion (DuPont) and XC-72R oil furnace carbon black (Cabot). After applying the MPL to one or both sides of the GDL, the MPL was dried under ambient conditions, baked at 280°C for 30 minutes, and then sintered at 330°C for 30 minutes. Prior to use, the carbon cloth was cleaned by a heat treatment at 450°C followed by a chemical treatment at 80°C for 1 hour with a 25% nitric acid aqueous solution. A variety of thicknesses and PTFE contents were used when fabricating the MPL. Paganin expresses PTFE content in terms of weight percent of PTFE to total weight of PTFE and carbon black mixture. This convention will also be used in this work. Paganin varied the PTFE content over a range of 10 – 40%, and varied the MPL thickness between 7.5 – 32.5 microns per side of the GDL. The tests in this work were performed using gases at saturated conditions, a cell temperature of 80°C, and back pressures of 1 atmosphere for both the anode and the cathode. Paganin concludes that the thinner MPLs do not provide a deep enough smooth contact surface to the catalyst layer and thus has higher electrical resistance, while the thicker MPLs increase the diffusion length of the gases and cause lower limiting currents due to diffusive losses. It is also concluded that the lower values of PTFE content are sufficient to enhance water and gas transport near the catalyst sites, and thus greater percentages of PTFE in the MPL could only decrease the conductivity of the layer. Paganin recommends the use of an MPL composed of 15% PTFE and 25 μm thick on both sides of the carbon cloth used for the diffusion media. The reason for applying an MPL on the gas channel side also is unclear and only shows minor improvements in performance.

Giorgi et al. [30] chose to use a spray technique in the application of an MPL onto a carbon paper GDL. The MPL ink was made by mixing a homogeneous suspension of carbon black (Vulcan® XC-72R, Cabot Corp.) and PTFE dispersion in an ultrasonic bath at room temperature for 25 minutes. Following application to the carbon paper, the MPL was dried in air for 1 hour at 120°C, baked at 280°C for 30 minutes, and finally sintered at 350°C for 30 minutes. MPL PTFE content was varied from 20 – 40% by weight. Giorgi then collected galvanostatic steady-state polarization curves for the oxygen

reduction reaction in 1 M H_2SO_4 and found that the 10 wt% PTFE MPL performed best. When porosity measurements were performed on the various MPL compositions, the 10 wt% MPL again performed better than all other compositions. Finally, the various electrodes to which MPLs had been applied were analyzed using impedance spectroscopy. Again, the 10 wt% MPL performed best, particularly at the mid to lower range of frequencies indicating that the MPL also has significant effect on the electrochemical losses in the cell, rather than simply enhancing the contact surface to lower the purely ohmic losses. This effect on electrochemical performance is likely due to the enhanced transport of water away from the catalyst sites. Rather than specifying a thickness for the MPL, Giorgi instead specifies a carbon loading of 2 mg/cm^2 for reasons that were not revealed in the published document. Giorgi concludes that a 10 wt% PTFE MPL is best, but makes no loading or thickness recommendation.

Jordan et al. [31] accepts that a low PTFE content is preferred but argues that oil furnace carbon black is not the best carbon black to use in the MPL. Experiments performed by Jordan indicate that an MPL made of acetylene black (Shawinigan®, Chevron Phillips) and PTFE outperforms an MPL made from oil furnace black (Vulcan® XC-72R, Cabot) and PTFE by up to 15% (increased cell power). Jordan argues that the decrease in surface area of the acetylene black (50 m^2/g) compared to the oil furnace black (250 m^2/g) causes a lower volume of micropores (smaller surface area means larger particles which causes larger pores) which enhances water transport from the catalyst sites. Jordan also experimented with various MPL loadings, where the loading likely refers to the total weight of the MPL rather than just the carbon black in the MPL. Jordan found that the optimal MPL loading was 1.25 mg/cm^2. It is worth noting that there was little increase in performance at lower current densities (such as those exhibited by fuel cell ribbons) since the cells were optimized for peak power density, which will typically occur between 0.4 and 0.6 Volts. Since the acetylene black only shows an increase of 15% at higher current densities and since 15% is likely within the statistical error of MEA fabrication the use of acetylene black for fuel cell ribbons is difficult to justify on the basis of this work.

Song et al. [9] performed independent investigations of MPL loading and composition. For the MPL loading investigation, the composition of the MPL was held

constant at 30 wt% PTFE. Loadings of 1.5, 3.5, and 10.0 mg/cm^2 were characterized using polarization performance and electrochemical impedance spectroscopy (EIS). The polarization data indicated that a loading of 3.5 mg/cm^2 was the optimal MPL loading, whereas the EIS analysis indicated that a loading of 3.5 mg/cm^2 was optimal for species transport within the fuel cell. For the MPL composition investigation, the loading of the MPL was held constant at 3.5 mg/cm^2, and the composition was varied over four different levels of PTFE content: 10, 20, 30, and 40 wt%. The composition study indicated that the 30 wt% PTFE MPL performed best based on polarization data. The EIS analysis indicated that the 30 wt% PTFE MPL was also optimal for species transport. It is important to note that the composition and loading studies were performed independently without and statistical analysis of possible interactions between loading and composition.

Henderson [28] performed an experimental investigation which accounts for interactions among MPL parameters to investigate polarization performance and adhesion quality at the MPL-catalyst layer interface. Adhesion at the MPL-catalyst layer interface was achieved by hot pressing the diffusion media with applied MPL to a catalyzed membrane. The polarization performance analysis done by Henderson allowed for varying MPL composition, MPL loading, hot press pressure, and hot press time. The optimal combination of parameters with respect to current density at 0.5 V was determined to be: MPL loading = 1.5 mg/cm^2, MPL PTFE content = 10 wt%, hot press time = 2 - 5 minutes, and hot press pressure = 500 psig. The performance criterion for the adhesion quality study was the apparent critical strain energy release rate at the MPL-catalyst layer interface when a peel test was performed as described by Chen [32]. Henderson's work indicates that the optimal combination of parameters for adhesion quality is: MPL loading = 1.5 mg/cm^2, MPL PTFE content = 33 wt%, hot press time = 8 minutes, and hot press pressure = 1500 psig.

Kaviany et al. [26] performed an analytically based study of the formation, distribution, and movement of condensed water within a PEMFC gas diffusion layer. The results of their analysis will be discussed herein, while the details of the equations will not. The results of the model indicate that water transport within gas diffusion media is enhanced when the diffusion media is comprised of two distinct layers, a coarse macroporous layer and a fine microporous layer. The water saturation within four

different dual layered gas diffusion media was analyzed. It was found that a diffusion layer with a fine structure adjacent to the catalyst layer, and a course structure adjacent to the gas channel provided the most advantageous distribution of water throughout the gas diffusion layer. Further analysis was performed to determine the ideal fraction of coarse structure within the media; it was found that the thickness of the coarse portion of the media should account for 70% of the total thickness. Therefore, for a carbon cloth substrate with a thickness of 350 μm, a microporous layer of 150 μm is prescribed. It is notable that this analysis did not include the effects of additional electrical resistance due to the added microporous layer, which is possibly the reason for the discrepancy between this analysis and the experimental results presented by other references which recommend a much thinner MPL.

Table 2.3 provides a summary of the references discussing the application of microporous layers on PEMFC diffusion media.

Table 2.3 - Summary of microporous layer recommendations.

Reference	Materials Used	Optimal hydrophobic polymer content	Optimal loading or thickness
Paganin [29]	PTFE and XC-72R	15 wt%	25 microns
Giorgi [30]	PTFE and XC-72R	10 wt%	1.25 mg XC-72R/cm^2
Jordan [31]	PTFE and acetylene black	none stated	1.25 mg total/cm^2
Song [9]	PTFE and XC-72R	30 wt%	3.5 mg total/cm^2
Henderson [28]	PTFE and XC-72R	10 wt% (optimal for performance)	1.5 mg total/cm^2
Henderson [28]	PTFE and XC-72R	33 wt% (optimal for adhesion)	1.5 mg total/cm^2
Kaviany [26]	analytical model	none stated	30% of thickness

2.4 GAS DIFFUSION MEDIA PROPERTY CHARACTERIZATION

There are a number of properties of gas diffusion media considered to be of importance to PEM fuel cell performance. The role of such properties in the PEMFC operating environment is described by Springer et al. [33]. The techniques associated with the ex-situ measurement of diffusion media properties are addressed thoroughly by Mathias et al [20]. Correlating these ex-situ properties and actual PEMFC performance are addressed by a variety of sources in more recent literature, most notably Williams et al [34], which will be discussed herein. Accurate measure of the diffusion media properties is essential to diffusion media development, as well as the development of correlations for use in PEMFC modeling.

The importance of gas diffusion media properties to the performance of PEMFC was addressed as early as 1996 by Springer et al. This paper utilizes impedance spectroscopy to determine which diffusion media properties have the greatest influence on the performance of PEM fuel cells. It is found that the porosity and tortuosity of the diffusion media both play a significant role, as well as effects attributed to limited permeability at higher current densities. The properties deemed important, as well as the relationships derived within this paper, have been used extensively in PEM modeling [35, 36]. Additionally, Springer stresses the importance of cell humidification. Humidification of varying cell components is closely linked to the hydrophobic content of the diffusion media. Likewise, permeability, porosity, and electrical conductivity, are closely linked to hydrophobic content due to the hydrophobic agent (typically PTFE) coating and/or filling pores within the media [20, 23, 24, 34].

The most complete work on gas diffusion media characterization was authored by Mathias et al. in the *Handbook of Fuel Cells-Fundamentals, Technology, and Applications* [20]. In this work, characterization methods for permeability, porosity, and conductivity are discussed in detail. Numerical values for these properties are also presented for some common PEM fuel cell gas diffusion materials. Although this work acknowledges the importance of diffusion layer characterization, it also notes that relatively few correlations existed at the time of publication, between ex-situ characterization results and in-situ performance.

Effective electrical conduction through the plane of the diffusion media is essential to ensure minimal losses in electrical potential between the reaction sites and the collector plates of the PEMFC. Due to the lack of a suitable standard, Mathias et al. proposed a method to characterize through-plane conductivity. The method involves the use of two parallel, high conductivity, non-corrosive blocks (i.e. graphite or gold) to apply pressure to the sample. The total resistance and applied pressure is recorded. Obviously, the measured value of resistance includes the contact resistance within the test fixture. In order to quantify the contact resistance, Mathias et al. propose measuring the resistance of various thicknesses of identically constructed material at a given pressure. Once these values are known, a plot of resistance versus thickness will identify the resistance at a thickness of zero; i.e. the total fixture contact resistance at the specified pressure.

Appropriate standards do exist for the measurement of in-plane conductivity of an isotropic porous media. The most common method is typically referred to as the four-point probe method, commonly referring to ASTM C611-98. Mathias et al. provide no unique characterization techniques for measuring in-plane conductivity of diffusion materials. However, it is noted that a typical carbon fiber paper used in PEMFC electrodes exhibits a resistivity an order of magnitude less in-plane than it does through-plane. The in-plane component of resistivity is most important for electron travel from the catalyst site under the gas channel to the land area of the collector plate. The in-plane electrical resistivity is also of importance for fuel cells which utilize lateral current collection [5, 6, 8, 18, 19, 37] .

Mathias et al. also discuss the characterization of diffusion material porosity. The simplest method discussed utilizes the uncompressed bulk density of the material ($\rho_{b,o}$), the density of the real (solid) phase of the material (ρ_r), the uncompressed thickness (d_o), and the compressed operating thickness (d), to arrive at an expression for the material porosity (ε).

$$\varepsilon = 1 - \left(\frac{\rho_{b,o}}{\rho_r} \right) \left(\frac{d_o}{d} \right) \tag{2.1}$$

The real phase density for carbon based diffusion materials is typically between 1.6 and 1.9 g/cm^3. Mathias et al. also argue that although many good methods are available to characterize the pore size distribution, some will yield poor results. This is attributed to the complexity of the porous network which is more difficult to characterize than a discrete set of pores. The most popular pore size measurement techniques are mercury porosimetry and capillary flow porosimetry. The mercury porosimetry method applies a pressurized column of mercury to a sample. The amount of mercury uptake at a given pressure can be attributed to the total volume for which a particular size of pore is responsible. The higher pressures correspond to small pores, while lower pressure mercury uptake corresponds to larger pores within the media. While mercury porosimetry forces a high surface tension fluid *into* pores under varying pressure, capillary flow porosimetry forces a low surface tension fluid *out* of pores under varying flow pressure. The first step in capillary flow porosimetry is to saturate the porous media with a low surface tension fluid such as Silwick™ silicon oil (20.1 dynes/cm). Following saturation, a gas pressure is applied across the media until flow breaks through for the first time. This presumably occurs through the largest pores, and the pressure at which this flow occurs is referred to as the bubble point. The flow pressure is then increased further causing progressively smaller pores to clear of the low surface tension fluid. The collected data can be used to plot the flow rate versus differential pressure for the initially saturated media. A similar plot can be generated for a dry sample of the material. The difference between the dry and wet curves can be used to deduce the pore size distribution within the media.

Gas permeability is another important parameter in the design of diffusion media for PEMFC. Permeability is sometimes expressed in units which are not based on fundamental physics, but rather based on testing standards developed years ago (i.e. Gurley seconds). Mathias et al. and others prefer a more fundamental approach to gas permeability characterization in diffusion media. Darcy's Law relates the pressure driven flux of a gas species to the pressure drop across the media.

$$Q = k_d \left(\frac{A}{\mu L_d} \right) \Delta P \tag{2.2}$$

In Darcy's Law, Q refers to the volumetric flow rate of the gas, k_d is the Darcy coefficient which is determined experimentally, A is the cross-sectional area through which the flow passes, μ is the viscosity of the gas, L_d is the length of the flow path through the media, and ΔP is the pressure differential across the media. The Darcy coefficient is typically expressed in the unit of Darcys, where 1 Darcy = 10^{-12} m^2. Additionally, it is reported that in-plane permeability is also of great interest for interdigitated flow fields.

Williams et al. [34] authored a paper titled, *Characterization of Gas Diffusion Layers for PEMFC*, in which they characterized a variety of commercially available diffusion materials as well as a material developed in-house. The purpose of this paper was to establish a relationship between ex-situ material properties and in-situ performance. A variety of material properties as well as performance related data were determined. Among the data compared was limiting current, in-plane electric resistivity, hydrophobicity, gas permeability, and pore size distribution. Electric resistivity measurements were performed using a four probe methods according to ASTM C611-98. Gas permeability coefficients were determined using Darcy's Law as described by Mathias et al. Pore size distribution was performed using mercury porosimetry, also described by Mathias et al. Overall porosity was calculated using the mercury porosimetry data, along with a method in which the media was saturated with decane (which fills hydrophobic and hydrophilic pores) and the wet weight was compared to the dry weight to establish the bulk material porosity. The most significant finding of this paper was the relationship between Darcy permeability coefficient and the limiting current density of the PEMFC. Experiments were run at a variety of cell temperatures and relative humidity's, and in each case, the limiting current increased linearly with increasing permeability coefficient. Williams et al. also state that although there is no direct relationship between pore size distribution and limiting current, there is an inherent relationship since pore size distribution affects permeability of the diffusion media.

2.5 CONTRIBUTIONS OF THIS WORK TO RIBBON STACK ADVANCEMENT

Improving the electrical properties of the GDL is paramount to the success of the fuel cell ribbon concept. Without a drastic reduction in the in-plane resistance of the GDL, a fuel cell ribbon would exhibit ohmic losses along the GDL so significant that the concept would be impractical even when the potential manufacturing cost reduction is considered. In addition to the electrical properties, other properties such as permeability and water transport must be considered. Characteristics of the GDL such as permeability and water transport are of diminished importance at low current levels (as observed in the literature) due to the lack of water production and need for reactants at the catalyst sites. But, as the resistive properties of the GDL are improved, the reactant and water transport properties of the GDL must also be enhanced to accommodate the increased water production and need for reactants.

Table 2.1 displays the performance achieved by a variety of scientists who fabricated alternative PEMFC stacks which utilize lateral current conduction. The performances referenced exhibit approximately only one-fifth of the performance attained by a conventional PEMFC stack operating on neat hydrogen and air at atmospheric pressure. The drop in performance is believed to be almost solely attributable to a lack of sufficient conductance of the diffusion media.

The work presented in this thesis aims to modify existing available diffusion materials or develop new diffusion materials capable of closing the gap which exists between the performance of conventional PEMFC stacks and laterally conducting PEMFC stacks. The ribbon GDL research was guided by analytical work to model the performance of a ribbon cell based on the electrical properties of the diffusion media.

3 MATHEMATICAL ANALYSIS

A variety of analytical methods were used to predict the theoretical limits for a fuel cell ribbon. Initially, a *simplified one dimensional mathematical model of the electrical conduction* along a fuel cell ribbon was derived in order to provide an estimate of the necessary in-plane electrical conductivity for which the fuel cell ribbon concept would be practical. Once the concept was deemed practical, the analysis was taken a step further to a *two dimensional finite element model of the electrical conduction* in the fuel cell ribbon. The finite element model provides an increased level of accuracy due to the elimination of many of the assumptions which are necessary for the one dimensional analysis. The rationale and methodology for these two models is discussed in this chapter.

Additionally, a variety of potential gas diffusion layer (GDL) fabrications were investigated. The determination of preferred GDL designs reflects both quantitative (e.g. property measurements), and qualitative (e.g. ease of fabrication) considerations. Particularly, the effects of fiber conductivity, fiber count, and binding and filling agents were investigated.

3.1 SIMPLIFIED MODEL OF FUEL CELL RIBBON PERFORMANCE

The purpose of the simplified fuel cell ribbon model is to provide an estimate for the necessary in-plane resistivity of the GDL, ρ_I, to achieve a specified loss in electrical potential. In addition, the simplified model provides a clear illustration of key features and a basis for comparison for more complex models. The assumptions and derivation of the one dimensional fuel cell ribbon model are detailed below.

3.1.1 Model assumptions

The following assumptions were used for the derivation of the simplified one dimensional fuel cell ribbon model:

- Steady state current generation

- No storage of charge within the GDL
- Same GDL material used on the anode and cathode
- Uniform current generation over the surface of the catalyzed membrane
- Infinite GDL conductivity perpendicular to the catalyzed membrane
- Absence of contact resistance at the GDL-catalyzed membrane interface

The first three assumptions are commonly accepted in most fuel cell models. The latter three assumptions are proven to be over simplifications of the electrical properties and conduction within fuel cell ribbons when further analysis is performed in this work.

3.1.2 Derivation of in-plane voltage drop for gas diffusion layer

Figure 3.1 is a diagram of an individual fuel cell ribbon consistent with the assumptions previously stated. The GDL on the anode and the cathode share identical values for their in-plane resistivity, ρ_I, while the through-plane resistivity for each GDL is assumed to be zero, effectively making the model one dimensional. The equal length arrows leaving the catalyzed membrane at the anode interface indicate a uniform current density, j, over the entire catalyzed area. Finally, the dimensions of the fuel cell ribbon are identified as the length of current travel in the x-direction, L, the width of the ribbon in the z-direction, w, and the thickness of each GDL in the y-direction, t.

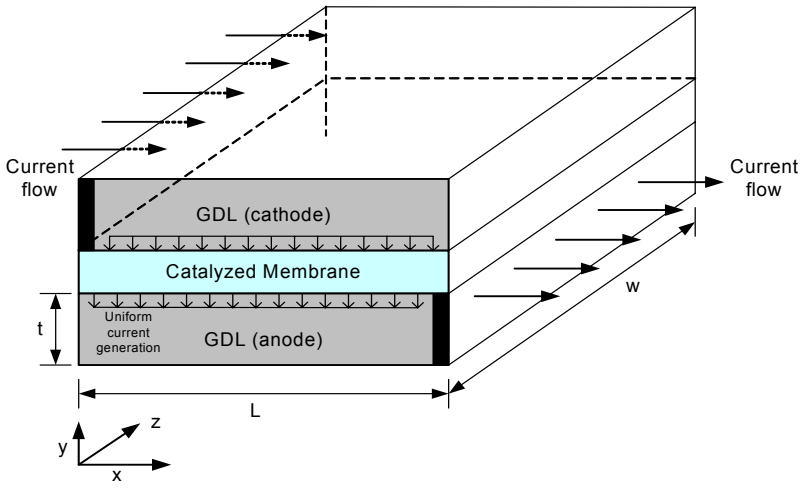

Figure 3.1 – Diagram of simplified fuel cell ribbon.

The potential losses in the cell as a function of the model variables were determined by a balance of charge transfer rate on a differential element of the fuel cell ribbon. Due to the symmetry that exists about the centerline of the membrane electrode assembly (MEA), only an analysis of the anode GDL was required to arrive at a relationship for the potential, φ, along the fuel cell ribbon. The resulting differential element and associated current flows can be seen in Figure 3.2.

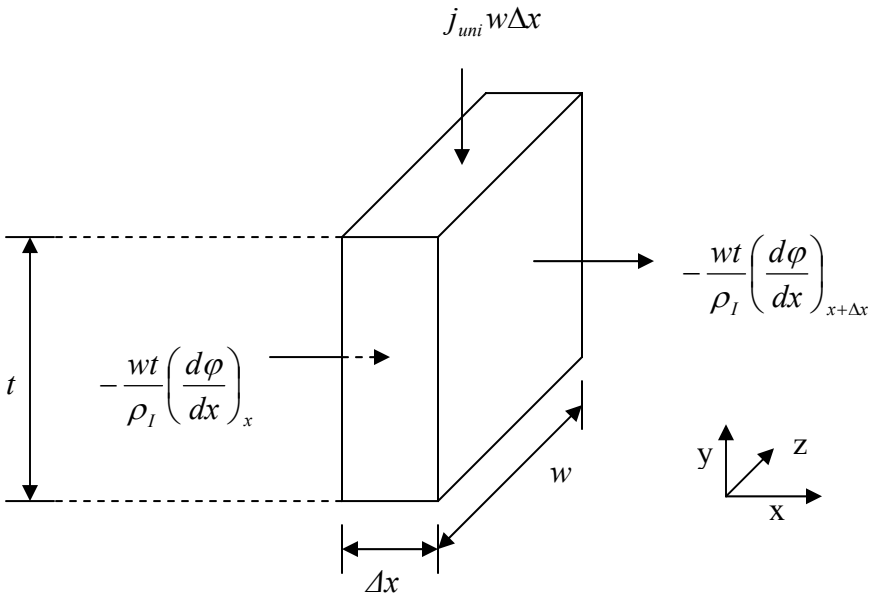

Figure 3.2 – Differential GDL element for derivation of 1-D fuel cell ribbon model.

A charge transfer rate balance yields:

$$\frac{wt}{\rho_I}\left[\left(\frac{d\varphi}{dx}\right)_{x+\Delta x} - \left(\frac{d\varphi}{dx}\right)_{x}\right] = -j_{uni} w\Delta x \qquad (3.1)$$

where the variable w (cm) represents the width of the fuel cell ribbon perpendicular to the direction of the potential gradient and parallel to the catalyzed membrane, t (cm) represents the thickness of the GDL measured perpendicular to the catalyzed membrane, ρ_I (Ω-cm) is the in-plane resistivity of the GDL, φ (V) is the electrical potential along the GDL, j_{uni} (A/cm^2) is the magnitude of the current density entering the GDL from the

catalyzed membrane, and Δx (cm) is the length of the differential GDL element parallel to the catalyzed membrane and parallel to the direction of the direction of the potential gradient. Taking the limit as $\Delta x \rightarrow 0$ yields the following second order differential equation:

$$\frac{d^2\varphi}{dx^2} = \frac{-\rho_I}{t} j_{uni} \tag{3.2}$$

In order to solve this equation two boundary conditions must be known. The first boundary condition states that the electric potential, φ, at $x = 0$, is equal to zero. This value is simply chosen to provide a reference point for the potential throughout the anode GDL. The second boundary condition which was used states that the potential gradient at the point $x = 0$ must be equal to zero. This condition exists because there is an absence of conductive media at the point $x = 0$ to carry current out of that end of the GDL. These two boundary conditions are stated in equation form below.

$$\varphi(x = 0) = 0 \tag{3.3}$$

$$\frac{d\varphi}{dx}(x = 0) = 0 \tag{3.4}$$

The second order differential equation along with the two boundary conditions was solved for an expression describing the potential in the anode GDL. This expression was evaluated at the position $x = L$ in order to determine the total potential drop across the length of the anode GDL of the simplified ribbon fuel cell. The total potential drop along the length of the anode GDL, $\Delta\varphi_{anode}$ is given by:

$$\Delta\varphi_{anode} = \frac{\rho_I}{2t} L^2 j_{uni} \tag{3.5}$$

where L (cm) is the length of the fuel cell ribbon in the direction of the potential gradient.

Due to the symmetry of the simplified fuel cell ribbon model, the total ribbon cell loss is simply twice the drop in the anode GDL. This relationship yields an expression for the total ohmic loss in both GDL's in a single fuel cell ribbon.

$$\Delta\varphi_{cell} = \frac{1}{t}\rho_I L^2 j_{uni} \tag{3.6}$$

3.1.3 Evaluation of the influence of ribbon characteristics

In order to characterize the effect of the parameters involved in equation 3.6, a current density, along with an acceptable value of potential loss in the cell were chosen. Typically a PEMFC operating at near atmospheric pressure, moderate humidity and temperature, and using air at the cathode will provide a potential of about 0.5 Volts at a current density of 1 A/cm^2. It was assumed that no more than a 20% decrease in cell power was acceptable due to the transition from a conventional PEM fuel cell to a ribbon cell. At a specified current density, a 20% drop in power corresponds to a 20% drop in cell voltage, or 0.1 V. Rearranging equation 3.6 yields an expression for ρ_I based on the allowable voltage drop, the GDL thickness, the ribbon length, and the current density of 1 A/cm^2 stated above.

$$\rho_I = \frac{\Delta\varphi_{cell} t}{L^2 j_{uni}} \tag{3.7}$$

By plotting ρ_I versus L, for varying GDL thicknesses, the influence of each parameter can quickly be seen. Figure 3.3 shows that for practical ribbon lengths of $L \geq 2$ cm, ρ_I must be less than 0.003 Ω-cm to meet the 20% loss goal, even for a GDL thickness as large as 0.1 cm. Currently, commonly used GDL materials exhibit resistivity values of approximately, $\rho_I = 0.015$ Ω-cm. Therefore, according to the one dimensional model a significant decrease (i.e. at least a five-fold decrease) in GDL in-plane resistivity is required to make the fuel cell ribbon concept feasible.

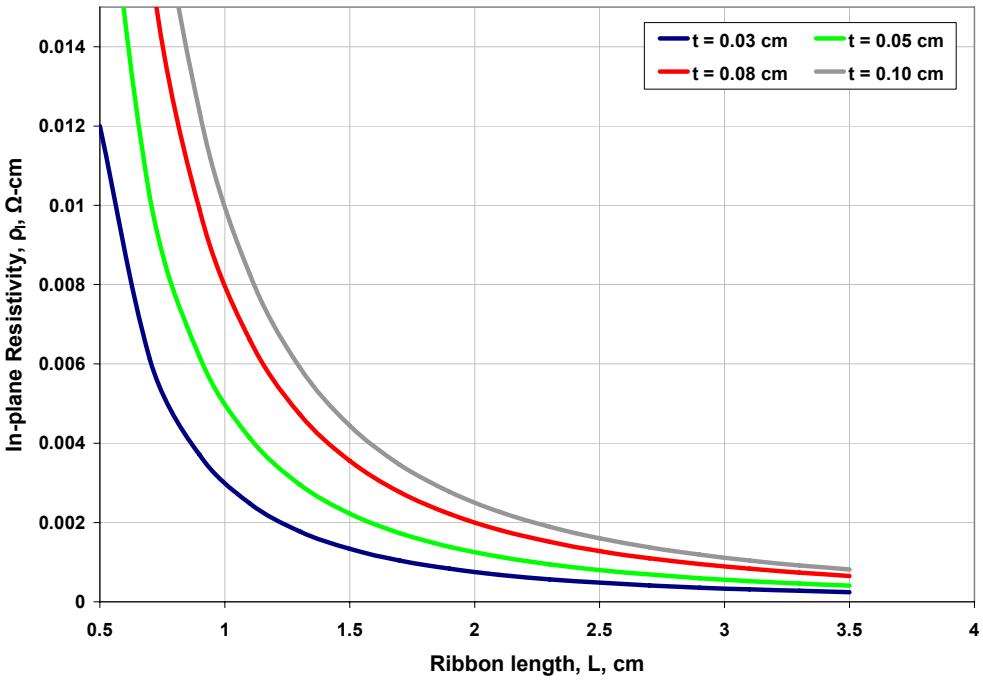

Figure 3.3 – In-plane resistivity required at a given ribbon length to limit potential drop to 0.1 V, at 1 A/cm^2 for varying GDL thicknesses.

3.2 TWO DIMENSIONAL MODEL OF FUEL CELL RIBBON PERFORMANCE

Although the one-dimensional model was useful for providing general trends and rough estimates of losses in the ribbon fuel cell arrangement, it was not complete enough to characterize the performance of a fuel cell ribbon prior to fabrication. The 1-D model lacked inclusion of variations in current density along the surface of the catalyzed membrane, and the effect of through-plane GDL resistance. Therefore, a two-dimensional model was developed based on the electrical properties of the GDL material. The two dimensional model takes the in-plane and through-plane resistivity of the GDL material into account, in contrast to the 1-D model which ignored the effects of current travel in the through-plane direction. The 2-D model was also useful for the determination of the optimum combination of physical dimensions and GDL material properties via a parametric study prior to experimental validation. The model was developed and implemented in FEMLAB® 3.1i developed by Comsol AB [38].

3.2.1 Model assumptions

The following assumptions were used for the development of the two dimensional finite element fuel cell ribbon model:

- Steady state current generation
- No storage of charge within the GDL
- Generation of current at a specific location on the surface of the anode catalyst layer is equal to the collection of current on the surface of the cathode catalyst layer at the adjacent location, (i.e. no in-plane ionic conduction within the membrane)
- GDL exhibits similar fuel and oxidant transport resistance in the ribbon configuration as it does in a conventional fuel cell configuration
- Resistive properties of the GDL can be sufficiently characterized by an experimental determination of the bulk in-plane resistivity (ρ_I) and the bulk through-plane resistivity (ρ_T) to construct an orthotropic conductivity tensor
- The current density at a given location on the anode catalyst is a function of the potential difference between that specific location, and the adjacent location on the cathode catalyst. Thus, the current density varies over the surface of the catalyzed membrane

3.2.2 Development of finite element model of the gas diffusion layer

As mentioned in the assumptions, this model can account for variation in the local current density along the catalyzed membrane surface. The local current density and local potential difference across the catalyzed membrane are very closely linked. An approximate correlation between local current density and local potential difference is based on data collected from a fuel cell operating in a conventional through-plane current collection test fixture. The voltage-current relationship observed in the conventional test is nearly uniform along the flow channel when operating at sufficiently large stoichiometric ratios [39]. The local voltage-current relationship should be nearly the same for a ribbon fuel cell using the same catalyzed membrane.

The geometry used for the 2-D finite element model, along with the associated subdomains and boundaries is presented in Figure 3.4. The catalyzed membrane is included as a boundary (boundary 4) rather than its own discrete subdomain. The thickness (y-direction) of the anode and cathode GDL's can be varied, along with the length of the ribbon cell (x-direction). Additionally, the anode and cathode GDL's are assigned identical orthotropic conductivity tensors, $\boldsymbol{\sigma}$, due to the fact that the same material will be used for each diffusion layer.

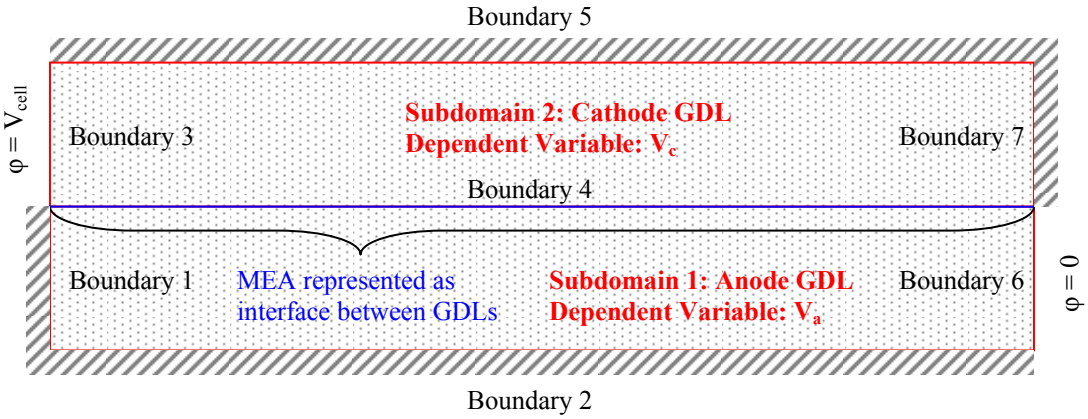

Figure 3.4 – Diagram of 2-D finite element ribbon cell geometry.

Prior to implementing a model, the material properties, and governing equations must first be established. The only material property required for this model is the orthotropic conductivity tensor, $\boldsymbol{\sigma}$. For this parameter, the resistivity in the in-plane (x) and through-plane (y) directions will be considered independently, thus resulting in a conductivity tensor in the form:

$$\boldsymbol{\sigma} = \begin{pmatrix} 1/\rho_I & 0 \\ 0 & 1/\rho_T \end{pmatrix} \tag{3.7}$$

where ρ_I is the in-plane resistivity and ρ_T is the through-plane resistivity.

Table 3.1 displays the equations governing the behavior within each subdomain, as well as the behavior at the boundaries of the geometry.

Table 3.1 – Subdomain and boundary equations for 2-D ribbon model.

Subdomain Settings			
Subdomain		**Dependent Variable**	**Governing Equation**
1 - Anode		V_a	$-\nabla \cdot (\sigma \nabla V_A) = 0$
2 - Cathode		V_c	$-\nabla \cdot (\sigma \nabla V_C) = 0$
Boundary Settings			
Boundary	**Subdomain**	**Type - (Description)**	**Governing Equation**
1	1	Neumann - (insulated)	$\vec{n} \cdot (\sigma \nabla V_A) = 0$
2	1	Neumann - (insulated)	$\vec{n} \cdot (\sigma \nabla V_A) = 0$
3	2	Dirichlet - (equipotential surface)	$V_C = V_{cell}$
4	2	Cathode - Inward current flux	$-\vec{n} \cdot (\sigma \nabla V_C) = j_{MEA}$
	1	Anode - Inward current flux	$-\vec{n} \cdot (\sigma \nabla V_A) = -j_{MEA}$
5	2	Neumann - (insulated)	$\vec{n} \cdot (\sigma \nabla V_C) = 0$
6	1	Dirichlet - (equipotential surface)	$V_A = 0$
7	2	Neumann - (insulated)	$\vec{n} \cdot (\sigma \nabla V_C) = 0$

The local current density along boundary 4, j_{MEA}, is given by:

$$j_{MEA} = A(V_C\text{-}V_A)^6 + B(V_C\text{-}V_A)^5 + C(V_C\text{-}V_A)^4 + D(V_C\text{-}V_A)^3 + E(V_C\text{-}V_A)^2 + F(V_C\text{-}V_A) + G \quad (3.8)$$

where the parameters A-G are determined by a curve fit to data for the catalyzed membrane that was measured using a conventional test fixture.

Ideally, the relationship between the local MEA potential difference (V_C-V_A) and the local current generation/collection (j_{MEA}) would be only a function of the catalyzed membrane characteristics. If this were the case, the same curve fit relating potential difference and current generation could be used for predicting the performance of the ribbon fuel cell for every diffusion media tested. A significant flaw with using the same

curve fit for all diffusion media is that each diffusion media type exhibits a different contact resistance at the catalyst-GDL, and the GDL-collector plate, interfaces. Therefore, in order to accurately predict the performance of a ribbon cell using a specific diffusion media, the performance of a conventional cell using the same diffusion media (and consequently similar interfacial resistances) must be established. *When using the finite element model for predictive purposes the local relationship between current density and potential difference was determined using a sixth order polynomial curve fit of previously collected data for our catalyzed membranes combined with the GDL of interest.* The predictions for specific diffusion media, in-house and commercially available, will be presented in Section 5.3.

In addition to predicting performance for specific GDL materials, the finite element model can also be used to conduct a parametric study to determine the best possible performance using a particular catalyzed membrane. This was accomplished by non-dimensionalizing the governing equations and solving the finite element model in terms of non-dimensional variable groupings. *When using the finite element model for the parametric study, the local relationship between current density and potential difference was determined using a polynomial curve fit of data collected for our catalyzed membranes combined with a high permeability, low through-plane resistance, reference GDL.* The following section presents the non-dimensional parametric study.

3.2.3 Parametric study of properties and dimensions

The goal of the parametric study of ribbon cell performance was to determine the combination of variable values which will yield the maximum possible fuel cell ribbon current for a specified cell potential. In order to determine the parameter groupings which would fully characterize the performance of a ribbon cell, the governing equations were first non-dimensionalized. The non-dimensionalization process yielded two variable clusters, one from the domain equations, and one from the boundary conditions, which determined the performance of the ribbon cell. Each of the dimensionless clusters of variables (Π parameters) was varied over reasonable ranges to provide a 3-dimensional map of performance as a function of the two Π parameters. The performance map

identifies the best performance and the necessary values of the Π parameters to achieve the best performance.

The parametric study and resulting performance map were based on the performance of a representative MEA. The sixth order polynomial used to relate the local current density to the local MEA potential difference in the parametric study was based on the data from the previously mentioned reference GDL with a standard catalyzed membrane operating in a conventional test fixture. The curve fit and associated coefficients are presented in Figure 3.5.

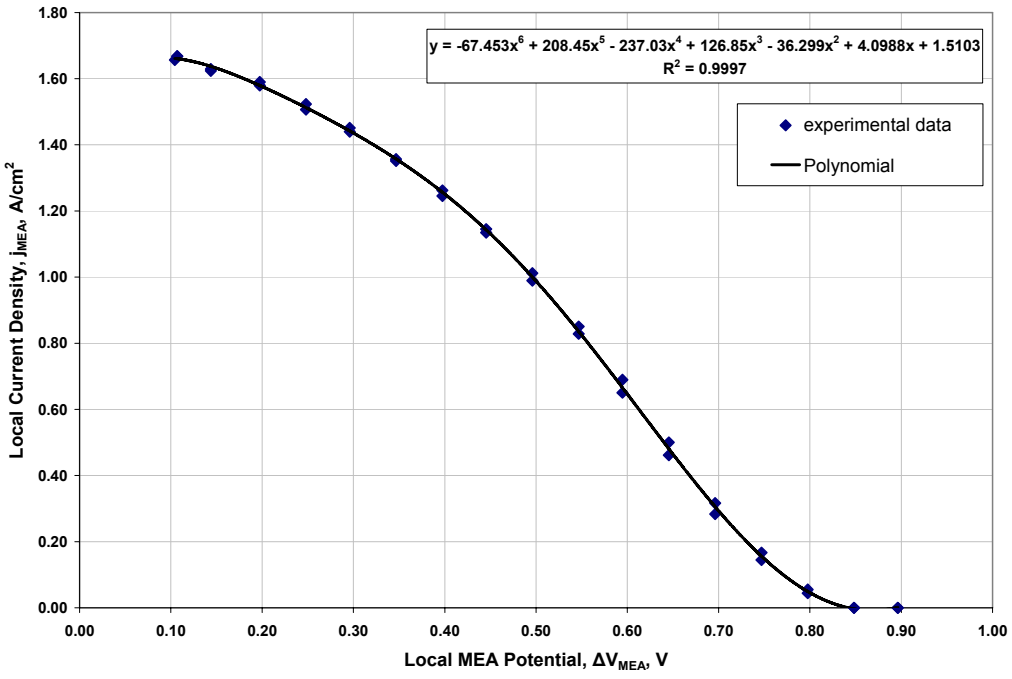

Figure 3.5 – Curve fit to relate local current density to local potential difference.

Equations 3.9-3.12b present the substitutions used to perform the non-dimensionalization for the subdomain and boundary condition equations. In these equations, x is the dimension along the plane of the GDL, L is the ribbon length in the x direction, y is the dimension through the thickness of the GDL, t is the GDL thickness, V_C is the local cathode GDL potential, V_{cell} is the output cell potential, i_{local} is the local current flux in the GDL traveling in the x direction, and j_{ref} is a reference value of local current flux based on the physical relationship between local potential difference across

the MEA and the local current generation at the MEA surface. The parametric study will be performed for an output cell potential of 0.5 V, therefore j_{ref} will be the average current density, 1.0 A/cm^2, achieved at 0.5 V in a conventional test fixture as shown in Figure 3.5 (this is based on the assumption of uniform current generation down the channel in a conventional test fixture). The capped variables in the following equations represent the dimensionless variables (e.g. $\hat{x}$ = dimensionless length) in the non-dimensional equations. The derivation of the Π parameters is based on the cathode subdomain and boundary condition equations. An identical result would be obtained if the same substitutions were performed on the anode equations.

$$x = \hat{x}L \tag{3.9}$$

$$y = \hat{y}t \tag{3.10}$$

$$V_C = \hat{V}_C V_{cell} \tag{3.11}$$

$$i_y = \hat{i}_y j_{ref} \tag{3.12a}$$

$$i_x = \hat{i}_x \left(\frac{j_{ref} L}{t} \right) \tag{3.12b}$$

The preceding relationships are generally self explanatory with the exception of the current scales in Equations 3.12a and 3.12b. The scale value for current density leaving the MEA is the current density in the conventional fixture, j_{ref}. Conservation of charge with an x-direction scale of L, and a y-direction scale of t, requires that the maximum x-direction current flux correspond to the value in parenthesis in Equation 3.12b.

The principle of conservation of charge applied to the entire gas diffusion layer domain yields a useful performance metric for the ribbon cell. In this formulation, the current leaving the current collector is the product of the average current flux over the

collector, $i_{cc,avg}$, and the collector area, t. This current must be equal to the integral of the current flux over the surface of the MEA:

$$i_{cc,avg} t = \int_0^L i_y dx = j_{ref} L \int_0^1 \hat{i}_y d\hat{x} \tag{3.13}$$

Rewriting Equation 3.13 in terms of the average non-dimensional current flux over the surface of the MEA, $\hat{j}_{avg}$, (where j is substituted for i to emphasize the distinction between current in general and current *at the MEA surface*) yields:

$$i_{cc,avg} t = j_{ref} L \hat{j}_{avg} \tag{3.14}$$

$$\hat{j}_{avg} = \frac{i_{cc,avg} t}{j_{ref} L} \tag{3.15}$$

In Equation 3.15 the denominator represents the total current which would be produced in a conventional test fixture, and the numerator represents the total current generated in the ribbon fuel cell. Equation 3.15 shows that the non-dimensional current averaged over the surface of the MEA, $\hat{j}_{avg}$, represents the ratio of the current produced in the fuel cell ribbon to the current produced if the fuel cell were operated in a conventional fixture. Thus, the value of $\hat{j}_{avg}$ represents a useful metric for the ribbon design.

The preceding scaling relationships (3.9-3.12) were substituted into the domain equation for the cathode GDL:

$$\frac{1}{\rho_I} \frac{\partial^2 V_C}{\partial x^2} + \frac{1}{\rho_T} \frac{\partial^2 V_C}{\partial y^2} = 0 \tag{3.16}$$

which resulted in:

$$\frac{\partial^2 \hat{V}_C}{\partial \hat{x}^2} + \frac{\rho_I}{\rho_T}\left(\frac{L}{t}\right)^2 \frac{\partial^2 \hat{V}_C}{\partial \hat{y}^2} = 0 \tag{3.17}$$

Therefore, the dimensionless variable Π_1 which corresponds to the product of the ratio of in-plane to through-plane resistance and the GDL aspect ratio is defined as:

$$\Pi_1 = \frac{\rho_I}{\rho_T}\left(\frac{L}{t}\right)^2 = \left(\frac{\rho_I L}{\rho_T t}\right)\left(\frac{L}{t}\right) \tag{3.18}$$

A similar substitution was performed for the cathode GDL boundary at which the current is collected. The governing equation for current flow at this boundary is:

$$i_x = \frac{1}{\rho_I}\frac{\partial V_C}{\partial x} \tag{3.19}$$

Substituting the scales from Equations 3.9, 3.11, and 3.12 yields:

$$\hat{i}_x = \frac{V_{cell} t}{\rho_I j_{ref} L^2}\frac{\partial \hat{V}_c}{\partial \hat{x}} \tag{3.20}$$

Therefore, the second Π parameter which corresponds to a dimensionless current flux is defined as:

$$\Pi_2 = \frac{V_{cell} t}{\rho_I j_{ref} L^2} \tag{3.21}$$

The values of Π_1 and Π_2 were varied within a reasonable range to arrive at the 3-dimensional performance map seen in Figure 3.6. This plot indicates that there are critical values for Π_1 and Π_2 at which the performance plateaus. The lower limits of the plateau region are approximately $\Pi_1 = 10$, and $\Pi_2 = 3$. Any further increase in these two values of

the Π parameters will provide relatively small increases in the ribbon cell performance. Figure 3.6 indicates that the ribbon cell performance at a specified voltage (here chosen to be 0.5 V) can be as high as 85% of the performance realized in a conventional current collection scheme at the same cell voltage.

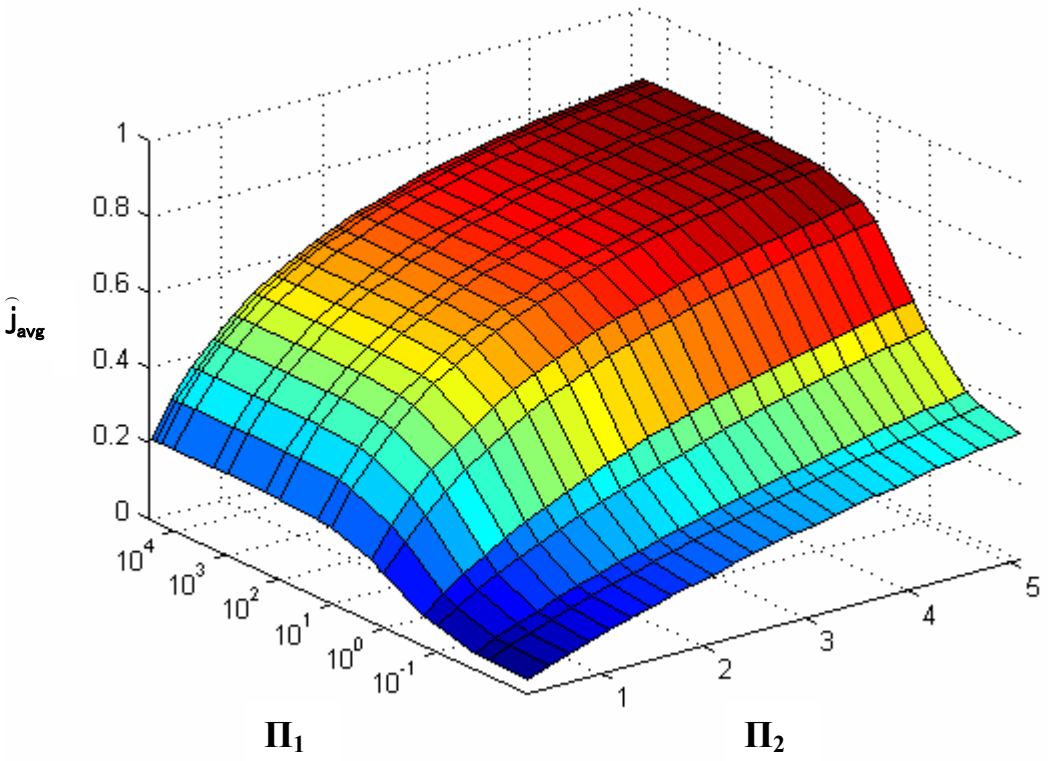

Figure 3.6 – Non-dimensional performance map for fuel cell ribbon.

Upon knowing the values of Π_1 and Π_2 that lead to peak performance, it is possible to consider the diffusion media characteristics that are required to achieve the values prescribed by the dimensionless analysis. The following section will discuss these characteristics in a qualitative and quantitative manner.

3.3 ANALYSIS OF GAS DIFFUSION LAYER PROPERTIES

A variety of variables exist in the construction of a porous carbon fiber material. Aside from the weave pattern, the most critical variables influencing diffusion media conductivity are the individual fiber conductivity; the number of fibers bundled together to form a tow; the amount and type of conductive filler in the interstitial space between fibers; and the effect that twisted tows can have on the through-plane conductivity.

The information obtained from the analysis and discussion of the aforementioned diffusion media construction variables was used to arrive at a set of ideal specifications for diffusion media for use in a fuel cell ribbon. Although it was possible to arrive at specifications for an ideal diffusion media, the actual manufacture of an ideal media is extremely difficult due to the fragility of high conductivity carbon fibers. For this reason, many of the materials actually presented in Chapter 5 vary significantly from the idealized diffusion media detailed in section 3.3.2.

3.3.1 Effect of fiber resistivity on bulk resistivity

The effect of fiber resistance in the in-plane direction was proven to be important in the 1-D analysis of section 3.1.3. The non-dimensional finite element analysis presented in the previous section shows how both in-plane and through-plane resistivity are important in the fuel cell ribbon architecture. It is important to be able to relate the material properties of individual carbon fibers to the bulk in-plane and through-plane resistive properties of the carbon fiber tows. It is typical for individual fiber properties such as axial fiber electrical resistivity to be reported by manufacturers, and sometimes even the axial tow electrical resistivity is reported, but no instance of a carbon fiber manufacturer reporting bulk radial electrical resistivity of a carbon fiber tow could be found. The bulk axial resistance of a carbon fiber tow is simply calculated by treating the bundle of fibers as a bundle of resistors in parallel and calculating an effective resistance of the tow as a whole. This can be done by applying the inverse additive property which exists for equal resistances in parallel. The axial resistance of a carbon fiber tow can be calculated according to equation 3.18:

$$\frac{1}{R_{tow}} = \left(\frac{n_{fibers}}{R_{fiber}} \right) \Rightarrow R_{tow} = \frac{R_{fiber}}{n_{fibers}} \tag{3.18}$$

where R_{tow} is the resistance (Ω) of a single tow, R_{fiber} is the resistance of a single fiber (Ω), and n_{fibers} is the number of fibers which make up the carbon fiber tow. Typically, since fibers are used in varying lengths, an actual fiber resistance is not reported by manufacturers, but instead a resistivity is reported. Therefore, in order to use the above equation, the resistance of an individual fiber of the desired length must be calculated according to:

$$R_{fiber} = \frac{\rho_{fiber} L_{fiber}}{\pi/4 \, D_{fiber}^{\,2}} \tag{3.19}$$

where ρ_{fiber} is the resistivity reported by the manufacturer (Ω-cm), L_{fiber} is the length to which the fibers are cut (cm), and D_{fiber} is the fiber diameters (cm).

Calculating the bulk radial resistance of a carbon fiber tow is not nearly as direct as the calculation of the bulk axial resistance of a fiber tow. Therefore, the calculation of bulk radial resistance requires the use of empirical methods based on research focused on a particular arrangement of conductive fibers. A model of this type requires significant experimental and analytical efforts and is beyond the scope of this work. Additionally, it has been suggested in the literature [40] that the contact resistance between the GDL and bipolar plate is 3-6 times the resistance of the GDL itself. Therefore, characterization of the bulk through-plane resistivity of gas diffusion media using an analytical model would be of little use since the contact resistance dominates in the through-plane direction of current travel.

3.3.2 Effect of tow size, carbon fill, and twisting on properties

A variety of factors other than fiber conductivity can affect the performance of the gas diffusion layer. Three factors which influence the quality of a GDL will be discussed

in a qualitative nature: tow size, conductive filler, and twisting of the carbon fiber tows prior to weaving.

Tow size of carbon fibers is typically designated by the number of continuous fibers axially aligned to form a tow. These tows are then subsequently woven to form the carbon based diffusion media. Typically for PAN based cloths, the tows are first twisted into yarns, while for pitch based cloth the tows are woven in an untwisted form due to their brittleness. The minimum tow size depends of the toughness of the fibers being used to form the tow. Weaker fibers require larger tow sizes to provide sufficient strength for processing and weaving, whereas stronger fibers can be processed using much smaller bundles of fibers. Therefore, PAN based carbon fibers can be configured into tows as small as a few hundred fibers, yet high conductivity pitch based carbon fibers are rarely configured in tows of less than 2,000 fibers. The size of the tows used to form the diffusion media has three major contributions to the final woven product. Figure 3.7 shows a cross-section of a plain weave commercially available GDL taken using scanning electron microscopy (SEM).

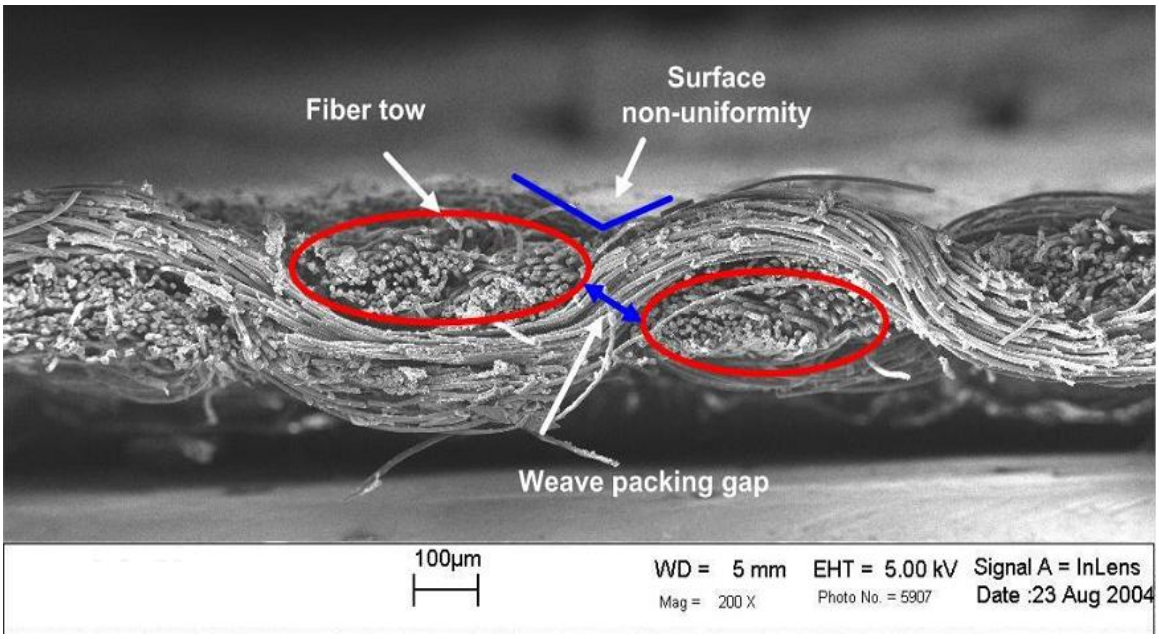

Figure 3.7 – SEM image of diffusion media detailing the effects of tow size.

Figure 3.7 illustrates that tow size affects the material thickness. By influencing the thickness of the material, the tow affects the rate of diffusion of the species through the diffusion media to the catalyst sites. The thickness of the GDL also directly affects the in-plane conductivity of the material if the material is treated as a homogeneous bulk. The tow size used in diffusion media also has a significant influence on the ability of tows to be packed tightly in the weave. It can be seen in Figure 3.7 that as the tow traveling in the plane of the diffusion media increases in size, that the tows circled in red become further apart. The weave packing gap causes a void of fibers oriented in the desired direction of electron flow, thus increasing the effective bulk in-plane resistivity of the material. Non-uniform in-plane resistivity of the GDL consequently means non-uniform current generation and heat generation which could cause hot spots along the catalyst layer and cause premature failure of the ionomer membrane. Perhaps the greatest effect that tow size has on GDL performance is on the uniformity of the surface at the GDL-catalyst interface. This effect is designated as surface non-uniformity in Figure 3.7. It can be seen that as the tow size increases, the depth of the cavity shown in blue becomes greater. Ideally the depth of the cavity would be very small in order to minimize the surface non-uniformities in the woven substrate. Therefore, in order to assure minimal surface contact resistance it is desirable to use fiber tows as small as possible which still provide ample strength and conductivity to the weave.

Application of conductive filler to the bulk of the diffusion media for the purpose of decreasing through-plane resistance has been supported in the literature [5]. It is believed that extremely small particles of conductive filler could decrease the interfacial resistance between fibers, thus providing greater conductivity in the radial direction of the tows. Figure 3.8 displays how the addition of conductive filler may aid in the contact among carbon fibers. Three fibers are present in the SEM micrograph and the proposed effect of conductive filler agglomerates is displayed. It can be seen that without the filler there is a gap between fibers in the absence of compression. Even when compression is applied, it is unlikely that the fibers will flatten enough to provide the desired intimacy of contact. Therefore, qualitatively, the addition of conductive filler such as carbon black (~30 nm diameter) provides an increased area of contact among fibers and will increase through-plane conductivity of the carbon fiber tows. The conductive filler drawn in

Figure 3.11 is approximately the size of Cabot Vulcan XC-72R oil furnace black. This is the same type of carbon black that is commonly used in microporous layers, and as a support structure for platinum catalyst.

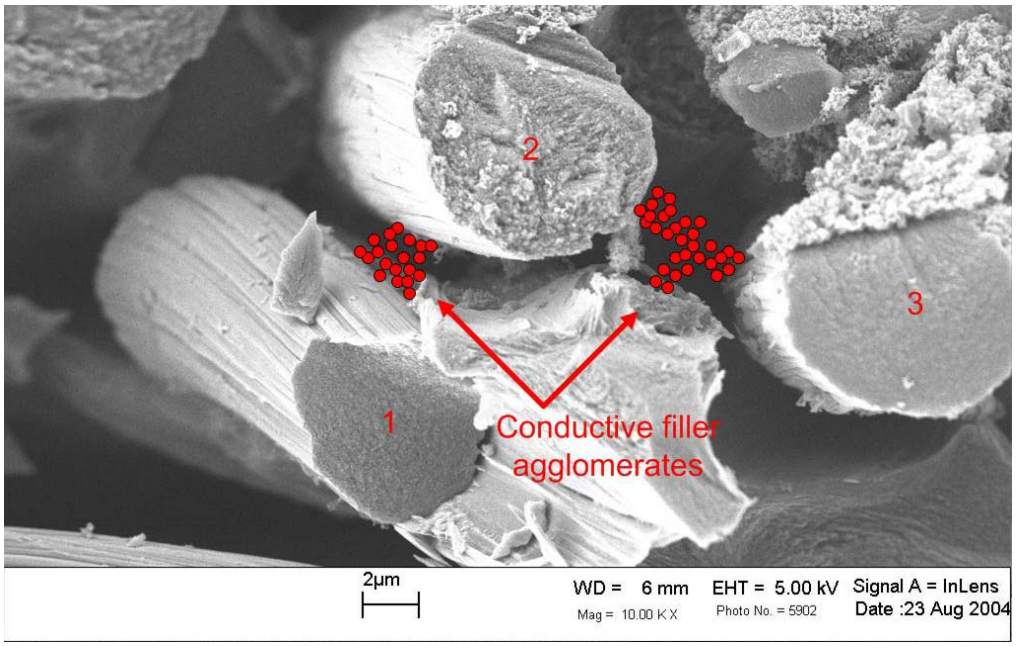

Figure 3.8 – Possible effect of added conductive filler agglomerates.

The conductive properties of a woven carbon fiber material could also be influenced by twisting the tows being used to construct the weave. Twisting the tows effectively reduces the need for radial conductivity from fiber to fiber. This occurs because the current will travel along the length of the twisted fibers therefore causing more of the bulk to be utilized since more fibers can come in direct contact with the catalyst layer if a twist is introduced. Figure 3.9 shows graphically how this can occur by showing a bundle of four fibers, each of which comes in contact with the lower boundary plane (the catalyst layer) at a different point along the length of the tow. If no twist were present, only the fibers that are in contact with the lower boundary plane at the far left end of the tow would ever come in contact with the catalyst layer. Therefore, twisted carbon fiber tows are more desirable for the construction of diffusion media. But, in order to have significant effect it is necessary for the tows to be twisted sufficiently for the tows to be of uniform diameter and have sufficient revolutions per length to utilize all fibers

around the circumference of the tow before the termination of the ribbon cell. Due to the fragility of some carbon fibers it is difficult to introduce sufficient twisting without fracturing the fibers.

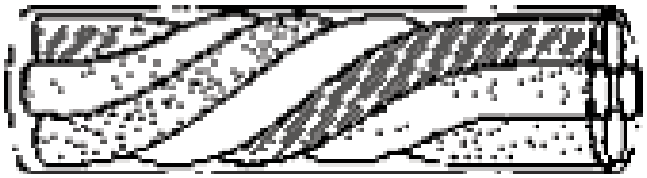

Figure 3.9 – Diagram of twisted carbon fiber tow [10].

3.3.3 Summary of preferred diffusion media characteristics

The preceding sections detailed the requirements and characteristics of diffusion media which would make a successful fuel cell ribbon. It was first determined that the bulk in-plane conductivity of a fiber tow varies according to the additive inverse law applied to electrical resistors in parallel. Therefore, *a large number of fibers oriented in the direction of current flow is a desirable characteristic.* The derived relationship is a useful tool for determining the number of properly oriented fibers needed to achieve the desired bulk in-plane conductivity following the determination of the desired Π parameter values and dimensions of the ribbon fuel cell. Additionally, it was determined that small fiber bundles are preferred, but that fiber strength is a limiting factor in the reduction of tow size. Therefore, *the smallest commercially available tows are the preferred material* for the construction of diffusion media in this work. It was also speculated that *the addition of conductive filler within the woven carbon fiber material may substantially reduce the through-plane resistance of carbon fiber tows*, although it could also reduce the porosity of the diffusion media causing negative effects on the ability of the material to transport gases. Finally, it was determined that *twisted carbon fiber tows could increase the utilization of fibers for conduction in the axial direction due to the increased number of fibers which would come in contact with the catalyst layer.* Thus, twisted tows could effectively reduce in-plane resistivity due to increased axial fiber utilization, and increase through-plane conductivity due to the spiraling effect of

moving the fiber from the catalyst surface up to the outer surface of the fuel cell ribbon. Thus, on the basis of electrical resistivity, the ideal gas diffusion media would appear to consist of a large number of low resistivity fibers arranged in small tows, likely containing carbon fill, and which utilizes twisted yarns to improve fiber utilization.

It is important to note that although it is possible to arrive at idealized criterion for the design of a diffusion media, that idealized designs are rarely possible or practical. Therefore, these design criteria will be used as guidance for the selection of diffusion media material and not as absolute requirements. The following chapter will deal with the determination of material properties for diffusion media. Chapter 5 will introduce the actual diffusion media tested in this work along with the experimental results obtained.

4 EXPERIMENTAL PROCEDURES

Chapter 2 discussed the important properties and treatments commonly used for fuel cell gas diffusion media. Chapter 3 introduced 1-D and 2-D models that relate fuel cell performance to the electrical properties of the GDL. In addition, Chapter 3 discussed some of the important characteristics of the carbon fiber substrate which will aid in achieving high performance ribbon fuel cells. This chapter will first discuss the carbon fiber substrate materials used in the fabrication of the gas diffusion media presented in this work. The substrates used in this work were commercially available carbon cloth's which were modified by applying bulk treatments and a microporous layer (MPL) on the surface of the cloths. The specifications for the application of bulk treatments to the substrate (i.e. hydrophobic polymer), and for the application of a microporous layer (MPL) to the substrate will be detailed in this chapter. The achieved loading of the treatments applied to the substrates will be presented in Chapter 5.

This chapter will also detail the methods and test apparatus' used to characterize three important properties of the fabricated diffusion materials: in-plane resistivity, through-plane resistivity, and Darcy air permeability. The results obtained from the material characterization methods will also be presented in Chapter 5. Finally, the results of the performance characterization for each GDL will be presented in Chapter 5.

4.1 FABRICATION OF GAS DIFFUSION MEDIA

The fabrication of cloth based diffusion media has many variables which influence the media's gas permeability, in-plane and through-plane electrical resistivity, and contact quality with the membrane electrode assembly (MEA). The main variables which influence these properties are the weave style, the fiber count in each yarn used to construct the weave, and the fiber conductivity. Each diffusion media is unique and the materials considered in this work will be presented in this section.

4.1.1 Commercially available gas diffusion media (ELAT)

The baseline for all experiments performed in this work will be ELAT® LT-1200W distributed by E-tek Inc. The basic construction of this diffusion media consists of twisted dual tow yarns of approximately 200 PAN based carbon fibers per tow, arranged in a plain weave. Thus, this material had two of the desirable characteristics (small tows and twisted yarns) identified for diffusion media. This construction yielded a cloth thickness of approximately 320 µm and an in-plane fiber density of approximately 19 yarns/cm in both directions. A proprietary amount of hydrophobic filler (likely PTFE) is applied to the bulk material to aid in gas and water transport. Additionally, an MPL composed of approximately 40% PTFE and 60% carbon black (type unknown) is applied at a thickness ranging between 100-120 µm to provide a smooth surface for catalyst layer contact, and to reduce interfacial resistance. Since this material comes with optimized proprietary treatments from the manufacturer, there is no need for the application of additional treatments. An SEM micrograph of a cross-section of the ELAT LT-1200W material can be seen in Figure 4.1. This figure is presented to illustrate the difference between the woven base, and the MPL in fuel cell gas diffusion media. The ELAT LT-1200W material will simply be referred to as ELAT throughout the remainder of this work.

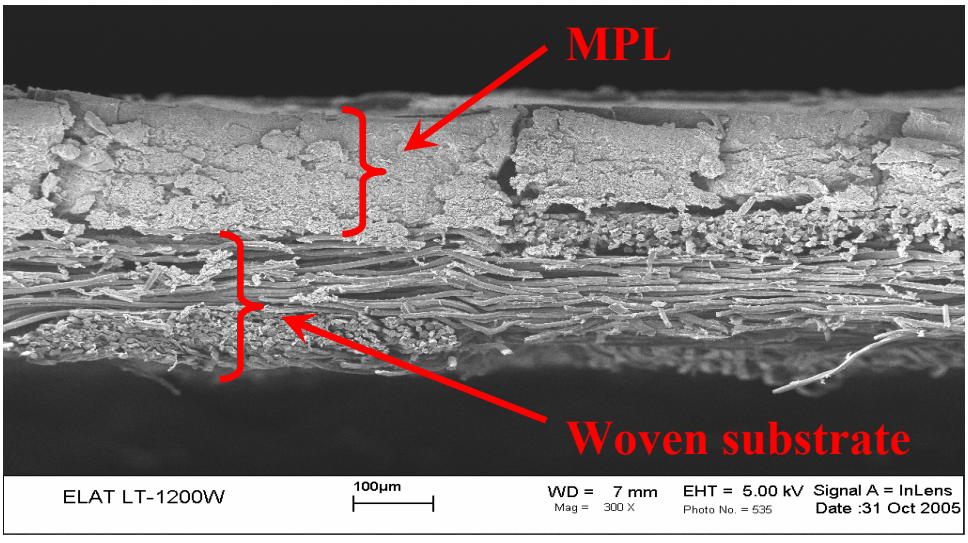

Figure 4.1 – SEM micrograph of ELAT gas diffusion media.

4.1.2 Increased thickness PAN based carbon cloth (ITPN)

In order to achieve lower in-plane resistance it is possible to increase the thickness and fiber density (fibers/cm) of the woven structure by using larger PAN based yarns, rather than changing the type of carbon fibers used. This was the logic employed when using what will be referred to as the increased thickness PAN (ITPN) based carbon cloth series of diffusion media. The ITPN woven carbon cloth is constructed of twisted carbon fiber yarns containing 6 tows, with each tow being made up of approximately 200 PAN based carbon fibers. Due to the increased size of the yarns used in the ITPN material compared to ELAT, the ITPN material is approximately 2-3 times the thickness of the woven structure used in ELAT. The other distinguishing characteristic of the ITPN material is the 5-harness satin weave (5HS) which is used to arrange the warp and fill yarns. The 5HS weave allows for the yarns to be in direct contact with the catalyst layer over a greater area than they would be in a plain weave, thus improving the contact between the fibers and the catalyst layer in the current carrying direction. On the other hand, the 5HS weave also reduces the number of times each yarn alternates between the top and bottom of the woven structure which could increase the through-plane resistance of the woven structure. The ITPN material was purchased in an untreated form from E-tek Inc. An SEM micrograph of the woven structure of the ITPN woven base material can be seen in Figure 4.2.

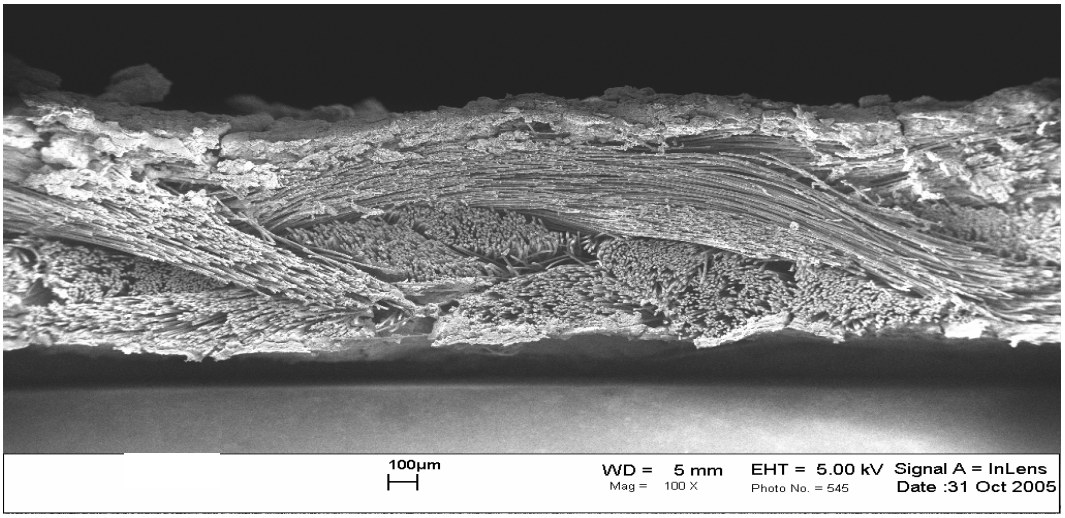

Figure 4.2 – SEM micrograph of woven ITPN material.

4.1.3 Coarsely woven pitch based carbon cloth (CWPT)

Another method for decreasing in-plane resistance is to use graphitized mesophase pitch fibers instead of the more common PAN based fibers used in most PEMFC gas diffusion media. Unfortunately, due to the fragility of graphitized high conductivity mesophase pitch based carbon fibers, these fibers are only available in tows of 1000 fibers or more. The added number of fibers in each tow causes materials constructed of woven pitch based fibers to have a very coarse structure in comparison to the woven structure achieved when PAN based yarns are used. The detrimental effects of a coarse structure in a PEMFC gas diffusion media include increased surface non-uniformity, which leads to higher interfacial resistances; and poorly developed pore structure, which can hinder effective water transport. Thus, with this material the desire for small twisted tows is compromised in favor of the need for low resistivity fibers. Nonetheless, the drastic decrease in fiber resistance makes pitch based carbon cloths an interesting candidate for use in the fuel cell ribbon architecture.

The coarsely woven pitch (CWPT) based carbon cloth used in this work was acquired from Mitsubishi Chemical of America Inc. of Chesapeake, VA. The woven material comes with a 2% epoxy sizing which was removed by heat treatment prior to further use. The CWPT material is not comprised of yarns but is rather constructed of single tows of 2000 fibers each. The reason for weaving tows rather than yarns is because pitch based carbon fiber tows are nearly impossible to twist into yarns due to the brittle nature of the high conductivity pitch fibers in comparison to PAN based carbon fibers. The weave construction of the CWPT material is a 2-by-1 twill, which is essentially a 3 harness satin (3HS) weave where the fill tows will pass over the top of two warp tows prior to passing under a single warp tow. Figure 4.3 displays an SEM micrograph of a section of the CWPT material which shows a single fill tow passing under a warp tow.

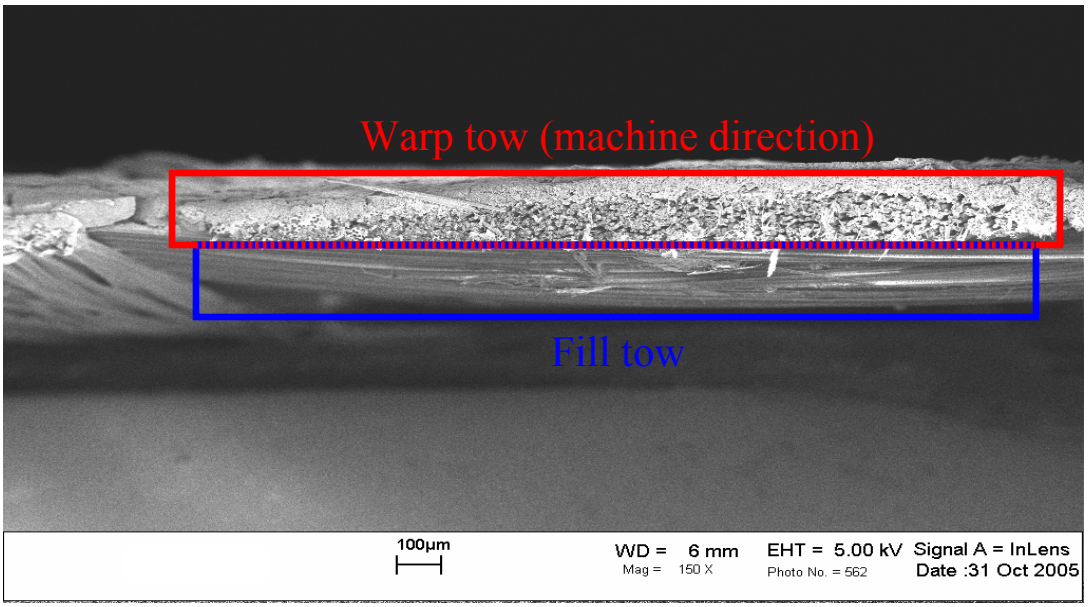

Figure 4.3 – SEM micrograph of woven CWPT material.

4.2 BULK TREATMENT OF GAS DIFFUSION MEDIA

Section 2.2.2 discussed the prevailing opinion in the literature that adding hydrophobic polymer to the bulk structure of the gas diffusion media enhances its water and gas transport characteristics. The ELAT material was supplied with a hydrophobic treatment already applied. For ITPN and the CWPT gas diffusion materials, bulk treatments were applied to the substrate. Each of the diffusion materials were treated in two different manners, creating a total of four in-house gas diffusers. Treatment A consisted of only PTFE in order to increase the hydrophobicity of the material. Treatment B consisted of PTFE and carbon black, where the carbon black was expected to reduce the bulk resistivity, and in particular the through-plane resistivity, of the material as suggested by Heinzel [5], and the PTFE was included to make the material hydrophobic.

A homogenous suspension of DuPont Teflon® (PTFE) was used in this work for the hydrophobic treatments of the diffusion media. The PTFE content in each diffusion material was based on the original untreated mass of the diffusion media. Most of the literature related to gas diffusion materials prescribe a hydrophobic polymer content consisting of 15-30 % of the final mass of the treated material. This work will reference all treatments to the untreated mass of the diffusion media substrate due to the fact that

two different treatments are being considered, causing the untreated mass to be a more useful point of reference. A mass of PTFE equal to 25% of the untreated diffusion media mass will be added to each substrate material for both treatments A and B. This value corresponds to 20% of the final mass when no other constituents are applied (Treatment A), thus resulting in a value within the range observed in the literature.

Treatment B also consists of the addition of PTFE equal to 25% of the untreated substrate mass, but further includes the addition of carbon black in an attempt to decrease the bulk through-plane resistivity of the diffusion media. Mathias et al. [20] state that the typical pore volume of carbon cloth materials is approximately 70% or greater. Due to the need for high permeability of the carbon cloth substrate, it was considered acceptable to fill a maximum of 20% of the total pore volume within the diffusion media. Assuming similar densities for the PTFE, carbon black, and carbon fibers, 20% of the pore volume would be filled if the added filler mass was 47% of the untreated mass of the woven material. A value of 40% of the untreated mass was chosen for the total mass of the PTFE and carbon black treatments combined, where 62.5% of the added mass is PTFE, and 37.5% is Vulcan® XC-72R carbon black. Therefore, treatment B consists of adding a mass of PTFE equal to 25% of the untreated mass (identical mass of PTFE per unit volume as treatment A), and a mass of carbon black equal to 15% of the untreated mass.

The application of each treatment required soaking the untreated woven cloths in the appropriate treatment. Each diffusion media substrate was first weighed, soaked in either treatment A or B, dried at 140°C for approximately 30 minutes to evaporate the isopropyl alcohol and/or de-ionized water, then weighed again to determine the added mass of the treatment. This process was repeated until the desired addition of mass was achieved. The mass addition was controlled by the level of treatment dilution, and the time the materials were allowed to soak. Following the addition of the desired mass, the diffusion media materials were heat treated at 180°C for 30 minutes, 280°C for 30 minutes, and then sintered at 350°C for 30 minutes according to the process observed in the literature [20, 29, 30].

The concentrations of the mixture used for each bulk treatment required significant adjustment to achieve successful treatment application. It was found that soaking each diffusion media for approximately 1 minute in a 5-10 wt% PTFE

suspension in de-ionized water was most suitable for treatment A. A 10% PTFE suspension was used for the CWPT material, while a 5% PTFE suspension was used for the ITPN material since the higher porosity of the ITPN material allowed for more of the suspension to be absorbed. The soaking process for treatment A in the proper concentration only needed to be performed once for each material.

The mixture used to apply treatment B was made by dispersing PTFE and carbon black particles in isopropyl alcohol (IPA), followed by ultrasonic agitation. The amount of IPA required to sufficiently suspend the carbon black was approximately 50 times the mass of the PTFE. The greater dilution of this mixture required longer soaking times for the application of treatment B. The desired mass was achieved by soaking the diffusion media in the carbon black/PTFE/IPA suspension for approximately 5 minutes, followed by drying at 140°C. The soaking process typically had to be repeated 4-6 times to achieve the desired addition of mass due to the low concentration of PTFE and carbon black.

4.3 APPLICATION OF THE MICROPOROUS LAYER

The literature related to the application of a microporous layer (MPL) on gas diffusion materials indicates that a MPL consisting of PTFE and carbon black enhances the performance of PEM fuel cells. It is believed that a thick MPL with high PTFE content will provide a smooth and compatible interface for adhesion of the gas diffusion layer to the catalyst later in a PEM fuel cell. This adhesion is critical in the ribbon stack arrangement. Yet, it is also expected that a thin MPL consisting primarily of carbon black would provide the lowest achievable bulk through-plane resistance of the MPL. The through-plane resistance of the MPL could have an effect in fuel cell ribbons, but the in-plane resistance is not expected to impact performance since the layer is very thin relative to the low resistivity substrate materials required for GDLs in fuel cell ribbons. Chapter 2 indicates that 10-30% PTFE in the MPL provided the best performance in PEMFCs. Experiments reported in the literature suggest that a total MPL loading of approximately 1.25-3.0 mg/cm^2 is desirable [9, 28, 30, 31]. Additionally, the literature indicates by analytical methods that a loading which makes up one third of the total thickness of the diffusion media is most desirable for water management within the GDL of PEMFCs

[26]. Previous work performed at the Energy Systems Laboratory at Virginia Tech indicates that an MPL consisting of 90 wt% carbon black and 10 wt% PTFE has sufficient adhesion ability and provides suitable performance in PEMFCs [28]. Therefore, in this work an MPL consisting of 90 wt% Vulcan® XC-72R oil furnace carbon black manufactured by Cabot Corp., and 10 wt% PTFE manufactured by DuPont under the trade name Teflon-30®, will be applied to the ITPN and the CWPT materials prior to adhering the diffusion materials to an MEA. The ELAT material is supplied with a MPL already in place.

A variety of methods of MPL application are suggested in the literature including spraying [30, 41, 42], screen printing [41, 42], brushing [31], rolling [41], tape casting [22], and vacuum filtering [29]. Careful consideration of the material to which the MPL is applied is necessary to determine the method of application that is most suitable. Due to the significant differences in the woven structure of the ITPN and the CWPT substrates, a different method of application will be used for each material. The MPL specifications for each material are detailed below.

The ITPN material has a very smooth surface due to the small twisted yarns used to construct the weave, and the 5HS weave pattern used to fabricate the cloth. Due to the smooth surface, a relatively thin MPL should be sufficient to provide ample water management and low interfacial resistance. Additionally, since the surface is already smooth, application of the MPL using an airbrush will provide a uniformly thick and smooth surface which can be adhered to the MEA. The target MPL loading for the ITPN material will be 1.5 mg/cm^2 in accordance with the surveyed literature. The MPL will be sprayed onto the ITPN material using an airbrush due to the simplicity and uniform thickness associated with this method of application.

Application of an MPL using an airbrush provides an MPL of uniform thickness and loading. A uniform thickness is desirable if the material to which the MPL is applied being has a smooth surface such as the ITPN cloth. But, application of a uniformly thick MPL to a material with an uneven surface simply results in a MPL which follows the surface contours. Due to the uneven surface of the CWPT material, application of a MPL using an airbrush is undesirable. Therefore the MPL was applied to the CWPT material using a tape casting technique. The advantage to the tape casting technique is that instead

of applying a uniform thickness, it applies a layer which has a smooth surface and fills in the contours of the surface to which it is applied. Due to the surface contours of the CWPT material it is difficult to specify a certain MPL loading since it varies from point to point on the diffusion media. Instead, an MPL which was one half the average thickness of the CWPT material was applied in order to achieve the desired MPL thickness of one third of the total thickness as suggested by Nam and Kaviany [26].

A mixture of 10 wt% PTFE and 90 wt% Vulcan XC-72R carbon black was homogeneously suspended in isopropyl alcohol to create the ink required for the MPL application. To achieve this suspension the PTFE was first mixed with the IPA in a ratio of 1 part PTFE to 300 parts IPA by mass. The 300:1 ratio provided ample dilution to accommodate the suspension of the carbon black within the mixture. When the MPL was applied using an airbrush (ITPN substrate), the MPL ink was used in the freshly prepared state. In order to tape cast the MPL (CWPT substrate), the mixture needed to be made more viscous. This was achieved by allowing the MPL ink to dry out until enough IPA had evaporated to achieve a viscosity similar to paste.

For the ITPN material the ink was applied by using an airbrush with an adjustable air/ink ratio to increase or decrease the flow rate and atomization of the ink at the nozzle exit. The optimal settings on the airbrush were determined in a previous work by analysis of the MPL surface and cross section using scanning electron microscopy (SEM) [28]. Prior to applying MPL ink or paste onto the diffusion media, the thickness of the media was measured using an electronic digital caliper, and the mass was recorded using a digital scale. Following the MPL application the diffusion media was dried at 140°C to evaporate the IPA, and subsequently measured and weighed. This process was performed once for the tape cast MPL, and multiple times for the MPL applied using the airbrush until the desired loading was achieved. Once the MPL application was completed, the diffusion media was heat treated at 140°C for 30 minutes, 280°C for 30 minutes, and sintered at 350°C for 30 minutes, in order to thoroughly dry the layer and sinter the PTFE particles.

4.4 SUMMARY OF GAS DIFFUSION MEDIA CHARACTERISTICS

The targeted values for the treatments discussed were obviously not met to an exact degree. The treatment levels actually achieved, as well as some important characteristics of the gas diffusion media substrates discussed previously will be presented in this section. The properties of the substrate material are summarized in Table 4.1, and the characteristics of the completed gas diffusion material used in this work are summarized in Table 4.2.

Table 4.1 – Summary of diffusion media substrate characteristics.

Substrate material	Tow size (# of fibers)	Yarn construction	Fiber density (yarns/cm)	Thickness (μm)
ELAT	200	2 ply - twisted	19	300
ITPN	200	6 ply - twisted	15	600
CWPT	2000	single ply - no twist	4.5	380

Table 4.2 – Summary of treated gas diffusion media characteristics.

Diffusion media designation	Actual added bulk treatment (% original mass)	Actual MPL loading (mg/cm^2)	Approximate MPL thickness (μm)	Final treated thickness (μm)
ELAT	unknown	unknown	110	410
ITPN-A	30	1.7	50	950
ITPN-B	46	1.6	50	1050
CWPT-A	24	4.3	180	550
CWPT-B	38	4.3	180	620

4.5 EVALUATION OF GAS DIFFUSION MEDIA PROPERTIES

Chapter 2 discussed the literature pertaining to the properties that have the greatest influence on diffusion media performance in a PEM fuel cell. In this work, the bulk in-plane resistivity and the through-plane area specific resistance were measured in order to evaluate a variety GDL materials (many of which were immediately discarded as

candidates for the fuel cell ribbon architecture) and to provide critical parameter data for the finite element model discussed in the previous chapter. Additionally, the air permeability of each diffusion media was evaluated. The air permeability measurements reveal how the gas diffusion materials fabricated for fuel cell ribbons compare to commercially available materials, which are considered sufficient diffusers in conventional PEM fuel cells. The permeability of the fabricated diffusion media was also important to measure so that the effect of the added carbon black in Treatment B could be evaluated. The permeability information will not be used in the modeling efforts at this time, but will likely be utilized in future research.

4.5.1 In-plane resistance

The in-plane resistance of the gas diffusion media was measured using a four edge system according to ASTM C611-98. The four edge method is ideal for low resistance materials because it eliminates the effect of the fixture and lead resistances. Figure 4.4 shows the fixture fabricated to measure the in-plane resistance of the diffusion materials used in this work.

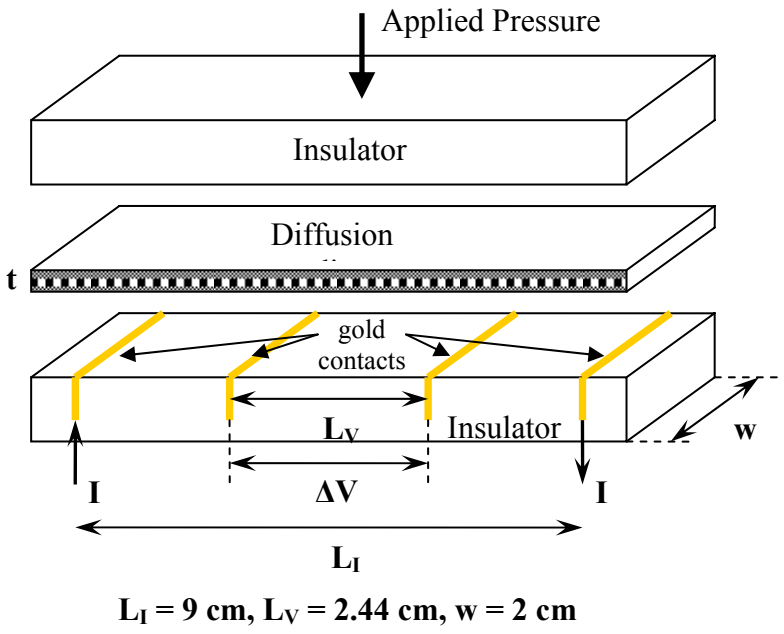

Figure 4.4 - Diagram of in-plane resistance measurement fixture.

In order to find the in-plane resistance of the diffusion media, current was passed through the media between the two contacts near the ends of the sample. The corresponding voltage drop was measured between two interior contacts. According to Ohm's law the resistance between the two interior contacts is equal to the voltage drop measured, divided by the applied current. In order to be able to compare diffusion materials with varying thickness, a thickness specific resistivity, ρ_I/t, was used as the performance metric as described by Mathias [20].

$$\frac{\rho_I}{t} = \frac{Rw}{L_V} \tag{4.1}$$

where ρ_I is the bulk resistivity of the media (Ω-cm), L_V is the length between the voltage measurement points (cm), R is the resistance calculated between the voltage contact points (Ω), t is the thickness of the diffusion media (cm), and w is the width of the diffusion media (cm). The quotient ρ_I/t can be expressed in units of Ω/square since the ratio L_V/w is essentially a measure of how many square units of diffusion media are lined up along the direction of current flow.

It is believed that the in-plane resistance of the diffusion media should have very little variation with the applied pressure on the test fixture since current likely only travels along fibers oriented in the preferred direction. Additionally, the true thickness of the diffusion material also changes with increased pressure, but is not possible to measure using the fixture in Figure 4.4. The in-plane resistance of the diffusion media was measured at many different fixture pressures to confirm that the resistance was not thickness or pressure dependent. It should be noted that with this technique, the effect of contact resistance is small and the measured value is a true property of the material. The results in Chapter 5 confirm that very little variation in resistance with applied pressure was measured.

4.5.2 Through-plane resistance

The methods used for the through-plane resistance measurements are a derivative of the method described by Mathias et al [20]. The method described by Mathias involves applying pressure to flat, high conductivity plates sandwiching a sample of diffusion media and measuring the resistance between the plates. Figure 4.5 is a diagram of the fixture used to measure the through-plane resistance of diffusion materials used in this work.

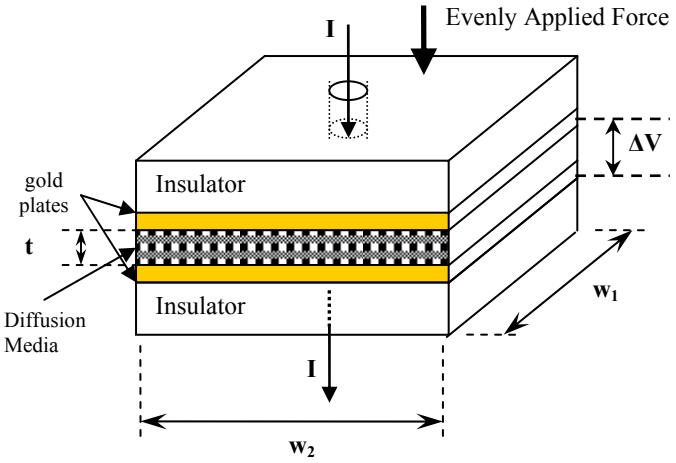

Figure 4.5 - Diagram of through-plane resistance measurement fixture.

A true four contact point resistance measurement was not possible through the plane of the diffusion media due to the lack of thickness to allow for separate voltage measuring contacts along the thickness of the material. The advantage of the four contact resistance measurement is that the resistance of the multimeter leads and contact plates is eliminated from the measurement, thus providing a value for the actual bulk resistance of the material of interest. Therefore, to make the measurements as accurate as possible an approximate four point method was used where one of the current sender/receiver leads and one of the differential voltage measurement leads were soldered together at the same point on each gold coated copper plate. This was done to eliminate the resistance of the leads from the measurement, which is significant compared to carbon cloth and carbon paper materials. This method could not eliminate the resistance of the gold contact plates,

but the plate resistance was measured to be less than 0.0001 Ω, which is negligible compared to the material resistances.

In order to combine the resistivity and the thickness of the diffusion media into a single metric characterizing the through-plane resistance, the following expression was used:

$$\rho_T t = R w_1 w_2 \tag{4.2}$$

where ρ_T (Ω-cm) is the resistivity of the bulk material, t (cm) is the thickness of the diffusion media, R (Ω) is the resistance calculated based on the applied current and the voltage drop, and the product $w_1 w_2$ is the area through which the current flows (cm^2). The resulting product $\rho_T t$ has dimensions of Ω-cm^2, which is commonly referred to as the area specific resistance. The area specific resistance is a convenient metric because the product of the area specific resistance and the current density is equal to the voltage drop in a conventional fuel cell arrangement. It is important to recognize that this technique does yields an area specific resistance which includes both bulk and contact resistance.

Unlike the in-plane resistance measurements, the through-plane resistance depends greatly on the force applied to the sample due to improved fiber to fiber contact at high compressive force within the media. Resistance data was collected for varying levels of applied force.

4.5.3 Darcy Permeability

The equation for Darcy permeability discussed in Chapter 2 did not include any inertial terms, and is thus only appropriate for laminar flow. The Darcy equation, Eq. 2.2, provides a relation between flow rate and pressure drop in porous media. Equation 2.2 is repeated here as equation 4.3 to aid in the discussion of Darcy permeability:

$$Q = k_d \left(\frac{A}{\mu L_d} \right) \Delta P \tag{4.3}$$

where Q is the volumetric flow rate of the fluid, k_d is the Darcy permeability of the media, A is the area of the porous media through which the flow passes, μ is the dynamic viscosity of the fluid, L_d is the travel length of the flow through the thickness of the diffusion media, and ΔP is the pressure drop across the diffusion media.

The Darcy permeability is a material property that characterizes the resistance to the flow of gas exhibited by the porous media. It can be seen in equation 4.3 that Q should vary linearly with ΔP, therefore the slope of a line connecting various common values of Q and ΔP would be equal to:

$$\frac{dQ}{dP} = k_d\left(\frac{A}{\mu L_d}\right) \tag{4.4}$$

At sufficiently large flow rates, the linearity inherent in Darcy's law breaks down due to the inertial effects of the higher velocity flow and Eq. 4.3 is no longer applicable. Equation 4.3 has been determined to be valid for Reynolds numbers less than 1 [43], where the appropriate length scale is an average characteristic length for the diameter of the pores within the material. Unfortunately, it is difficult to determine the pore size within PEM fuel cell diffusion media, and even more difficult to reconcile all pore size information into an appropriate characteristic average. It has also been proposed that the square root of the Darcy permeability coefficient, k_d, can be used as the length scale for Reynolds number determination in flow through porous media.

$$\mathrm{Re} = \left(\frac{Q}{A}\right)\frac{\rho_f k_d^{1/2}}{\mu} \tag{4.4}$$

where Q is the volumetric flow rate of the fluid, A is the area of the porous media through which the flow passes, ρ_f is the density of the fluid, μ is the dynamic viscosity of the fluid, and k_d is the Darcy coefficient of the media as defined in equation 2.2. Unfortunately, the limit on Reynolds number is not very well established for porous media when $k_d^{1/2}$ is used as the length scale for the Reynolds number as it is in Eq. 4.4. Therefore, in order to truly quantify the Darcy permeability of a material, the slope from the linear region of a

curve describing Q as a function of ΔP should be used to determine k_d. This process is presented for each of the five diffusion material used in this work in Chapter 5.

The experimental apparatus to measure the Darcy coefficient of the in-house diffusion materials is shown in Figure 4.6. MKS Instruments manufactured the flow controller and it was calibrated for dry, room temperature air. The flow controller has a set point input, and an actual value output so that the actual real time flow rate could be recorded. The differential pressure transducer has a range of 0-2.5 kPa and was manufactured by Barocel. The differential pressure transducer also has an analog 0-10 V voltage output to relay the real time pressure differential read by the transducer to the data acquisition software. The calibration of the pressure transducer was confirmed using a differential slant monometer. The sample holder has a barbed inlet fitting for a tubing connection and the outlet was open to the surrounding atmosphere. Since the sample fixture exhausted to the atmosphere, the low side of the differential pressure transducer was also left open to the atmosphere. The air used for the experiment was compressed Grade D breathing air supplied by AirGas, located in Radford, VA.

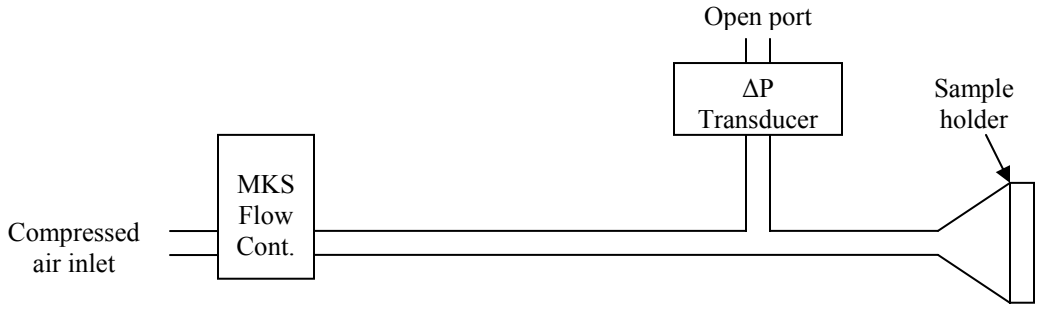

Figure 4.6 - Diagram of through-plane permeability measurement apparatus.

The flow rate and pressure differential attained for dry air flowing through each diffusion media was measured and monitored in real time using National Instruments LabView® software. The flow rate was started at 500 sccm and was adjusted in increments of 500 sccm up to a maximum value of 15,000 sccm for each diffusion media. The flow rate data was then plotted as a function of the differential pressure and linear regression was used to fit a line to the linear region of the curve with a forced intercept at

the origin. The slope of the line was then used to calculate the value of k_d for each material of interest. The results of these experiments are presented in Chapter 5.

4.6 FUEL CELL PERFORMANCE USING NOVEL GAS DIFFUSERS

More important than any ex-situ property characterization is the actual polarization performance of a MEA in combination with each of the five gas diffusion materials presented in this work. This section will detail the process for fabricating the test cells, and the process for characterizing the performance of each cell in a ribbon configuration, and a conventional configuration. Three different test fixtures were used in this work, a serpentine flow field conventional fixture (SFFC), a serpentine flow field ribbon fixture (SFFR), and an open flow field ribbon fixture (OFFR). The test fixtures were connected to a fuel cell test stand which controlled the fuel cell operating conditions. The details of each test fixture as well as the test stand and operating conditions will be discussed in this section.

4.6.1 Fabrication of test cells

Prior to characterizing the performance of each test cell it was necessary to assemble the necessary components of the fuel cell. There are three main components which make up the test cells used; MEA, GDL, and gaskets; all of which can be seen in Figure 4.7. The GDL materials used in this work were described earlier in this chapter.

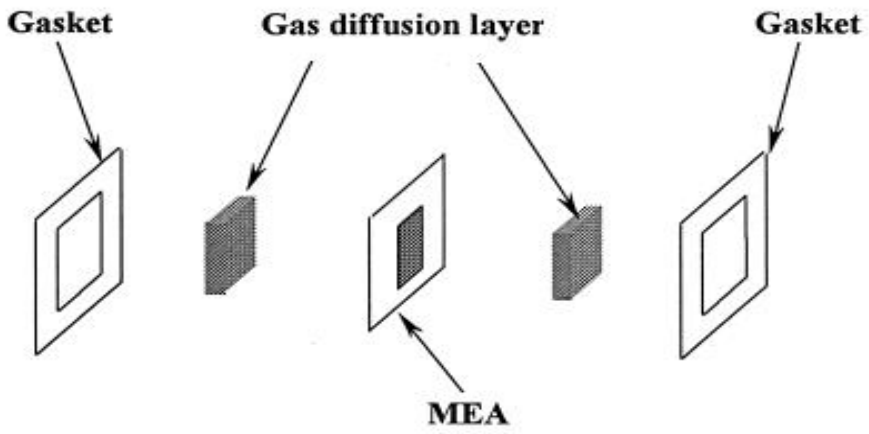

Figure 4.7 - Diagram of MEA-GDL-gasket sandwich [1].

The MEAs used in this work were purchased from Ion-Power Inc. The platinum catalyst loading was specified to be 0.4 mg/cm^2. The membrane material used in the MEAs is Nafion® N-112, which is a solution cast Nafion® film approximately 50 µm thick manufactured by DuPont. An SEM micrograph of an Ion-Power MEA used in this work can be seen in Figure 4.8 below.

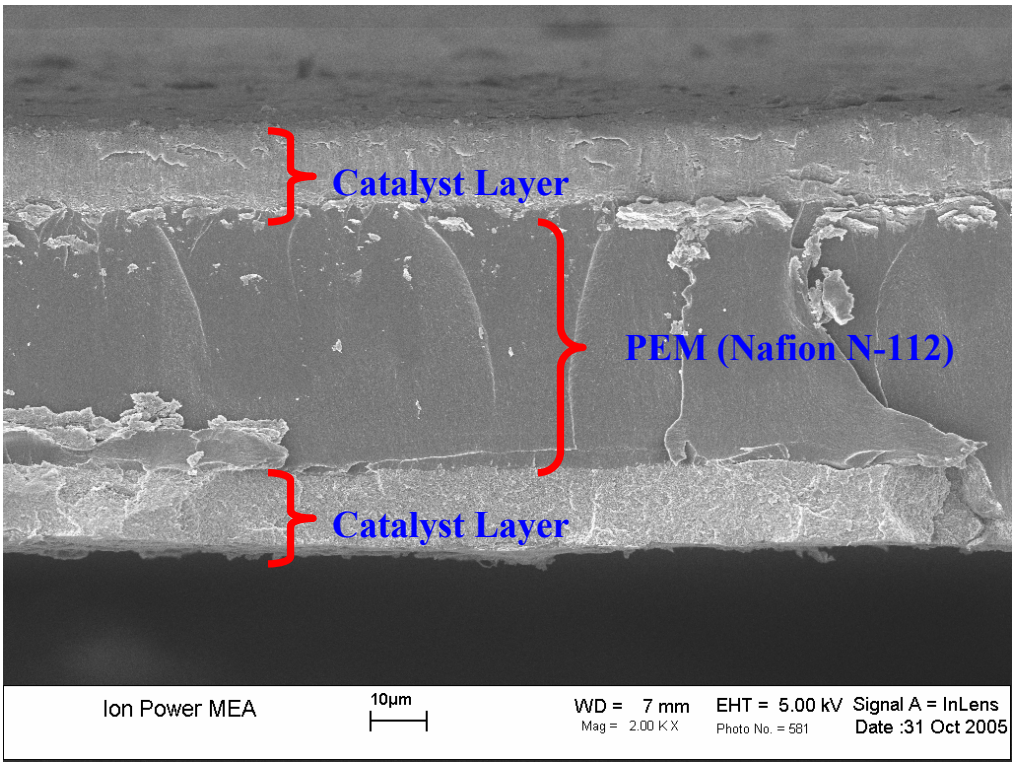

Figure 4.8 – SEM micrograph of an Ion-Power MEA.

In order to reduce the interfacial resistance between the MEA and the applied GDL, each diffusion media was hot pressed to an MEA prior to testing. The hot pressing procedure was performed at a gage pressure of 3.4 MPa, and a temperature of 140°C, for 5 minutes according to previous work [28]. Once the MEA and GDL were adhered together, Teflon® coated fiberglass fabric was used to gasket the GDL to ensure the gases would not leak when the cell was placed in the test assembly of interest. Finally, the sandwich composed of the gasketed GDL's and the MEA were placed inside the appropriate cell fixture and connected to the test station for testing. The test fixtures used in this work will be detailed in the following three sections.

4.6.2 Serpentine flow field conventional test fixture (SFFC)

The conventional method of current collection is to collect the current generated by a fuel cell in a direction perpendicular to the MEA. This method only requires the travel of the electrons through the thickness of the GDL, which is typically on the order of 200-500 μm. Another advantage of this method is the large cross section of conductive material (GDL) through which the current can travel. A large cross section, small travel distance, and relatively low resistance cause the ohmic losses within the GDL to be minimal in this configuration. This is absolutely the best current collection scheme for a single cell due to the minimal ohmic losses in the GDL. The problems that arise with regard to cost and manufacturing when this current collection scheme is employed in a fuel cell stack were detailed in Chapter 1.

A picture of the SFFC test fixture for a conventional through-plane method of current collection is displayed in Figure 4.9. The aluminum end plates are simply a means for clamping the fixture (using bolts) to apply pressure to the MEA-GDL-gasket sandwich to ensure ample electrical contact and gas sealing. The graphite blocks act as the serpentine flow channel and as the current collectors. The gold coated plates under the graphite blocks are electrically connected to the graphite blocks and are used as a connection point to the voltage sensing wires and the current carrying cables attached to the load. An electrical insulator between each gold coated plate and the aluminum end block cannot be seen but is there to avoid a short circuit when the bolts are attached to

both end blocks. The SFFC test fixture was manufactured by Fuel Cell Technologies Inc. of Albuquerque, NM.

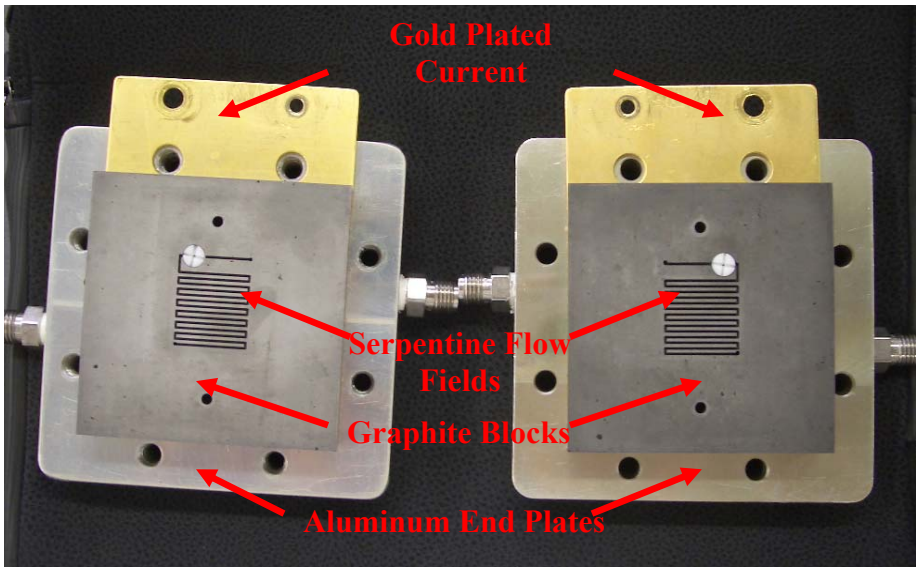

Figure 4.9 – Serpentine flow field conventional fuel cell test fixture (SFFC).

Polarization data using the SFFC test fixture was taken for each of the five test cells operating under optimized cathode relative humidity. Each test cell was tested using 2 or more gasket thicknesses. This was done in order to determine which gasket thickness provided the optimum combination of low contact resistance, and high gas permeability. The gasket selection process is detailed further in Chapter 5 where the polarization data is presented.

4.6.3 Serpentine flow field ribbon test fixture (SFFR)

When collecting current in the plane of the GDL the electrons have a long travel distance, and a small cross-sectional area through which to travel. The in-plane current collection scheme is a complete contrast to the large cross-section and short distance utilized in the conventional method of current collection. This current collection scheme certainly causes increased ohmic losses within the GDL of a PEM fuel cell, but the hope

is that the sacrifice in power will be offset by reduced manufacturing difficulty, time, and consequently cost as discussed in Chapter 2.

The test fixture displayed in Figure 4.10 was adapted to force the current generated by the cell to travel along the plane of the GDL and into collector plates situated at the edge of the gas channel. To do this, polyetherimide (PEI) blocks were machined to be identical to the graphite blocks used in the SFFC test fixture. The PEI blocks were then machined on the edge to allow for 316 stainless steel collector plates to be inserted at the edge of the gas channels. The SFFR fixture can be seen in figure 4.7. Rather than using the gold coated plates for voltage and current collection, the stainless steel plates are now used because the PEI insulates the gold coated plates from the GDL.

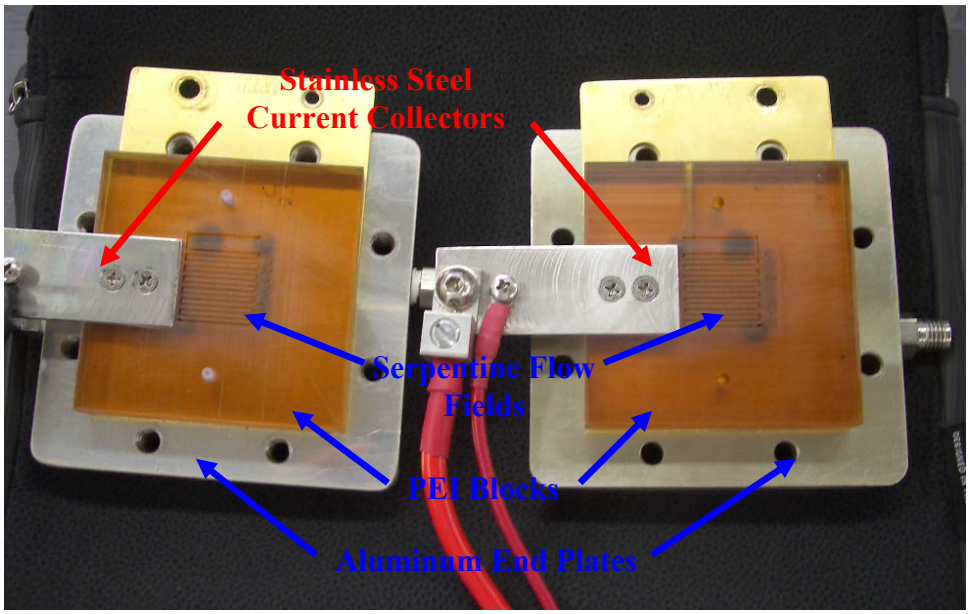

Figure 4.10 – Serpentine flow field ribbon fuel cell test fixture (SFFR).

It is important to notice that this test fixture does not eliminate the compressive nature of the flow field on the GDLs. This was done to capture only the effects of the added GDL resistance due to increased electron travel length, while keeping all other flow and compression characteristics identical to the SFFC test fixture. Polarization data for the test cells operated in the SFFR test fixture under optimized cathode relative humidity are presented in Chapter 5. The same gasket combinations were used in this test fixture as are used in the SFFC fixture.

4.6.4 Open flow field ribbon test fixture (OFFR)

Once it was determined which gas diffusion layer performed the best in the SFFR test fixture, the same cell was tested in the OFFR fixture. Tests were performed in the OFFR fixture to investigate the case in which there is no compression of the GDL against the MEA by the flow field. Additionally, since the OFFR fixture has much a much larger flow area, the velocity of the gas is significantly lower (for similar volumetric flow rates) in the OFFR configuration than it is in a serpentine flow field. The reduced gas velocity can cause complications with water removal. The water removal issue and the issue of interfacial resistance in the OFFR fixture will be discussed further in Chapter 5.

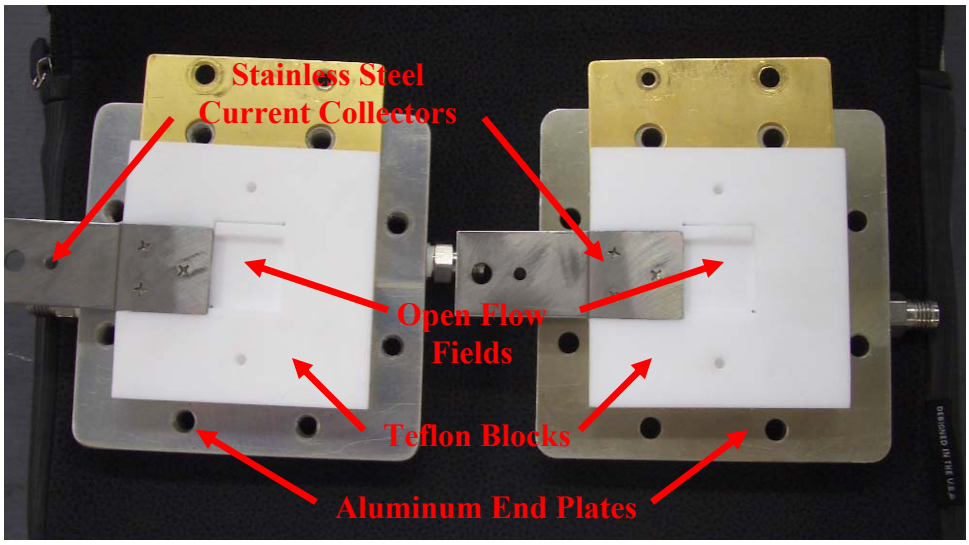

Figure 4.11 – Open flow field fuel cell ribbon test fixture (OFFR).

4.6.5 Operating conditions

PEM fuel cells are very sensitive to the conditions under which they are operated. For example, as the cell temperature (T_{cell}) is decreased, the activation overpotential increases as evidenced by an increased Tafel slope [44]. But, if the cell temperature is increased too much, the polymer membrane will begin to degrade at an unacceptable rate. Therefore, a balance is needed when choosing the operating temperature of a PEM fuel cell. An operating temperature of 80°C is typical for PEMFCs which use Nafion®

membranes, and will be used in this work. A similar balance is needed when choosing other operating conditions as well.

In this work, all tests were run using air at the cathode and hydrogen at the anode in a cell in which the exit pressures or "back pressures" (BP_a and BP_c) were at atmospheric pressure. The preference for operating at atmospheric pressure was based upon the assumption that fuel cell ribbons are most suitable for small scale power systems which typically lack the power to supply compressed air to the fuel cell stack. In order to assure that sufficient air and hydrogen were supplied to the cell, the gases were controlled to flow at a rate (Q_{H2} and Q_{AIR}) corresponding to six times the stoichiometric reaction rate at a current density of 1 A/cm^2.

The final two parameters which are typically controlled in experimental fuel cell testing are the inlet hydrogen relative humidity at the anode (RH_a) , and the inlet air relative humidity at the cathode (RH_c) . Drying of the membrane or catalyst layers is a major concern in PEMFC operation because the electrolyte becomes a very poor proton conductor in a dry state. The drying typically occurs at the anode electrode since there is no water produced there, and because protons leaving the anode tend to drag water across the membrane to the cathode. In order to eliminate the possible effects of electrolyte drying at the anode electrode, the inlet stream of hydrogen was maintained at 100% relative humidity for all experiments performed for this work. Electrode drying can also occur at the cathode if air at less than 100% relative humidity is supplied at a flow rate which is large enough to transport water out of the cell at a rate greater than the cell is producing water. Another phenomenon which is common at the cathode electrode is electrode flooding. Electrode flooding occurs when the cell produces water at a rate far greater than the air stream is removing water, thus filling the GDL and catalyst layer pores with water and blocking the flow of air to the catalyst sites. Each gas diffusion media handles the transport of water and air differently. Therefore it is necessary to adjust the humidity conditions at the cathode in order to achieve the best possible performance for each cell. The baseline testing conditions used in this work are summarized in table 4.3 below. The optimized cathode relative humidity will be presented along with the acquired polarization data in Chapter 5.

Table 4.3 – Summary of baseline test conditions.

Control Paramteter	Units	Value
Cell temperature (T_{cell})	°C	80
Anode relative humidity (RH_a)	%	100
Cathode relative humidity (RH_c)	%	optimized
Hydrogen flow rate (Q_{H2})	sccm	225
Air flow rate (Q_{AIR})	sccm	550
Anode back pressure (BP_a)	kPa-ga.	0
Cathode back pressure (BP_c)	kPa-ga.	0

4.6.6 Fuel cell test stand

All tests were performed using a test station manufactured by Fuel Cell Technologies Inc. of Albuquerque, NM. The tests station was outfitted with mass flow controllers manufactured by MKS Instruments for hydrogen and air, dew point setting humidifiers for the anode and cathode gas flows, a fuel cell assembly temperature controller, an electronic load manufactured by AMREL, digital back-pressure regulators, and an electrochemical impedance spectroscopy analyzer. All of the above components were controlled using programs written in LabView by Fuel Cell Technologies Inc.

Each of the baseline test parameters listed in table 4.3 could be directly controlled using the test stand, with the exception of the anode and cathode relative humidity. In order to control the humidity at the cell inlet the dew point humidifiers were simply set at a temperature corresponding to the appropriate dew point to achieve the desired relative humidity at the cell temperature of 80°C. Figure 4.12 shows the test stand used to perform the experiments presented in this work.

Figure 4.12 – Test stand manufactured by Fuel Cell Technologies Inc.

4.7 SUMMARY OF EXPERIMENTAL PROCEDURES

The overall experimental procedure can be summarized as follows:

- Fabricate test cell by hot pressing desired GDL to MEA
- Evaluate cell performance in the SFFR test fixture using gaskets slightly thinner than the post hotpress GDL thickness
- Reduce gasket thickness and evaluate cell performance until an apparent maximum is achieved
- Evaluate cell performance using the preferred gaskets in the SFFC test fixture
- Place the test cell in the SFFR fixture and reduce gasket thickness to confirm that the apparent maximum performance truly is the maximized performance
- Use resistance fixtures to evaluate the in-plane and through-plane resistance of the GDL material
- Evaluate GDL air permeability using the Darcy permeability apparatus

5 RESULTS AND DISCUSSION

This chapter will first discuss the results obtained from the material property experiments for in-plane resistance as a function of applied stress, through-plane resistance as a function of applied stress, and Darcy permeability, as described in Chapter 4. This chapter will also present the applied through-plane resistances measured for each diffusion media when clamped between two silver coated copper plates in the fuel cell test assembly. The values obtained for through-plane resistance as a function of applied stress, and those obtained for Darcy permeability are used in Section 5.1 to distinguish the advantages and disadvantages of the two different bulk treatments; Treatment A and Treatment B. The applied through-plane resistance of the different diffusion materials measured in the cell test fixture when the fixture bolts are torqued to the specified operating torque (565 N-cm) are used in Section 5.2 to compare the experimental results to the dimensionless analysis of Chapter 3. The values obtained for in-plane resistance as a function of applied stress are used to evaluate treatment options (Section 5.1), and to aid in the finite element fuel cell ribbon performance predictions.

Section 5.2 will discuss the polarization performance achieved from a standard membrane electrode assembly (MEA) when each gas diffusion media is applied as the gas diffusion layer for the MEA, for two different test fixtures. The first test fixture utilizes through-plane current collection (SFFC), and the second test fixture utilizes in-plane current collection (SFFR). The best performing gas diffusion media also underwent additional testing to characterize its performance in a test fixture utilizing an open flow field (OFFR) configuration while still collecting current in the plane of the diffusion media. The results from the OFFR fixture are presented in Section 5.4. Each of the three test fixtures was discussed in Chapter 4.

The final section of this chapter describes a variation of the finite element model discussed in Chapter 3. As noted in Chapter 3, the finite element model requires the input of an expression to characterize the local MEA performance. The necessary expression was achieved by testing each diffusion media with a standard MEA in the SFFC test fixture and fitting a sixth order polynomial to the data representing current density versus cell potential. The finite element model also requires the input of electrical resistivity

values for the diffusion media of interest. The in-plane resistance information from Section 5.1 was used to satisfy this requirement.

5.1 MATERIAL PROPERTIES

As described in Chapter 4, this work explores five different diffusion materials. The first is the commercially available ELAT® LT-1200W available from ETEK Inc. The second and third materials are each relatively thick PAN based woven materials with different treatments. These materials are designated as ITPN-A, and ITPN-B. The final two materials are pitch based materials again having different bulk treatments, CWPT-A, and CWPT-B. A thorough description of the treatments and bulk material used in each gas diffusion media was presented in Chapter 4. The properties of in-plane resistance, through-plane resistance, and air permeability, are presented for each material in this section along with a comparison of each property for all of the materials of interest.

5.1.1 Through-plane resistance under varying applied stress

ELAT LT-1200W, which will subsequently be referred to only as ELAT, exhibits extremely low through-plane resistance due to the fact that it was designed with through-plane current collection in mind. Measurements of through-plane resistance were performed at various values of compressive stress. As force is applied, the diffusion media is compressed and the through-plane resistance decreases due to improved fiber to fiber contact. Figure 5.1 shows the results from the through-plane resistance measurements expressed as area specific resistance as a function of applied stress. The presented results include both the bulk resistance of the diffusion media and the contact resistance with the gold plates. Here no attempt was made to separate bulk resistance and contact effects. A more detailed discussion of these effects is presented by Mishra [40]. In general, the contact resistance is roughly 3 to 5 times greater than the bulk through-plane resistance for graphite bipolar plates in contact with carbon fiber based diffusion media. It is expected that contact resistance in the gold plated fixture is less than that

reported for contact with bipolar plates. However, since the contact resistance was not quantified these results were not used to predict a bulk resistivity of the material.

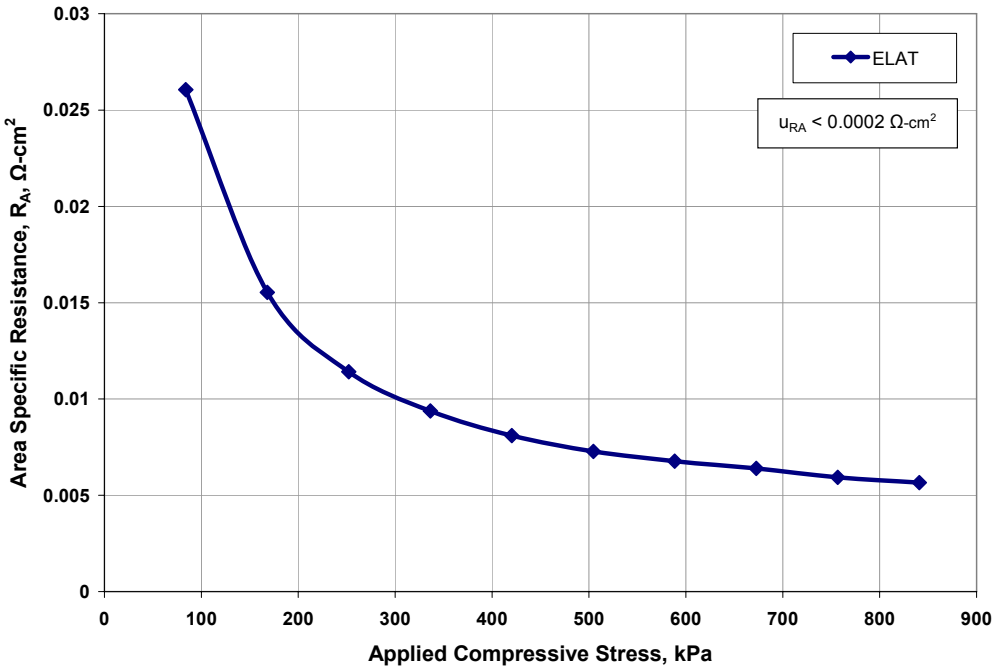

Figure 5.1 – Area specific resistance values obtained for ELAT LT-1200W.

Figure 5.2 displays the results of the through-plane resistance measurements for the ITPN-A and ITPN-B diffusion materials. Due to its increased thickness, the through-plane resistance of the ITPN-A material is approximately twice the resistance observed for ELAT at all levels of applied stress due to the additional thickness (and thus longer length of current travel) of the ITPN-A material.

The most significant difference between treatment A and treatment B is that treatment B includes the addition of carbon black into the bulk of the diffusion media. The carbon black was introduced based on the existing literature noting a decrease in through-plane resistance as a result of the inclusion of carbon black in the bulk structure of carbon paper based gas diffusion media [5]. Therefore, it is expected that the ITPN-B material will exhibit reduced through-plane resistance in comparison to the ITPN-A material. It can be seen that the carbon black does appear to reduce the through-plane resistance of the diffusion material regardless of the applied stress. The range of

resistance reduction observed was 18-32% depending on the applied stress, while the average reduction over all stress levels was 24% as shown in Figure 5.2.

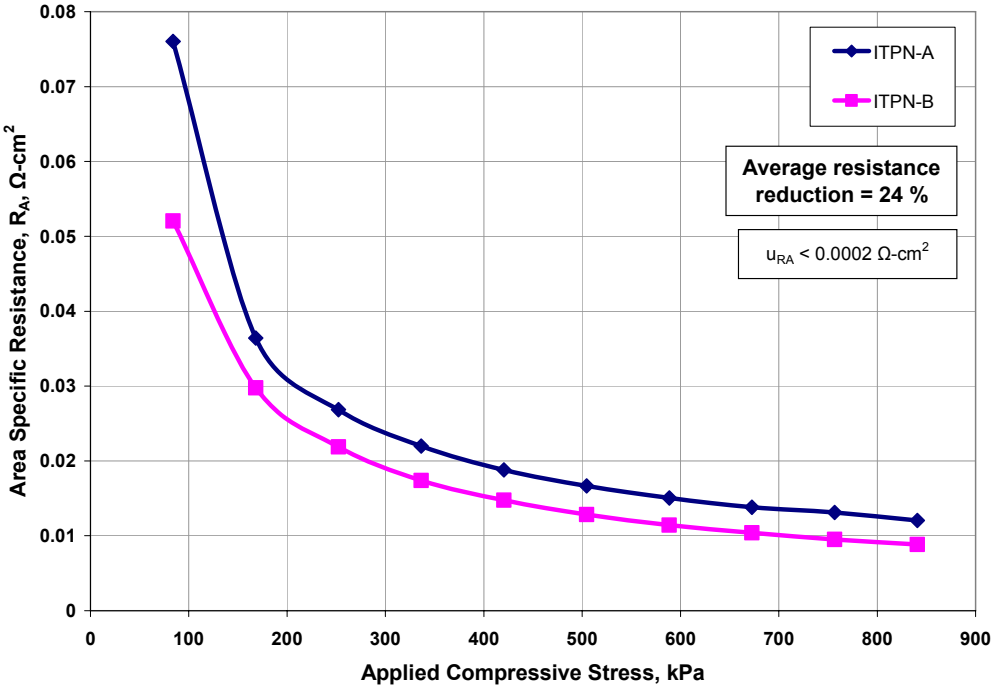

Figure 5.2 – Comparison of area specific resistance values obtained for ITPN series.

The distinguishing characteristic of the CWPT materials is that they are constructed of pitch based carbon fibers rather than the more commonly used PAN based fibers. The purpose of using the pitch based fibers was to reduce the in-plane resistance of the cloth. Since pitch based fiber tows are only available in sizes larger than PAN based tows, the weave is more coarse and the surface less even, thus, it is expected that the through-plane resistance of the CWPT materials will be greater that the through-plane resistance observed for ELAT. The through-plane resistance results for the CWPT-A and CWPT-B materials are presented in Figure 5.3. It can be seen in the figure that the CWPT-A material and the CWPT-B materials exhibit through plane resistances approximately twice the through-plane resistance of ELAT. At stresses below 300 kPa it appears that the through-plane resistance of the CWPT-B material is greater than the CWPT-A material. The only explanation of this behavior is that stress levels lower than 300 kPa are not sufficient to make good contact with such coarse materials. Therefore,

the values of resistance below 300 kPa are predominantly measures of the contact resistance between the materials and the gold coated copper plates. The resistances observed at applied stresses greater than 400 kPa indicate that the through-plane resistance of the CWPT-B material is lower than the through-plane resistance of the CWPT-A material. The data indicates that the resistance was reduced by an average of 13% at stress levels above 400 kPa. The observed range of reduction observed for applied stresses greater than 400 kPa was 8-17%.

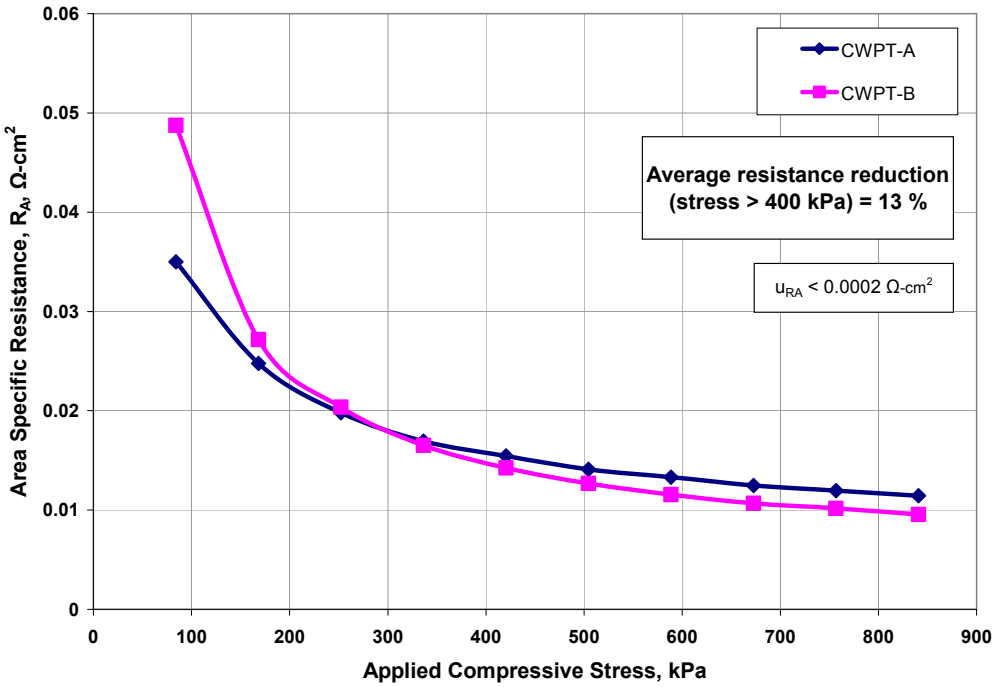

Figure 5.3 – Area specific resistance values obtained for CWPT-A and CWPT-B.

5.1.2 In-plane resistance under varying applied stress

The results obtained for the in-plane resistance measurement, expressed as Ω/sq., of ELAT is shown in Figure 5.4. It can be seen that the in-plane resistance shows very little variability with applied load. This result confirms the belief that current flowing in the plane of the diffusion media travels almost exclusively along continuous carbon fibers arranged in that direction, therefore diminishing the effect of compressing the fibers into

a tighter configuration. The high in-plane resistance of ELAT is expected since it was designed for through-plane current conduction in mind.

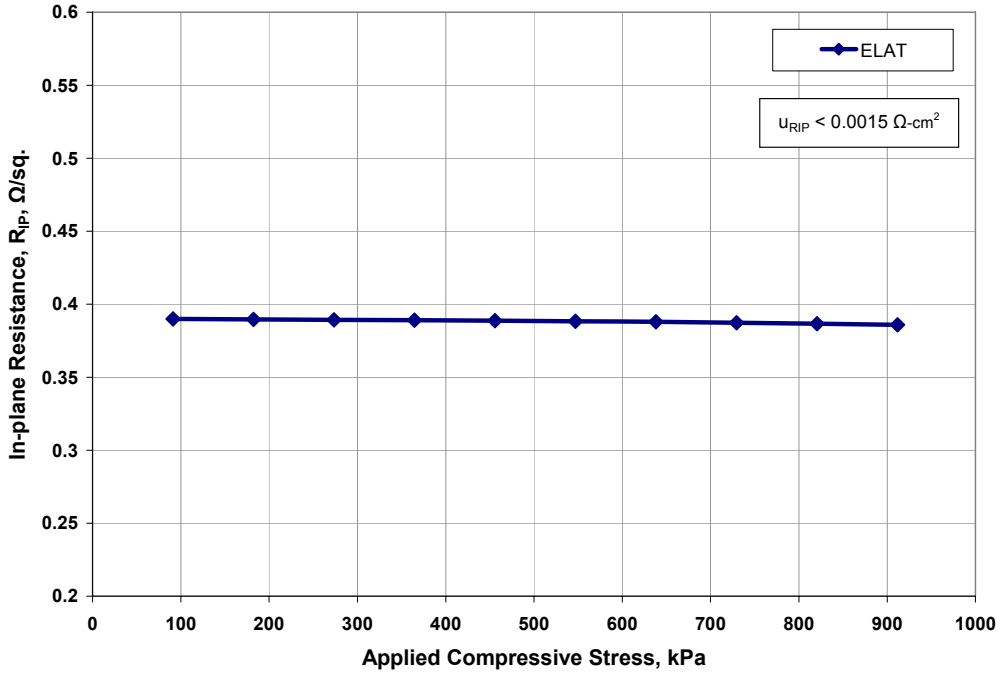

Figure 5.4 – In-plane resistance values obtained for ELAT LT-1200W.

The results obtained for the in-plane resistance of the ITPN-A and ITPN-B materials are displayed in Figure 5.5. Again, there is very little variation in resistance with varying applied stress, as was observed with ELAT. Similar to the doubling of through-plane resistance observed when ITPN-A is compared to ELAT, a halving of in-plane resistance is also observed. This phenomena exists because when the thickness is doubled the travel lengths for electrons is doubled when the direction of travel is through the plane, but the area perpendicular to the direction of travel is also doubled when electrons are traveling in the plane of the material. It can also be seen that the carbon black added when Treatment B was applied to the ITPN material caused a reduction in in-plane resistance by 7%. This result is attributed to the carbon black filling in surface non-uniformities and thus facilitating an even distribution of current along the entire surface of the diffusion material. Due to the even distribution along the surface of the material, greater fiber utilization is achieved.

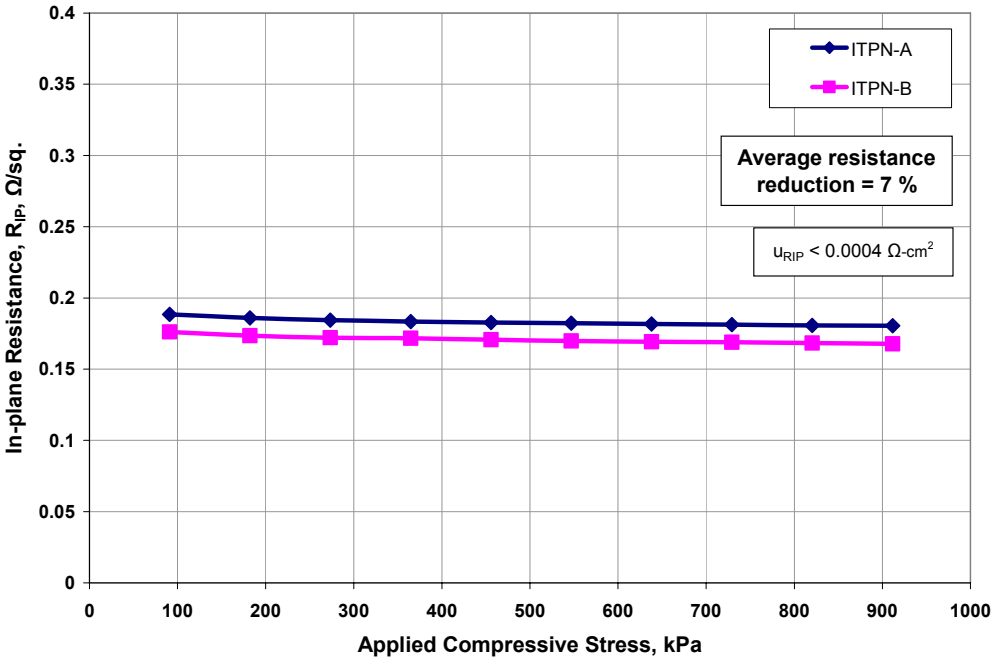

Figure 5.5 – In-plane resistance values obtained for ITPN-A and ITPN-B.

Although the through-plane resistance of the CWPT-A and CWPT-B material is much higher than the through-plane resistances exhibited by ELAT, it is expected that the CWPT materials will exhibit much lower in-plane resistance due to the lower resistivity of pitch based fibers compared to PAN based fibers. Figure 5.6 illustrates that the CWPT-A material exhibits an in-plane resistance of approximately 0.042 Ω/sq. This value is a full order of magnitude lower than the in-plane resistance of ELAT, and one fifth the resistance exhibited by the ITPN materials. This result is significant since in-plane current conduction is paramount in the fuel cell ribbon architecture. The in-plane resistance curve for the CWPT-A material exhibits an increase in resistance above a certain applied load. The observed increase is due to fiber breakage just above the gold contact edges since the stress at those points is extremely large. Resistance values above the threshold of fiber breakage will not be considered when the CWPT-A material is compared to the CWPT-B material.

The in-plane resistance measured for the CWPT-B material is only 14% lower than the in-plane resistance measured for the CWPT-A material. This is likely due to the carbon black filler more effectively distributing the current across the width of the

material at the current source edge. Minimal decrease in in-plane resistance was expected due to the fact that the current traveling in the plane of the material is expected to travel exclusively along the fibers oriented in the proper direction. But, the results for the CWPT materials seem to indicate that that carbon black filler near the surface can provide better utilization of the properly oriented fibers for coarsely woven material which inherently have non-uniform surfaces. To a lesser degree, the same phenomenon was observed for the ITPN diffusion materials.

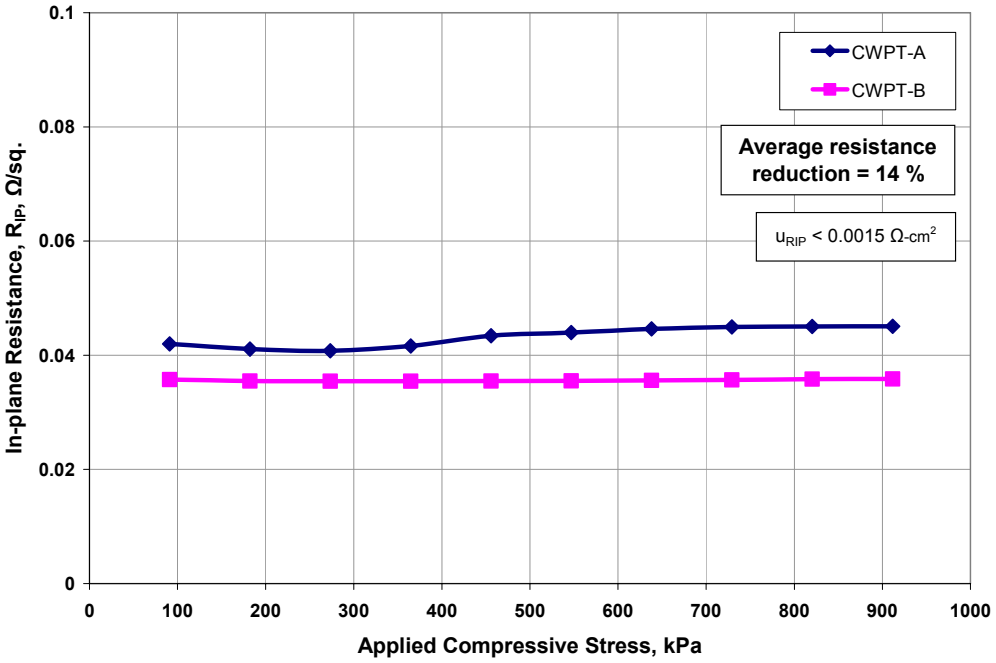

Figure 5.6 – In-plane resistance values obtained for CWPT-A and CWPT-B.

5.1.3 Darcy Permeability

The ELAT material exhibited a Darcy permeability coefficient, as described in Chapter 2, of 8.1 Darcys (1 Darcy = 10^{-12} m^2). This value of Darcy permeability alone does not provide much information. However, since ELAT is a widely accepted diffusion media, its permeability is useful for setting a reference point for the four remaining diffusion materials which were tested in this work. The data collected to determine this value of dry air permeability is shown in Figure 5.7. Only the data from the linear region

of the curve representing flow rate, Q, as a function of pressure drop across the media, ΔP, is used to determine the Darcy permeability coefficient. As noted previously, Darcy's law is not valid at flow rates and pressure differentials outside of this linear range because the inertial affects of the flow dynamics (which Darcy's law ignores) begin to take effect.

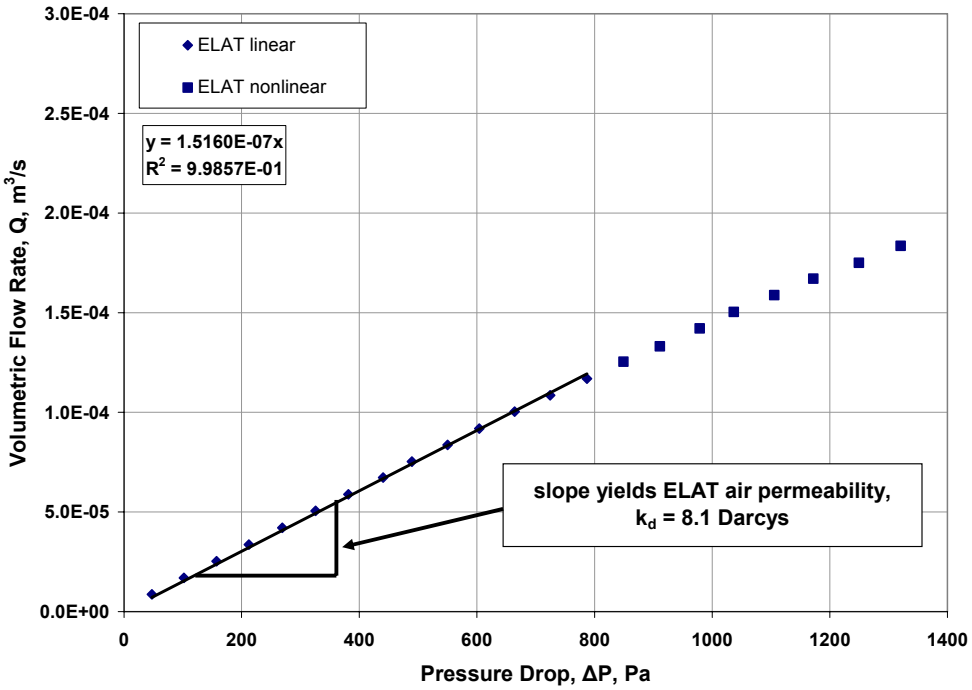

Figure 5.7 – Dry air permeability data obtained for ELAT LT-1200W.

The Darcy permeability for the ITPN-A material is presented in Figure 5.8, and indicates a value of 144 Darcys for the measurement of Darcy air permeability. This indicates that this material is much less resistant to the flow of air through it than ELAT in a dry environment. The large difference between the Darcy permeability of ELAT and ITPN-A is attributed to the thick and dense MPL which exists on the surface of ELAT versus the lower loading of MPL on the surface of the ITPN-A material.

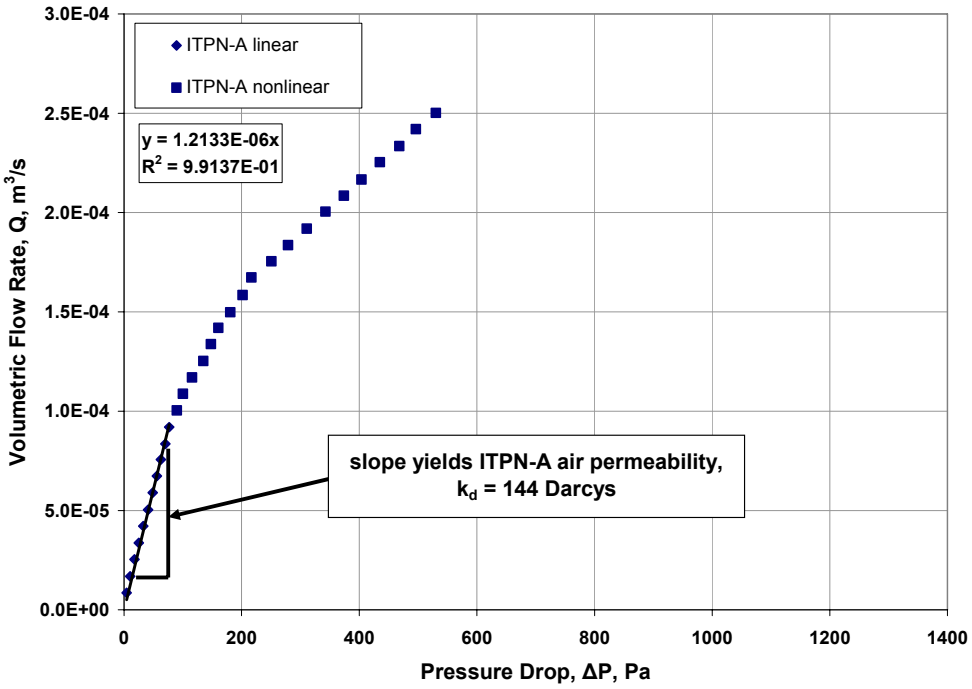

Figure 5.8 – Dry air permeability data obtained for ITPN-A.

The effect of the carbon black filler is evident when the air permeability of the ITPN series materials is compared. The Darcy permeability data for the ITPN-B material can be seen in Figure 5.9. The data indicates a dry air permeability of 35.8 Darcys in the linear region of the curve, thus indicating that the ITPN-B material exhibits four times the flow resistance of the ITPN-A material. This increase in flow resistance is attributed solely to the addition of the carbon black filler. Although the increased flow resistance of ITPN-B is significant when compared to ITPN-A, the Darcy permeability of ITPN-B is still greater than the permeability exhibited by ELAT. Therefore, it is concluded that the ITPN-B material exhibits sufficient permeability for use as a gas diffusion layer in a PEM fuel cell.

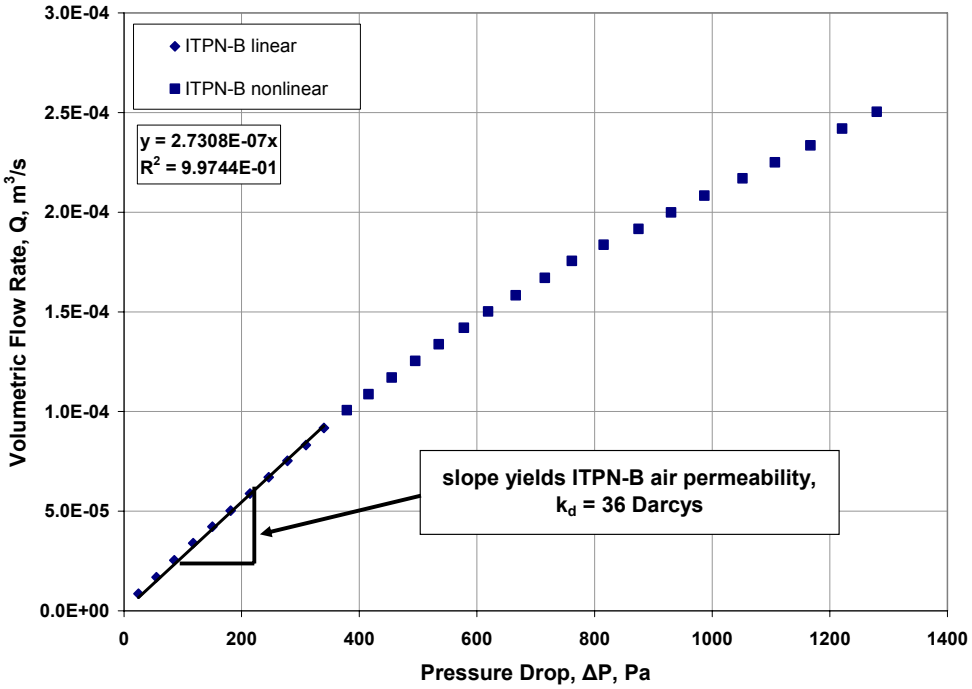

Figure 5.9 – Dry air permeability data obtained for ITPN-B.

The results for the permeability experiment performed on the CWPT-A material are presented in Figure 5.10. According to the slope of the linear region, the CWPT-A material exhibits a Darcy permeability of 113 Darcys. This value which is much higher than the permeability of ELAT indicates that the CWPT-A material has suitable permeability for use in PEM fuel cells.

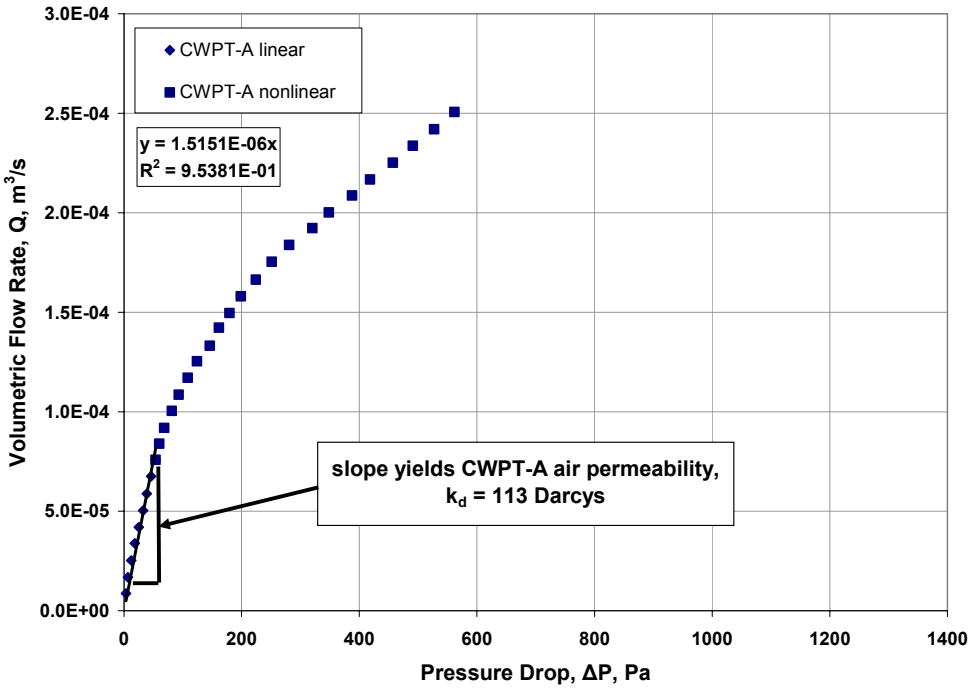

Figure 5.10 – Dry air permeability data obtained for CWPT-A.

The dry air permeability data (Figure 5.11) exhibits a significant reduction in permeability for the CWPT-B material as opposed to the CWPT-A material. This result was expected due to the addition of the carbon black filler into the bulk of the CWPT-B material. Although the Darcy permeability of the CWPT-B material in comparison to the CWPT-A material, the CWPT-B material still exhibits Darcy permeability three times the values observed for ELAT. Therefore, the CWPT-B material is likely still adequately permeable for use in PEM fuel cells.

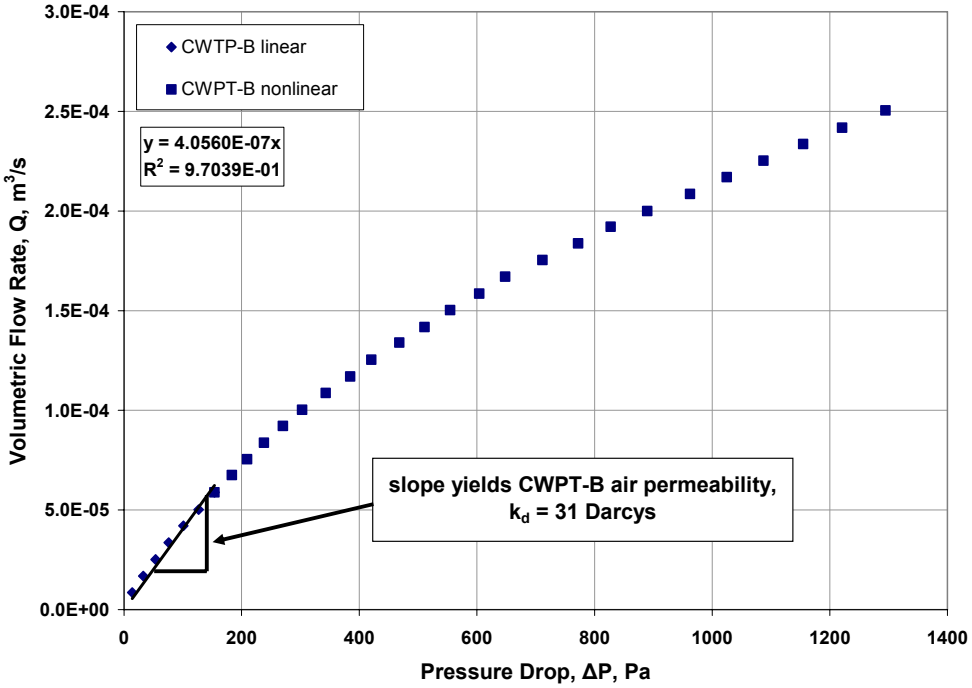

Figure 5.11 – Dry air permeability data obtained for CWPT-B.

5.1.4 Applied through-plane resistance in cell fixture

The through-plane resistance as a function of applied compressive stress data presented in Section 5.1.1 is useful for comparing Treatment A and Treatment B. Unfortunately, the stress imposed on the GDL when a fuel cell is assembled in one of the test fixtures is unknown. What is known is the torque applied to the bolts of the fixture (565 N-cm) regardless of the GDL being used. Therefore, since the bolt torque is the same regardless of the GDL material, the total force exerted on the MEA-GDL-gasket combination within the fixture must also be constant regardless of the material. Although the total force exerted within the fixture is constant, the manner in which the force gets distributed within the fixture depends on the elasticity of the GDL and gasket being used. Thus, determination of the GDL stress within the fuel cell fixture is problematic. Instead, the GDL resistance was measured directly in the fixture for a specific gasket-GDL combination. The chosen gasket was the one that yielded the best performance at 0.5 V.

The through-plane resistance measurements between two silver coated copper plates within the fixture serve two purposes. First, the resistance values obtained in this

manner when the diffusion media is paired with the appropriate gaskets is a useful indicator of the actual through-plane resistance which should be used in the dimensionless analysis presented in Chapter 3. Second, the through-plane resistance measured can be compared to the through-plane resistance versus applied stress curves presented in Section 5.1.1 to infer an apparent stress on the GDL within the cell test fixture at the given bolt torque of 565 N-cm. The results of the through-plane resistance measurements in the cell fixture, and the inferred apparent stress on the diffusion media within the fixture are summarized in Table 5.1. The values obtained for applied through-plane resistance in this manner were used in Section 5.2.4 to compare the experimental ribbon results to the dimensionless analysis presented in Chapter 3. The average apparent stress for all materials was approximately 500 kPa. To facilitate comparisons at a common stress, Table 5.1 also presents results for the through-plane resistance at 500 kPa as determined from the curves in Section 5.1.1 for each material.

Table 5.1 – Applied through-plane resistance and apparent stress of materials in cell fixture.

Material	Results with gasket yielding optimal current density		Area specific resistance at 500 kPa (Ω-cm^2)
	Area specific resistance in cell fixture (Ω-cm^2)	Approximate apparent stress on material in cell fixture (kPa)	
ELAT	0.0063	670	0.0073
ITPN-A	0.0159	520	0.0167
ITPN-B	0.0079	950	0.0128
CWPT-A	0.0299	120	0.0141
CWPT-B	0.0279	160	0.0127

5.1.5 Summary of material properties

A variety of materials were tested to determine their suitability for use in fuel cell ribbon assemblies. The experimental results for the physical properties of the materials of interest in this work indicate a wide range of in-plane resistance, through-plane resistance, and Darcy permeability.

The ITPN series of diffusion media utilizes a woven carbon fiber structure very similar to the woven structure used in ELAT due to the fact that the same type of carbon fibers were used to generate the woven structure. The greatest difference between the woven structure of the ITPN series and ELAT is that the ITPN series was woven in a manner which caused the material to have more fibers in the plane and thus have a greater thickness that is approximately twice the thickness of ELAT. The increased thickness was chosen in order to reduce in-plane resistance, as seen in Figure 5.12. The consequence of a thicker diffusion media is increased through-plane resistance as indicated in Figure 5.13 which shows through-plane resistance at a compressive stress of 500 kPa. Figure 5.13 indicates that the resistance of the ITPN-A material is approximately twice the resistance of the ELAT material when a compressive stress of 500 kPa is applied. This result indicates that the contact resistance in the through-plane resistance fixture is likely very small relative to the bulk material resistance for materials that exhibit uniform surfaces (i.e. ELAT and ITPN-A). In addition, the greater thickness leads to reduced permeability and can be seen in Figure 5.14.

The reduction in in-plane resistance, which is so critical to fuel cell ribbon development, was achieved by the CWPT materials. The CWPT materials exhibited an in-plane resistance which was an order of magnitude smaller than the in-plane resistance of ELAT.

The effect of the carbon black included in treatment B was evident in all three material property measurements. The results obtained for the Darcy permeability of the five materials indicates that the filler drastically reduces the permeability of the filled fabrics, but that the filler is not significant enough to cause the permeability to drop below the acceptable benchmark of 8.1 Darcys associated with the ELAT material. Chapter 6 will provide a graphical comparison of the physical properties for the diffusion

materials discussed. It should be noted that the materials filled with carbon black and Teflon (ITPN-B and CWPT-B) exhibit nearly identical values of Darcy permeability. This indicates that the carbon black filler is the component that dictates how well the diffusion media transport dry air.

Figures 5.12-5.14 present comparisons of in-plane resistance, through-plane resistance measured in the fuel cell test fixture, and Darcy air permeability.

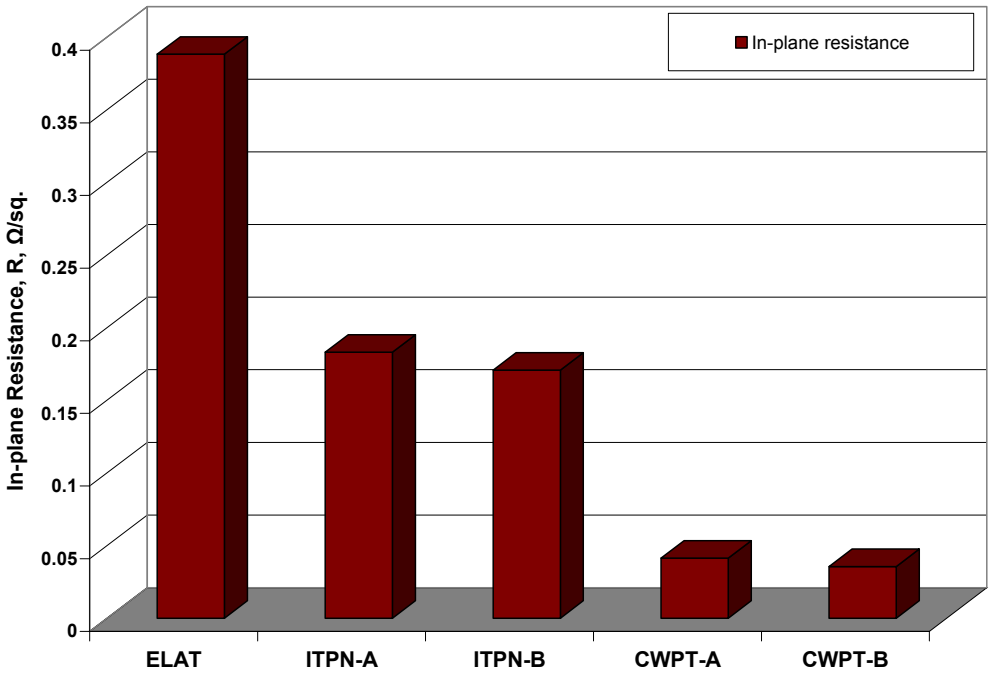

Figure 5.12 – Summary of average in-plane resistance results.

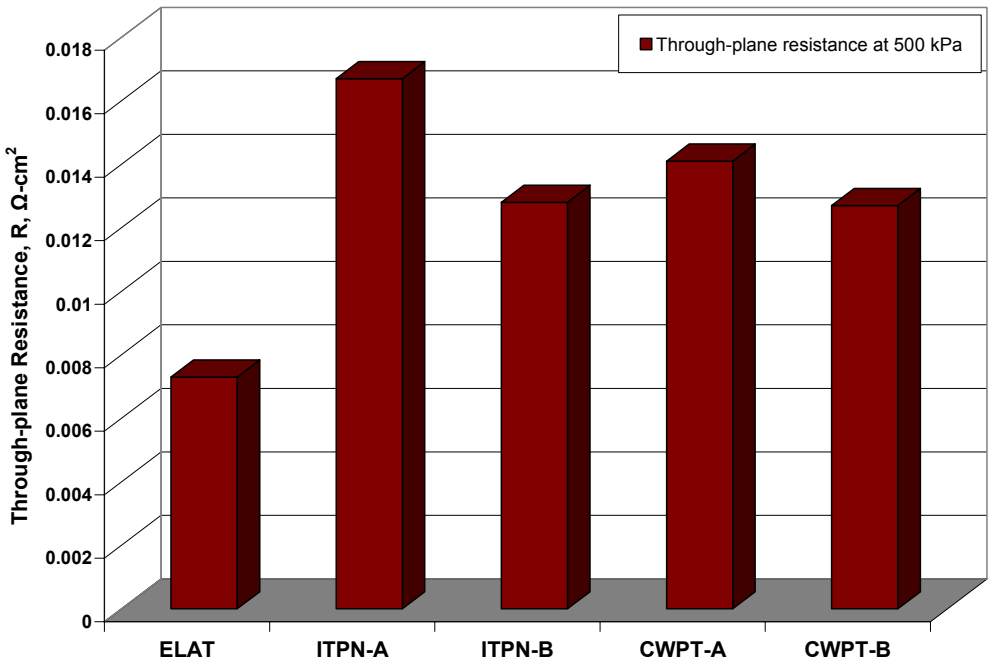

Figure 5.13 – Summary of through-plane resistance results in cell fixture at a compressive stress of 500 kPa.

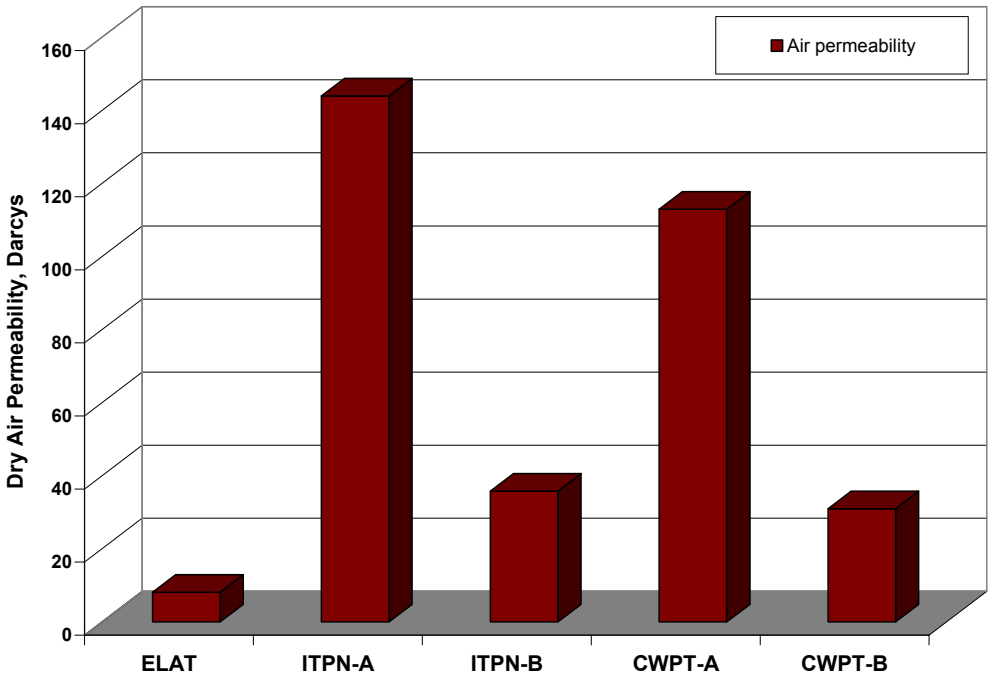

Figure 5.14 – Summary of Darcy air permeability results.

5.2 POLARIZATION PERFORMANCE

Although it is important to characterize the ex-situ bulk properties of diffusion media, it is even more important to observe how each diffusion media performs in a fuel cell environment. Each gas diffusion media discussed in this work was applied as a gas diffusion layer to a commercially available MEA purchased from Ion-Power Inc. The ex-situ properties serve only as a guide in material selection but provide little insight into how the materials will perform under the conditions in a fuel cell, i.e. water acceptance and rejection, heat rejection, and interfacial resistance between the diffusion media and the MEA. Therefore, the polarization data obtained from PEM fuel cells utilizing each of the five diffusion materials discussed herein are presented in this section.

Additionally, high frequency resistance (HFR) measurements will be presented for each material. High frequency resistance is considered to be the purely ohmic contribution to the losses in a PEM fuel cell. The measurement is performed by applying a high frequency (typically 1-10 kHz) AC voltage perturbation (typically 0.01-0.1 V) through the cell. The change in phase of the wave when it returns to the frequency response analyzer can be broken into real and imaginary components of impedance. If the appropriate frequency is chosen for the AC voltage perturbation, the response will not include an imaginary component of impedance. The lack of an imaginary component in the returned AC signal indicates that the capacitive effects of the electrode have been eliminated from the impedance measurement, therefore only the purely ohmic portion of the cell impedance is measured.

There is a fine balance between contact resistance, bulk through-plane resistance, water transport, and air permeability when it comes to selecting the level of compression imposed on the gas diffusion layer in every PEM fuel cell. Because of all of these sometimes competing phenomena, there must be a balance achieved in the choice of gaskets used when the test cell is assembled. Therefore, for each diffusion media under consideration, a variety of gasket thicknesses were utilized to determine where the optimum point of compression existed in the fuel cell ribbon assembly with serpentine flow channels. The current density when operating at 0.5 Volts in the SFFR fixture was used as the criteria for determining which gasket combination was the most suitable

match to each gas diffusion layer. HFR measurements were also performed at each gasket thickness to characterize the sum of the through-plane GDL resistance and the contact resistances existent in the cell.

5.2.1 ELAT LT-1200W diffusion media performance

As with the ex-situ property characterization, the polarization data from a cell using ELAT is provided here as a reference point for the other materials of interest. Figure 5.15 displays the process for optimizing the performance of ELAT in a ribbon cell configuration under varying GDL compression. It can be seen that the cell performs best in the SFFR fixture when a 210 µm gasket is used. Since the gaskets used are essentially incompressible (PTFE coated fiberglass fabric), the GDL is assumed to be the same thickness as the gasket used.

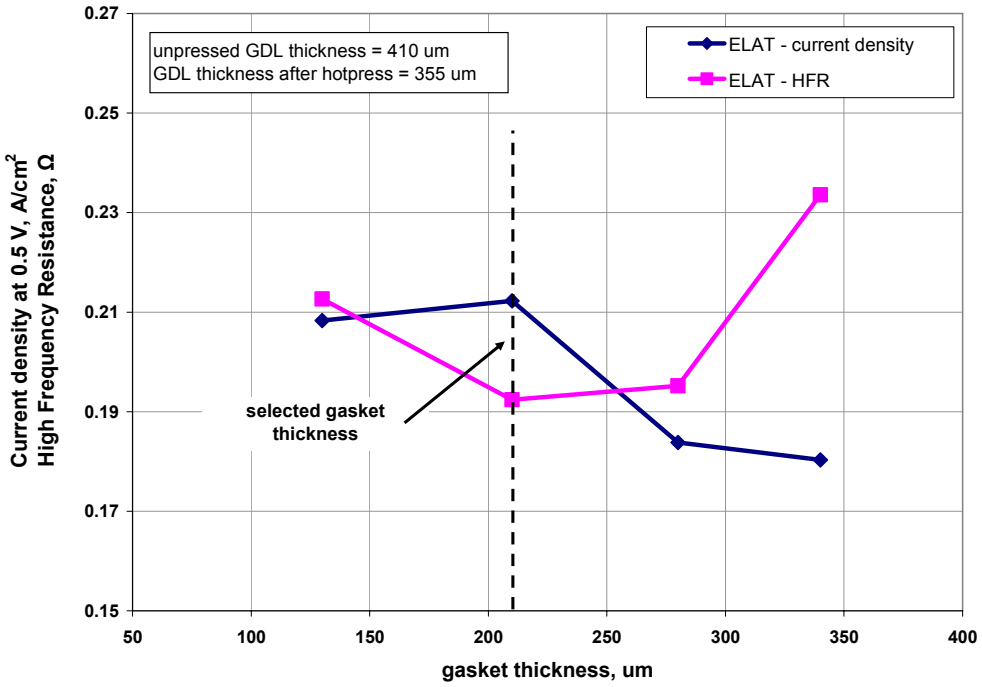

Figure 5.15 – Gasket optimization plot for ELAT operating at 0.5 V.

Figure 5.16 is a graph showing two polarization curves obtained for ELAT when the 210 µm gasket was used. It can be seen that the ELAT material does not perform particularly well when arranged in a ribbon configuration, only achieving 29% of the current density at 0.5 Volts in comparison to the conventional current collection arrangement. This result was expected since the non-dimensional model of Chapter 3 indicated that a material exhibiting the resistive properties of ELAT would perform poorly when adapted from a conventional configuration to a ribbon configuration.

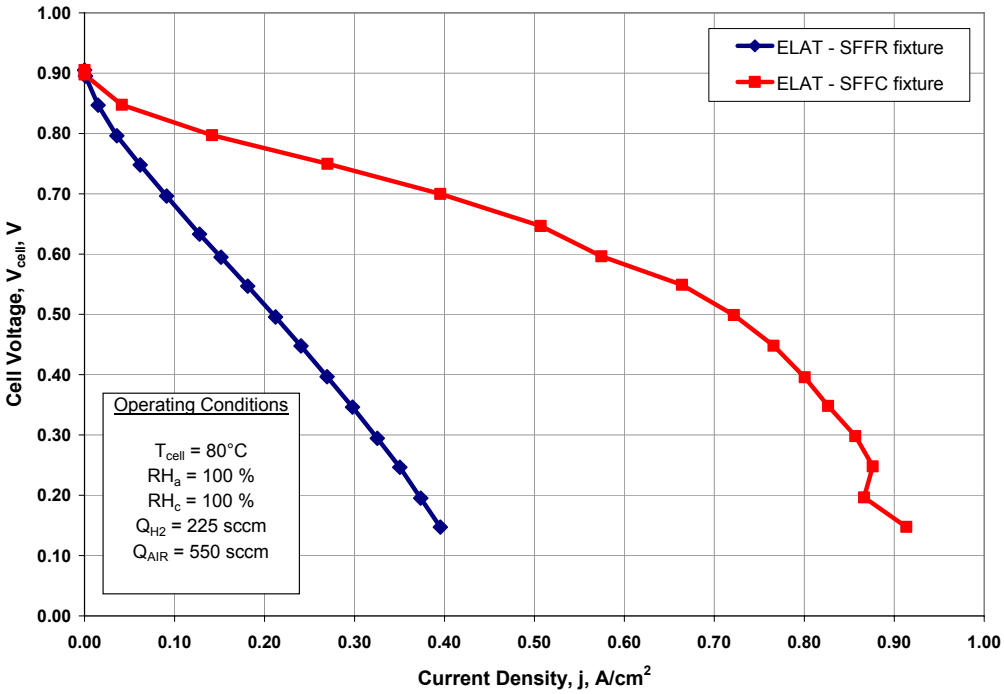

Figure 5.16 – Experimental polarization data for an MEA using ELAT.

5.2.2 ITPN series diffusion media performance

The ITPN-A diffusion media performed significantly better in a ribbon configuration than ELAT. Figure 5.17 indicates that the current density at 0.5 Volts reaches a peak when a 340 µm gasket was used. The achieved current density of 0.34 A/cm^2 at 0.5 V for the ITPN-A material is 62% greater than the performance achieved using ELAT. This difference is attributed solely to the greater thickness, and thus larger current carrying capacity, of the ITPN-A material.

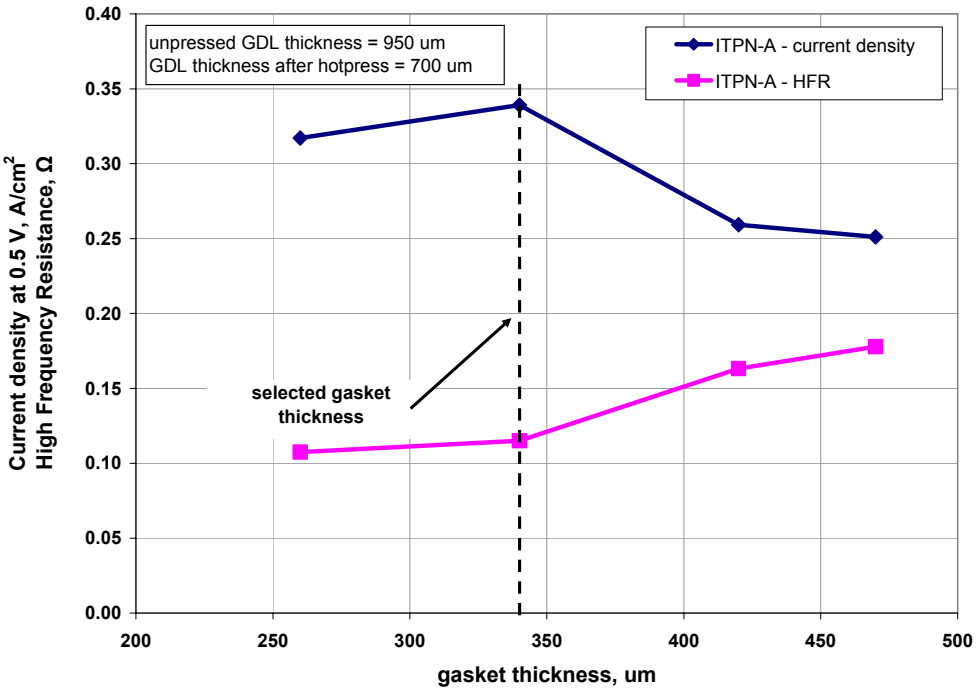

Figure 5.17 - Gasket optimization plot for ITPN-A operating at 0.5 V.

Figure 5.18 shows how the ITPN-A material performed in a ribbon cell test fixture compared to the performance achieved in a conventional test fixture. The results indicate that the ITPN-A material performs at 58% of the conventional current density at 0.5 Volts. This fraction of performance is far greater than the 29% observed for the commercially available ELAT diffusion media.

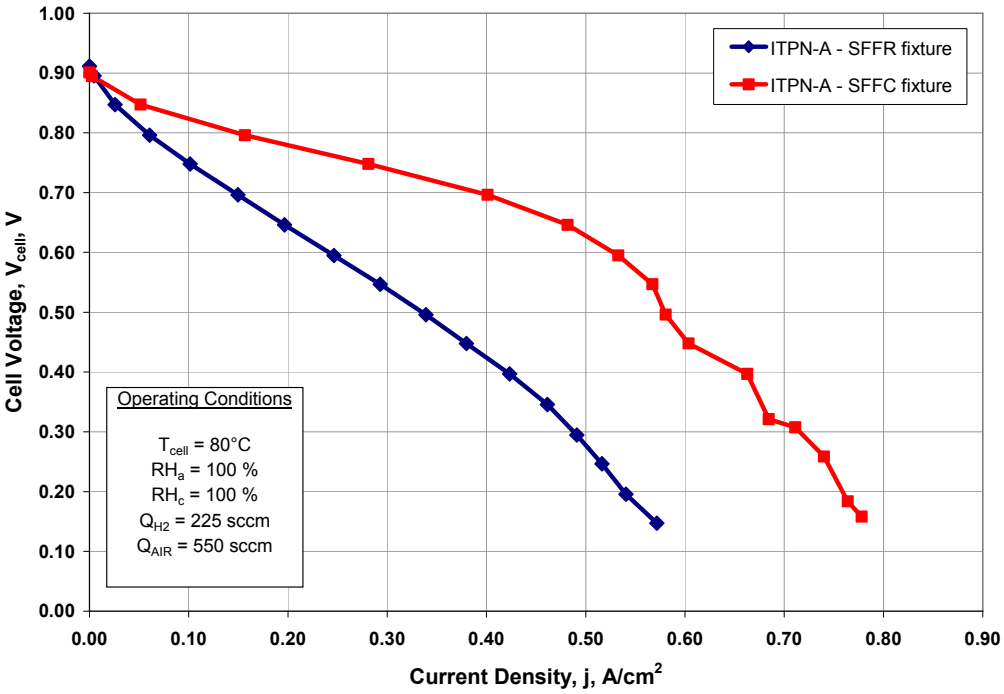

Figure 5.18 - Experimental polarization data for an MEA using ITPN-A.

Figure 5.19 displays the gasket optimization for the ITPN-B material. Similar to the ITPN-A material, the peak performance was achieved when a 340 µm gasket was used. The changes in performance as a function of gasket thickness are not as drastic for the ITPN-B material as they were for the ITPN-A material. This is likely due to the added carbon black filler reducing the effect of compression on the through-plane resistance of the material. If the majority of the interstitial space between carbon fibers is already filled with a conductive material, then squeezing the conductive carbon fibers together is less important to reduce through-plane resistance. Unfortunately, this reduced dependence on compression did not translate into added performance.

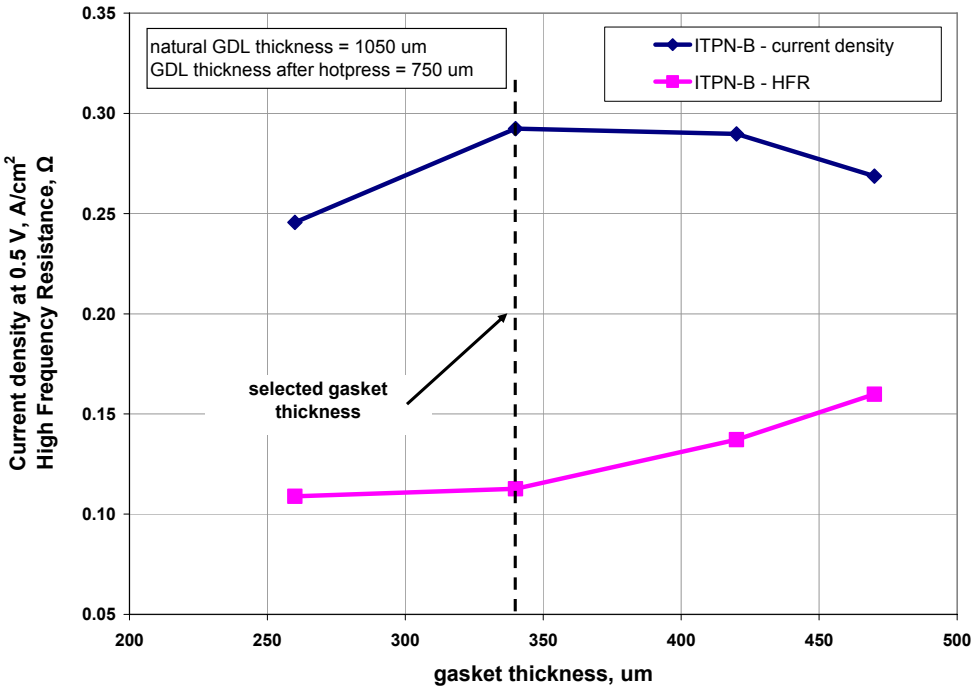

Figure 5.19 - Gasket optimization plot for ITPN-B operating at 0.5 V.

Figure 5.20 displays the polarization data collected for the MEA using the ITPN-B gas diffusion layer. It can be seen that the ITPN-B material performs quite well in a ribbon fixture when compared to the performance in the conventional fixture, achieving 72% of the current output at 0.5 Volts. But, it is also evident that the performance of the ITPN-B material is inferior to the ITPN-A material at higher current densities. This is likely due to the added resistance to gas flow or water transport through the ITPN-B material as evidenced by the reduced value of air permeability observed.

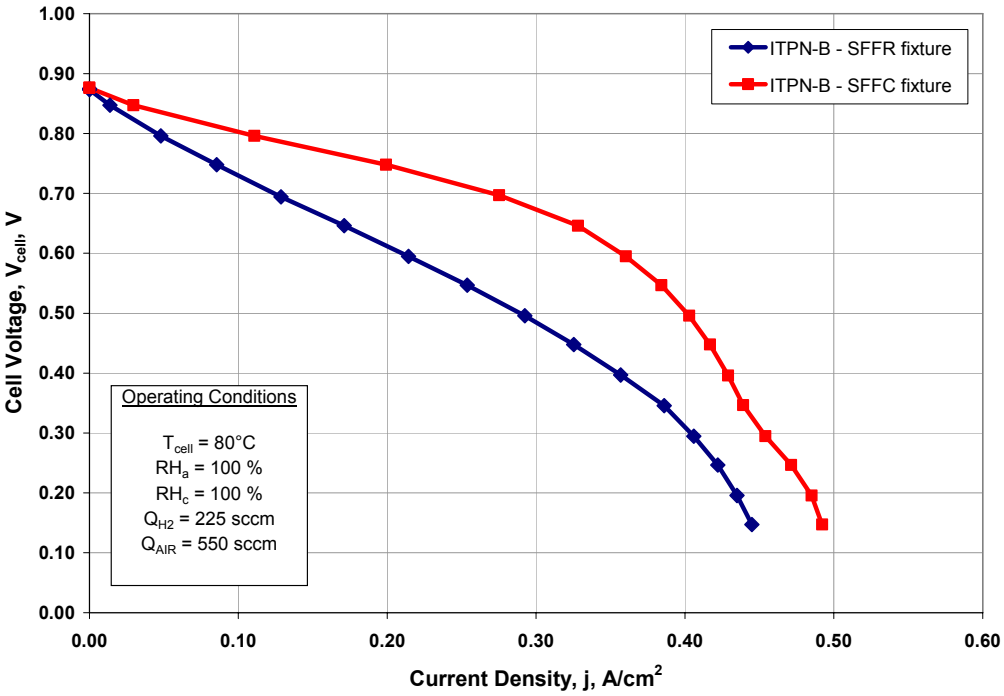

Figure 5.20 - Experimental polarization data for an MEA using ITPN-B.

5.2.3 CWPT series diffusion media performance

The CWPT-A material performed best when operated at 75% relative humidity at the cathode inlet. The gasket optimization for the CWPT-A material can be seen in Figure 5.21. The performance is very low when a 380 µm gasket is used, and the associated high frequency resistance (HFR) is quite high. In contrast, the performance increases significantly, and the HFR drops significantly when the gaskets were reduced to a thickness of 280 µm. Additional reduction in gasket size was not performed past 280 µm since a very marginal increase in performance was observed when the change from 340 µm gaskets to 280 µm gaskets was performed.

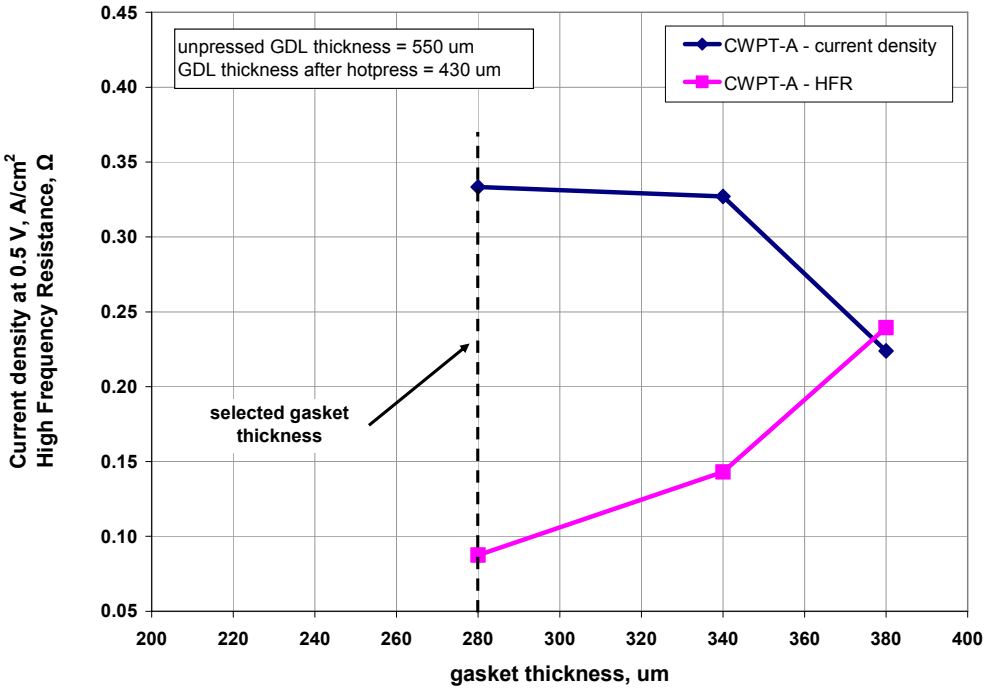

Figure 5.21 - Gasket optimization plot for CWPT-A operating at 0.5 V.

The polarization data collected for the cell fabricated using the CWPT-A material can be seen in Figure 5.22. The displayed experimental data indicates that the cell using the CWPT-A material as a gas diffusion layer achieved 78% of the current density at 0.5 V in the SFFR fixture as was achieved in the SFFC fixture. Although the percentage achieved in a ribbon arrangement relative to a conventional arrangement is very good compared to the other materials, the actual current density is lower than what was observed in the test cell using the ITPN-A material. This is due to the significantly greater performance observed in the SFFC fixture for the ITPN-A test cell compared to the CWPT-A test cell.

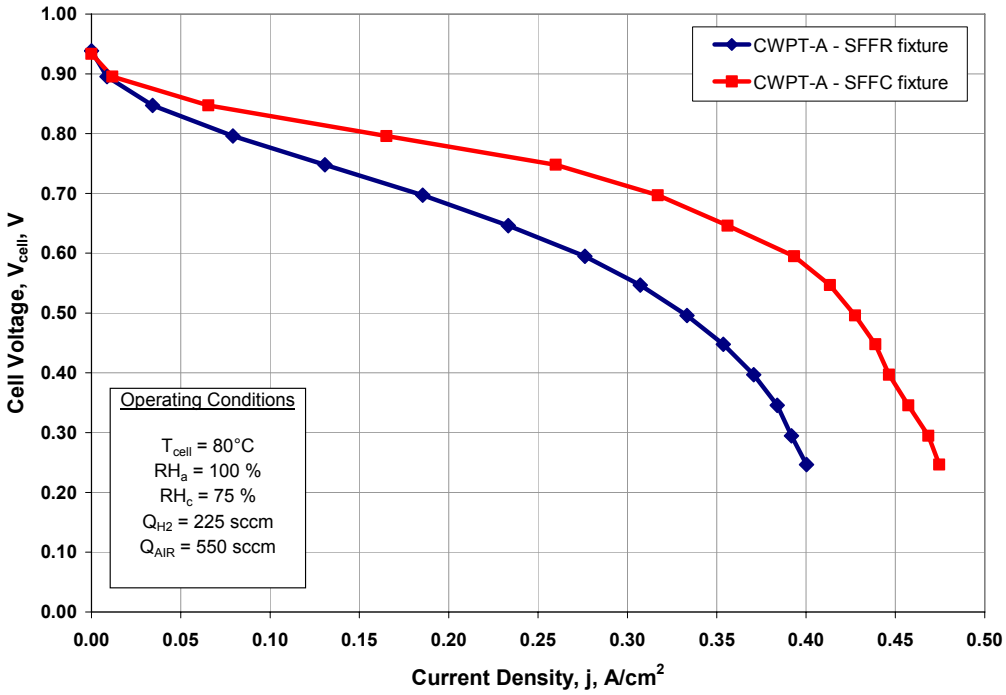

Figure 5.22 - Experimental polarization data for an MEA using CWPT-A.

The CWPT-B material exhibited an interesting trend in its gasket optimization. Figure 5.23 shows that when the gasket size was reduced from 380 µm to 340 µm, that the HFR increased from 0.08 Ω to 0.15 Ω. The reason for this is not well understood since increased compression should decrease through-plane resistance and the contact resistance at the GDL-MEA interface. One possible explanation is that since the CWPT-B material performed so well in the SFFR fixture using 380 µm gaskets, it was also tested in the OFFR fixture before being tested with a 340 µm gasket in the SFFR fixture. It is likely that when the test in the OFFR fixture was performed, that the GDL partially delaminated from the MEA due to the lack of compression against the GDL surface in the OFFR fixture. This is the most probable explanation for the increased HFR observed when the cell was tested in the SFFR fixture using 340 µm gaskets. The data collected for the CWPT-B test cell in the OFFR fixture will be presented in a later section.

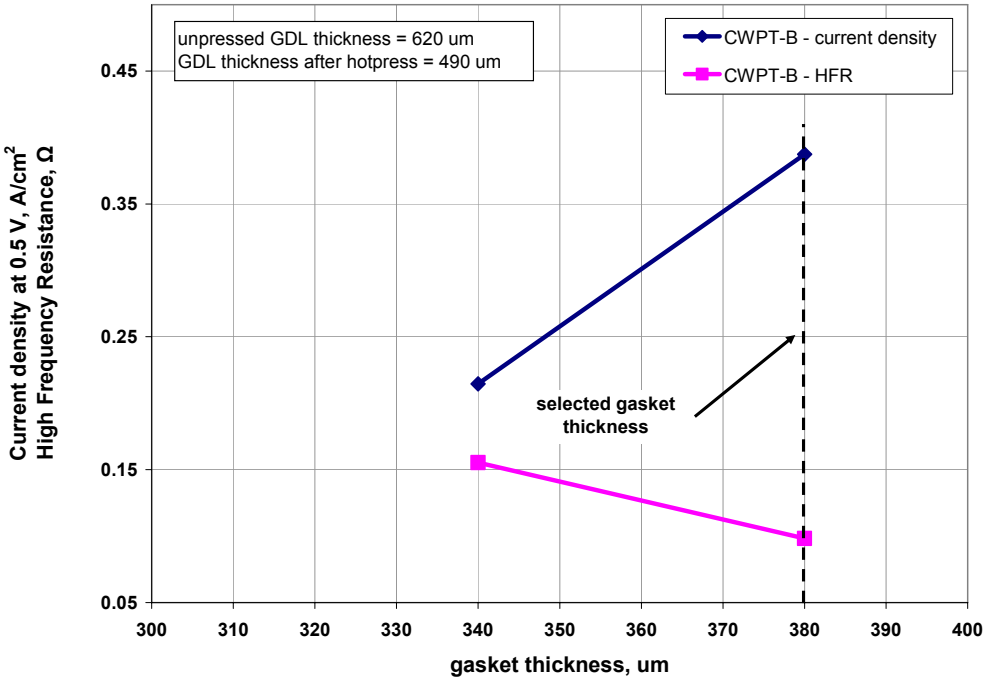

Figure 5.23 - Gasket optimization plot for CWPT-B operating at 0.5 V.

The polarization data collected from the CWPT-B test cell using the 380 µm gaskets in the SFFC and the SFFR test fixtures is presented in Figure 5.24. It can be seen that the CWPT-B material performed in the SFFR fixture at 66% of the performance achieved in the SFFC fixture at 0.5 V. More important than the ratio of performances is the absolute performance of 0.39 A/cm^2 which was produced at a cell potential of 0.5 V. This value for current density is significantly greater than any value observed in the literature for laterally conducting fuel cell stacks operating at 0.5 V. A more in depth investigation of the performance of the CWPT-B test cell will be presented in Section 5.4.

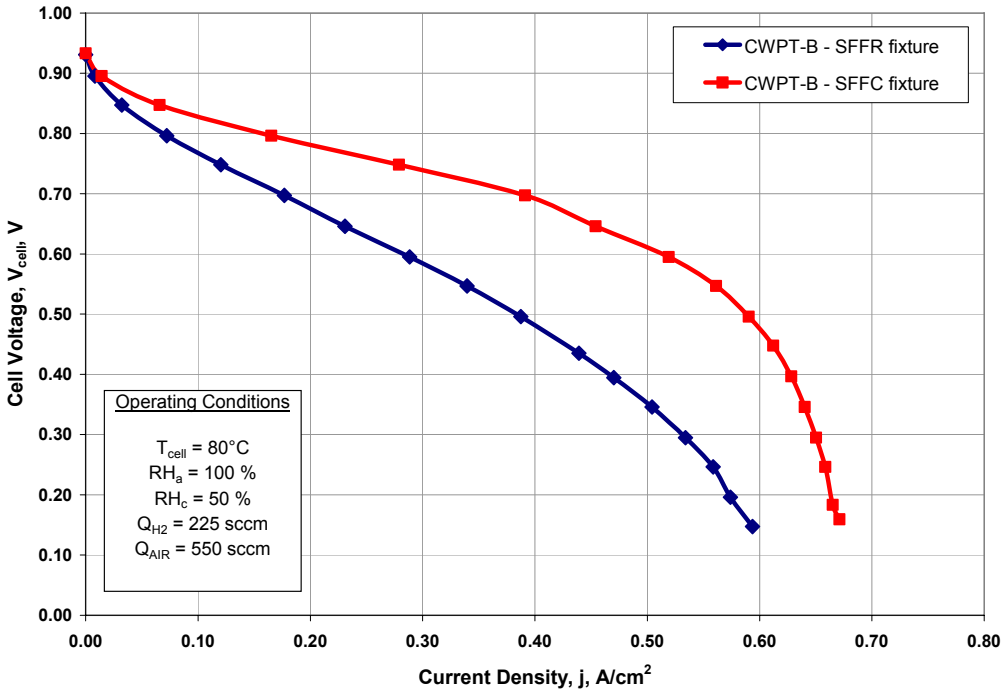

Figure 5.24 - Experimental polarization data for an MEA using CWPT-B.

5.2.4 Summary and comparison of GDL performance results

The performance metric utilized in this work is average current density at 0.5 V. Experimental data for ribbon cells using each of five different GDL's were presented in the previous section. The performance of the five cells designed and tested at the Energy Systems Laboratory (ESL) at Virginia Tech, along with the performance observed in the literature is summarized in Figure 5.25.

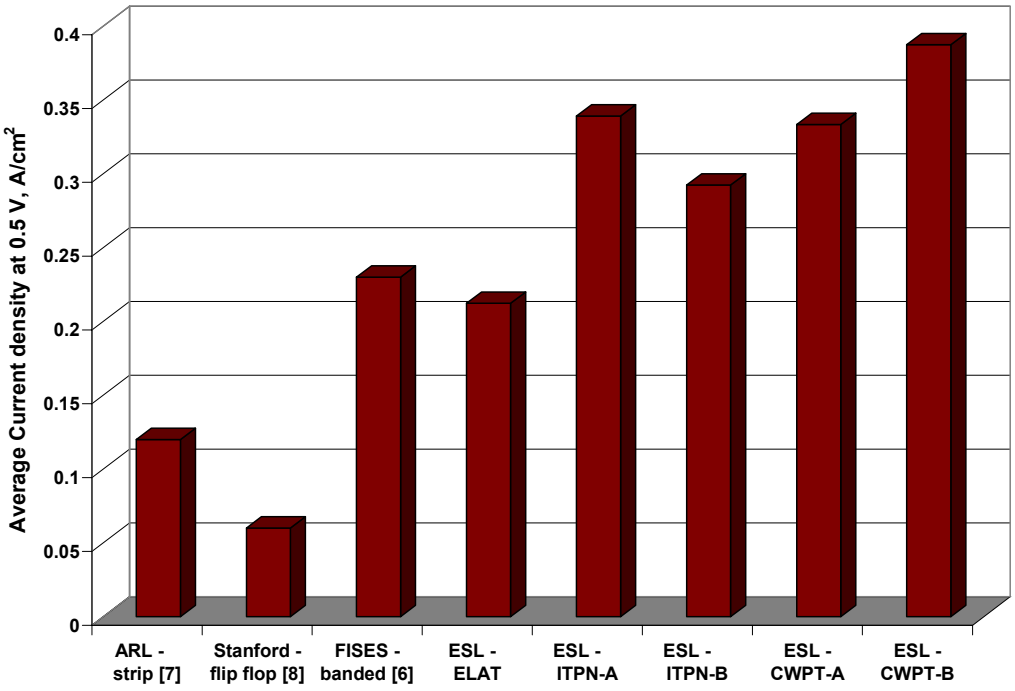

Figure 5.25 – Comparison of ESL material to cells observed in literature.

5.2.5 Comparison of achieved performance to dimensionless analysis

The performance surface from the dimensionless analysis presented in Figure 3.6 of Chapter 3 is again displayed here as Figure 5.26 for reference. This surface indicates the expected ratio of fuel cell ribbon current density to conventional fuel cell current density which can be expected for a diffusion material which exhibits a certain combination of Π parameter values when each cell is operated at 0.5 Volts. The dimensions of the test fixture used to generate the conventional and ribbon cell data

presented in this section, along with the resistive properties characterized in Section 5.1 were used to determine the Π parameters for each of the five diffusion media materials considered in this work. Upon determining the Π values for each material, the experimentally determined dimensionless current density was calculated and compared to the predictions presented in Figure 5.26 below. It is important to note that the curve fit used to characterize the MEA performance for the non-dimensional analysis is for a generic cell operating under idealized conditions and it cannot account for gas diffusion layers which exhibit different mass transport resistance or contact resistance between the GDL and the MEA. In addition, the performance surface shown in figure 5.26 was determined using an idealized geometry for the fuel cell ribbon concept.

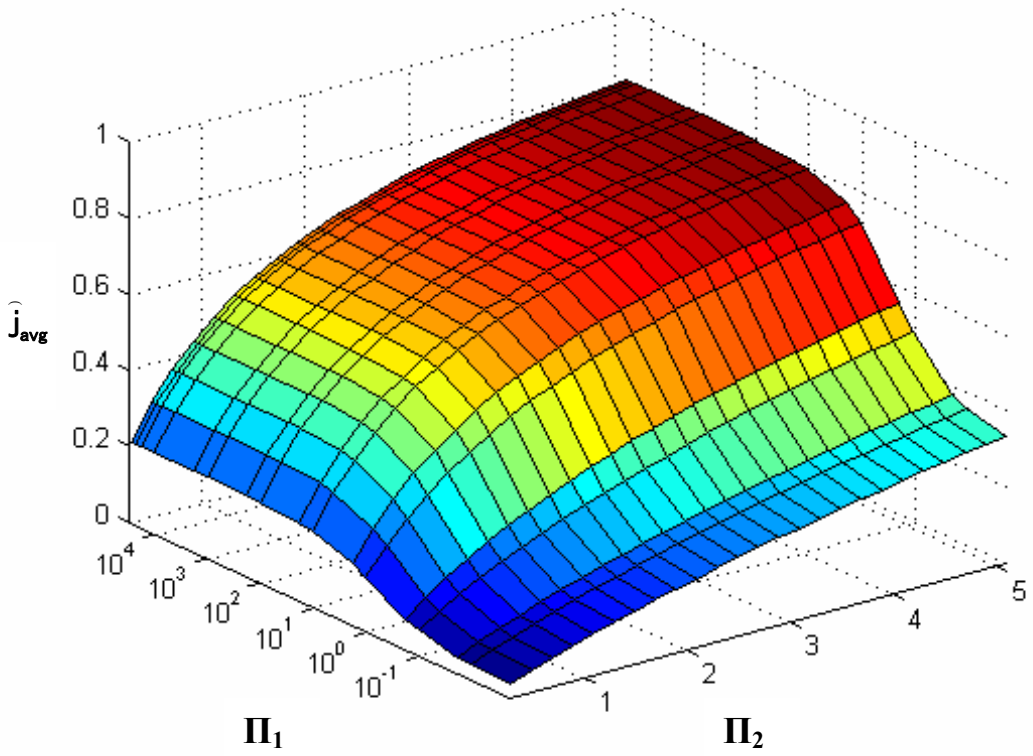

Figure 5.26 – Dimensionless performance map for fuel cell ribbon.

Even with these limitations and relatively simple physics, reasonable agreement is achieved among the experimental data and the non-dimensional model. Table 5.2 shows the Π parameters for each diffusion media, the dimensionless current density achieved experimentally, and the dimensionless current density as determined by the non-dimensional model presented in Chapter 3. Finally, the difference between these two values, using the experimental results as the reference point, can be seen in the final column of Table 5.2.

Table 5.2 – Comparison between dimensionless current density ratio predictions and experimental current density ratio for each diffusion media at 0.5 Volts.

Material	Π_1	Π_2	$\hat{j}_{exp}$	$\hat{j}_{model}$	% Difference
ELAT	310	0.35	0.29	0.24	19.9
ITPN-A	58.2	0.92	0.58	0.43	25.6
ITPN-B	109.7	1.42	0.73	0.54	25.1
CWPT-A	7.01	5.54	0.78	0.81	3.4
CWPT-B	6.46	4.66	0.66	0.78	18.4

**coefficents for MEA V-j realtionship: A = -67.45, B = 208.45, C = -237.0, D = 126.9, E = 36.3, F = 4.1, G = 1.5*

Three major problems exist with comparing experimental data to the results obtained from dimensionless analysis. First, the dimensionless analysis uses an idealized geometry for the fuel cell ribbon concept due to the assumption that an equipotential surface can be achieved at the edge of the GDL. Second, each diffusion material exhibits unique surface and bulk characteristics, therefore causing the presence of unique contact resistances for each diffusion media which cannot be captured when an idealized current-voltage relationship is used to characterize the MEA performance as was done for the dimensionless analysis. Finally, the dimensionless analysis does not incorporate the effects that water production can have on gas transport within the GDL.

The first two problems with the dimensionless analysis can be eliminated by modifying the curve fit used to characterize the MEA current-voltage relationship. When the MEA current voltage relationship is characterized using the *actual* diffusion media of interest in the SFFC fixture, the contact resistances associated with that particular

material, and the bulk through-plane resistance of that material are implicitly included in the MEA current-voltage relationship. The inclusion of the contact resistances in the material specific MEA relationship eliminates the inaccuracies associated with using a generic reference material in the non-dimensional model. Additionally, the total through-plane GDL resistance is captured in the material specific MEA relationship. The results of this modified model are presented in the following section.

5.3 FINITE ELEMENT PREDICTIONS FOR SPECIFIC MATERIALS

Due to the inability of the dimensionless analysis to account for unique contact resistances at the GDL-MEA and GDL-collector plate interfaces, and to capture the total through-plane resistance of the GDL (bulk and contact), an MEA performance curve for each of the diffusion material discussed in this work was generated by collecting data from a cell using the GDL of interest in the SFFC test fixture. When the MEA is characterized using a cell in the SFFC fixture, the only additional resistance introduced due to the conversion from a conventional method of current collection, to a ribbon method of current collection, is the in-plane resistance of the GDL. Using the material specific MEA voltage-current relationship, a new finite element performance prediction was made for each material.[*] This section will present the material specific MEA relationship in the form of a sixth order polynomial for each gas diffusion media. The presented MEA relationship (which captures through-plane effects), along with the in-plane resistance data presented in Section 5.1 were used to generate figures showing how the potential varies along the length of the gas diffusion layers, and how local current density varies along the cathode MEA surface. Finally, a predictive polarization curve was generated for each diffusion media of interest to compare to experimental data and to identify the shortcomings of the finite element model presented in Chapter 3.

[*] Since through-plane resistance (both bulk and contact) is reflected in the material specific polarization curves, the bulk through-plane resistance (ρ_T) in the finite element model from Section 3.2 was set to a very small value. This effectively made the model a 1-D model. Therfore, the model could have been implemented as a solution to a set of ODE's. However, since the finite element model was already constructed, it was more expeditious to simply modify the through-plane resistivity.

5.3.1 ELAT LT-1200W diffusion media prediction

Figure 5.27 presents the data used to generate the sixth order polynomial which is characteristic of the relationship between local current density and local MEA potential when the ELAT gas diffusion media is used as the diffusion layer in the fuel cell. This is simply the data collected in a SFFC fixture, but reversed to display current density as the dependent variable.

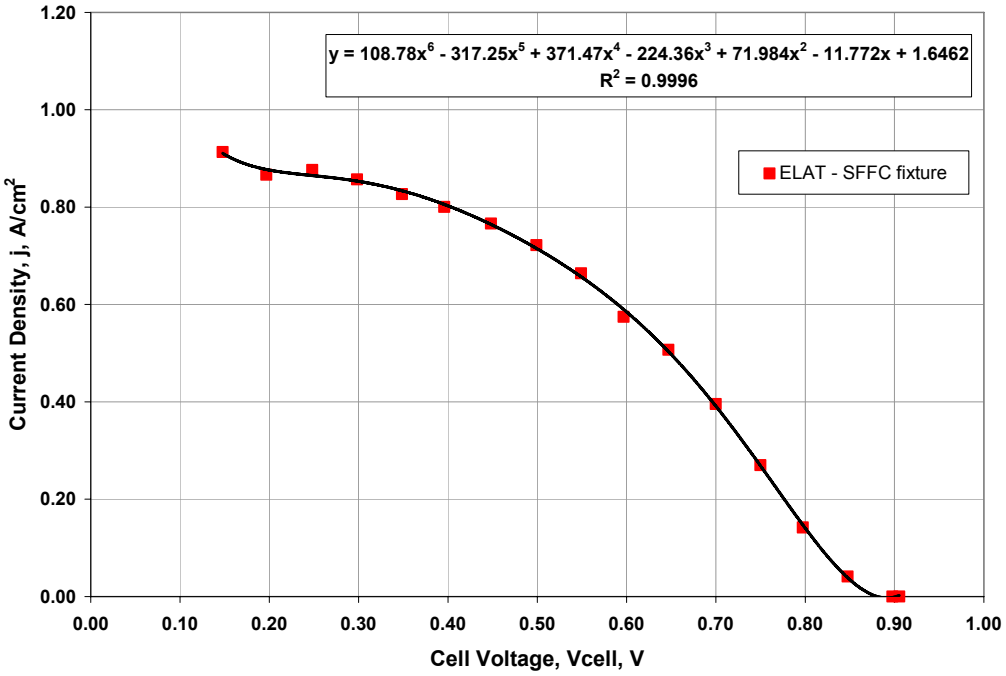

Figure 5.27 – Curve fit to characterize MEA performance when using ELAT.

Once the relationship presented above and the in-plane resistive data from Section 5.1 was substituted into the finite element model it was possible to generate Figure 5.28. Figure 5.28 shows the variation in potential along the anode and cathode GDLs when the cell potential between the current collectors is specified to be 0.5 V. Figure 5.29 shows the variation in current density leaving the MEA at the cathode. It can be seen that both the GDL potential and the local current density vary significantly due to the high in-plane resistance of ELAT.

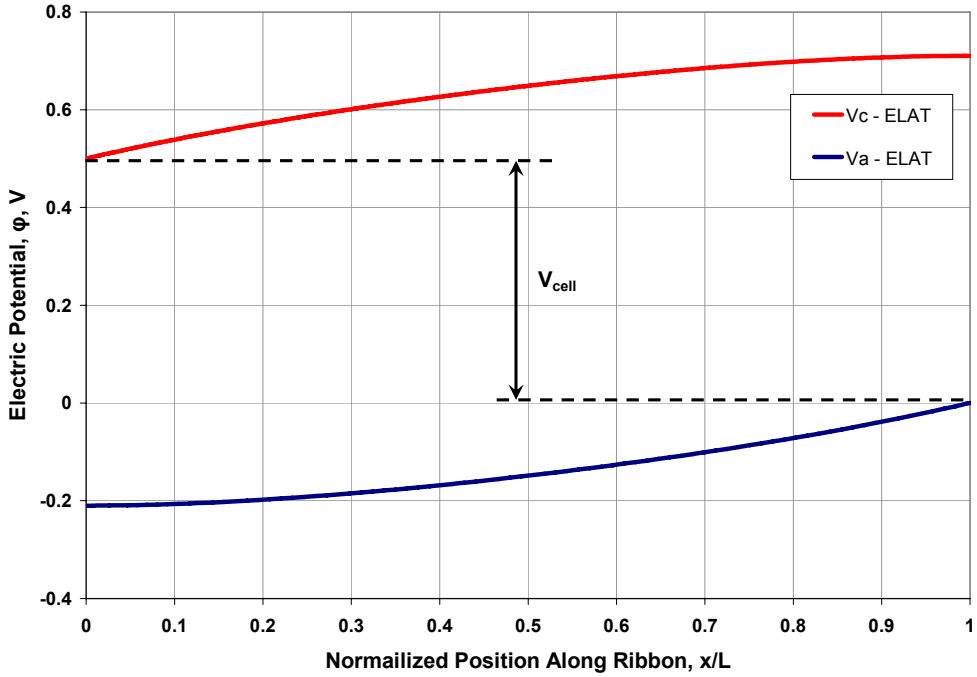

Figure 5.28 – Voltage variation for ELAT ribbon at 0.5 V.

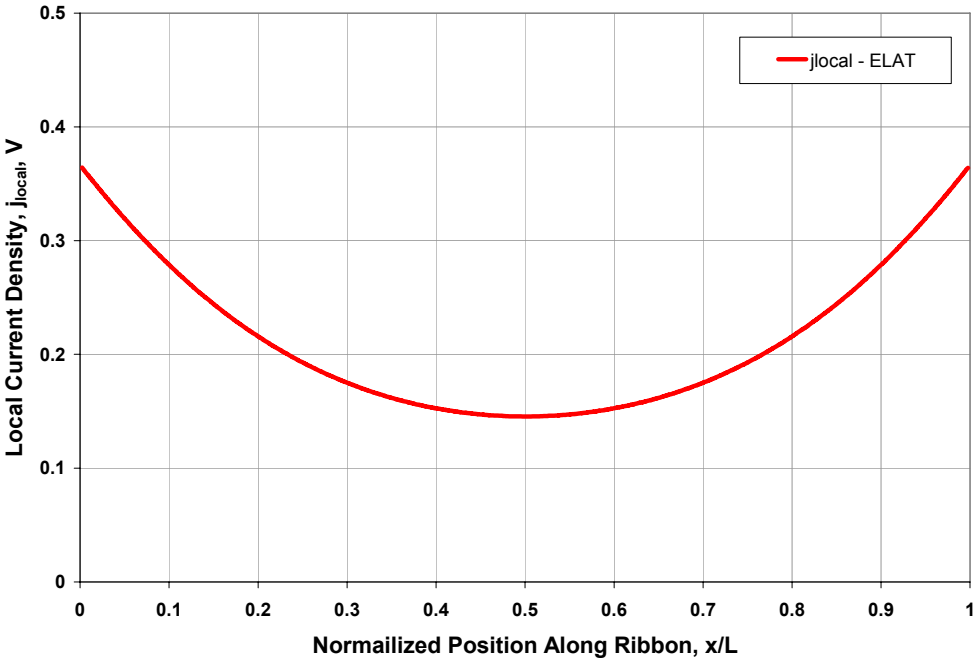

Figure 5.29 – Local current density variation for ELAT ribbon at 0.5 V.

A model which can only evaluate a single point is of little use for an energy system such as a PEM fuel cell due to the potentially dynamic nature of the power load. Therefore, a prediction of the polarization performance of the ELAT material was also performed using the finite element model. Rather than looking at the local potential and current generation as was done in Figures 5.28 and 5.29, a polarization curve looks at the output potential and current of a fuel cell. Figure 5.30 presents the predicted and experimental polarization behavior of an MEA using ELAT as the GDL.

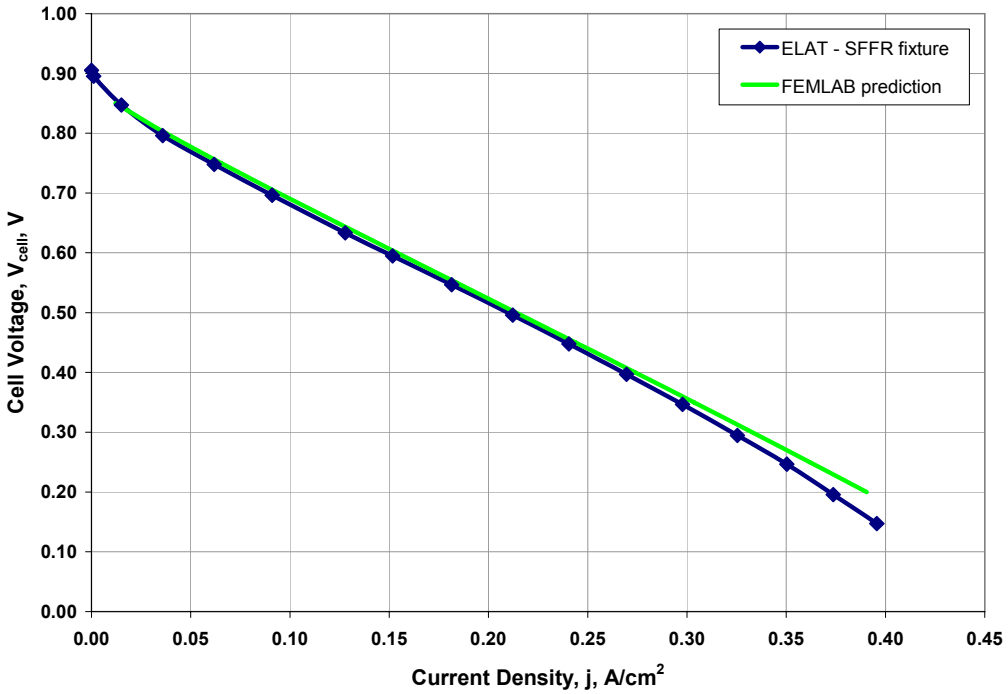

Figure 5.30 – Finite element results and experimental data for ELAT ribbon cell.

The polarization predictions for the cell using ELAT as a GDL agree quite well with the experimental results. The average deviation in current density between the two curves at voltages less than or equal to 0.8 V is less than 3%. This level of error is likely within the range of error associated with fuel cell performance measurements when parameters such as relative humidity and temperature are considered.

5.3.2 ITPN series diffusion media prediction

The same process used for the fuel cell using ELAT gas diffusion layers was followed for the cells using the ITPN-A and ITPN-B materials. Figure 5.31 shows the curve fit relating local current density to local MEA potential gradient obtained from data collected using the conventional test fixture for the ITPN-A material. Due to the lower in-plane resistance of the ITPN-A material compared to ELAT, the local GDL potential (Fig. 5.32), and local current density (Fig. 5.33), both show significantly less variation with position along the fuel cell ribbon.

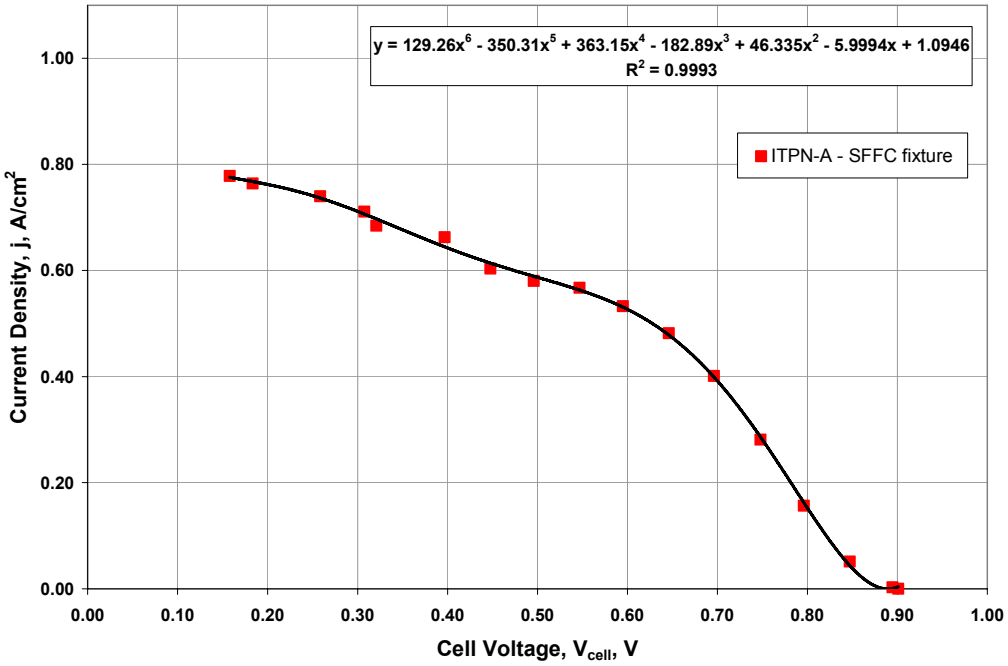

Figure 5.31 – Curve fit to characterize MEA performance when using ITPN-A.

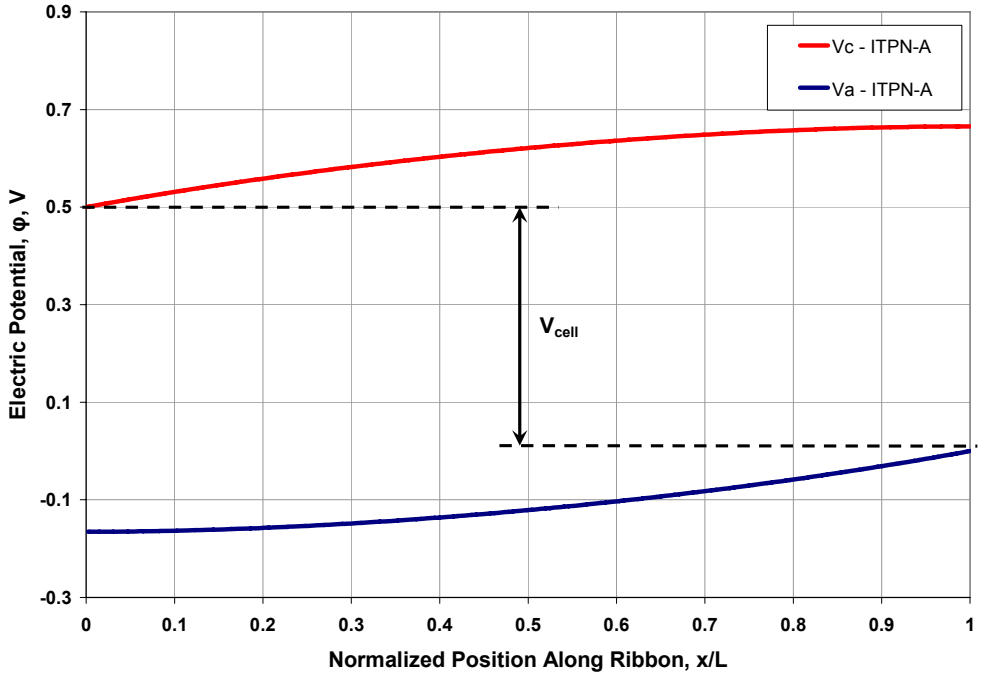

Figure 5.32 – Voltage variation for ITPN-A ribbon at 0.5 V.

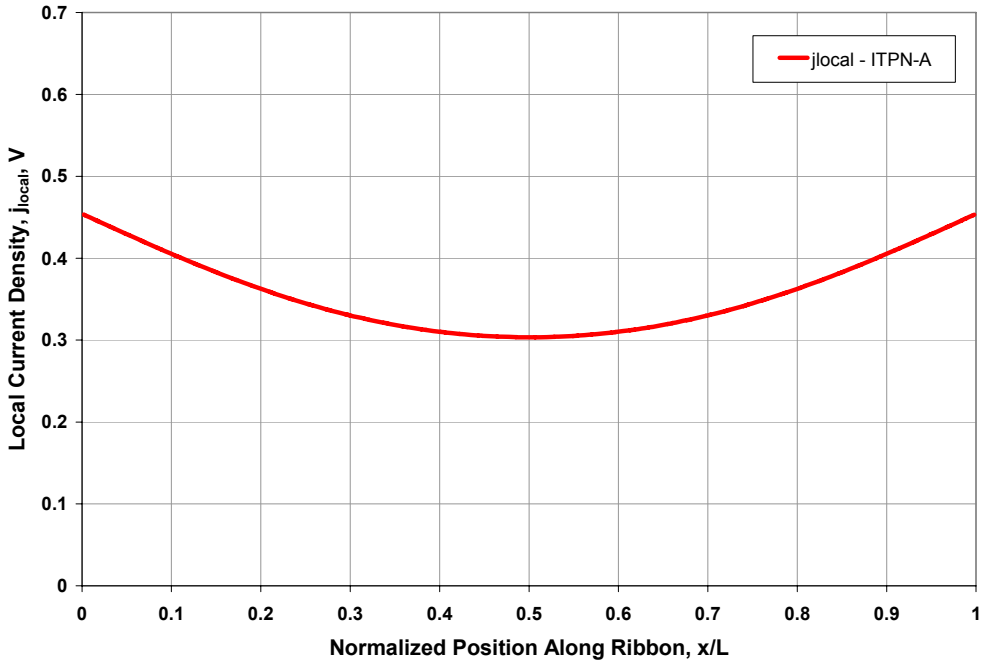

Figure 5.33 – Local current density variation for ITPN-A ribbon at 0.5 V.

The finite element predictions for the performance of the ribbon cell using the ITPN-A diffusion media were again reasonably accurate when the simplicity of the physics included in the model is considered. The average deviation in current density between the prediction and the experimental data at cell voltages less than or equal to 0.85 V is approximately 6%. The prediction and experimental data for the ITPN-A test cell can be seen in Figure 5.34.

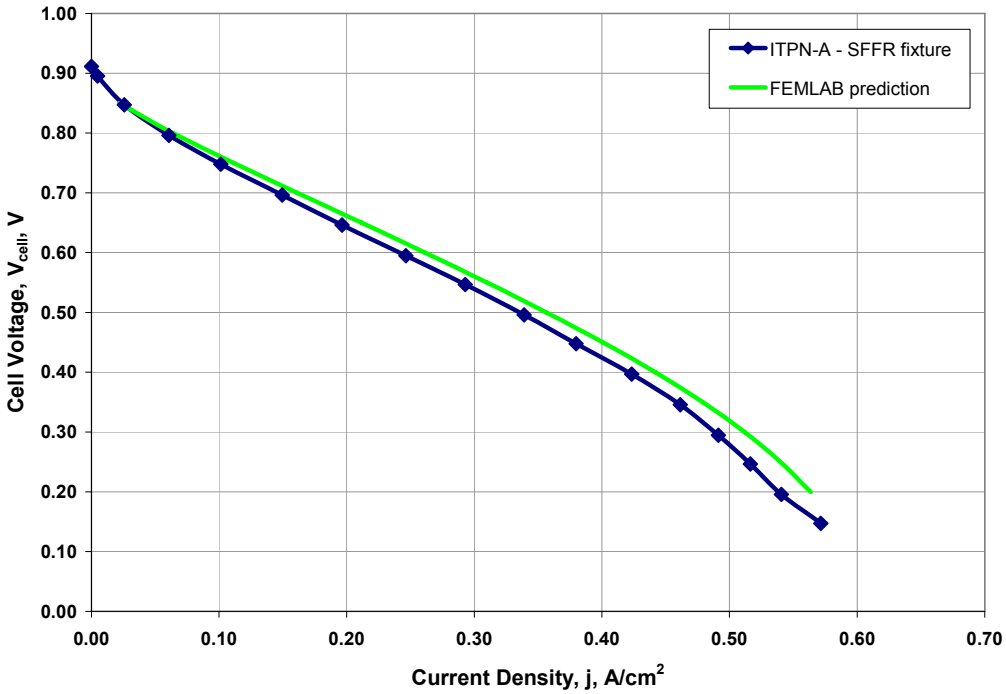

Figure 5.34 – Finite element results and experimental data for ITPN-A ribbon cell.

Figure 5.35 shows the curve fit used to characterize the MEA performance of the ITPN-B ribbon cell. Since the ITPN-A material and the ITPN-B material have similar resistive properties it is not surprising to see in Figures 5.36 and 5.37 that similar variation occurs in the GDL potential and local current density for both materials.

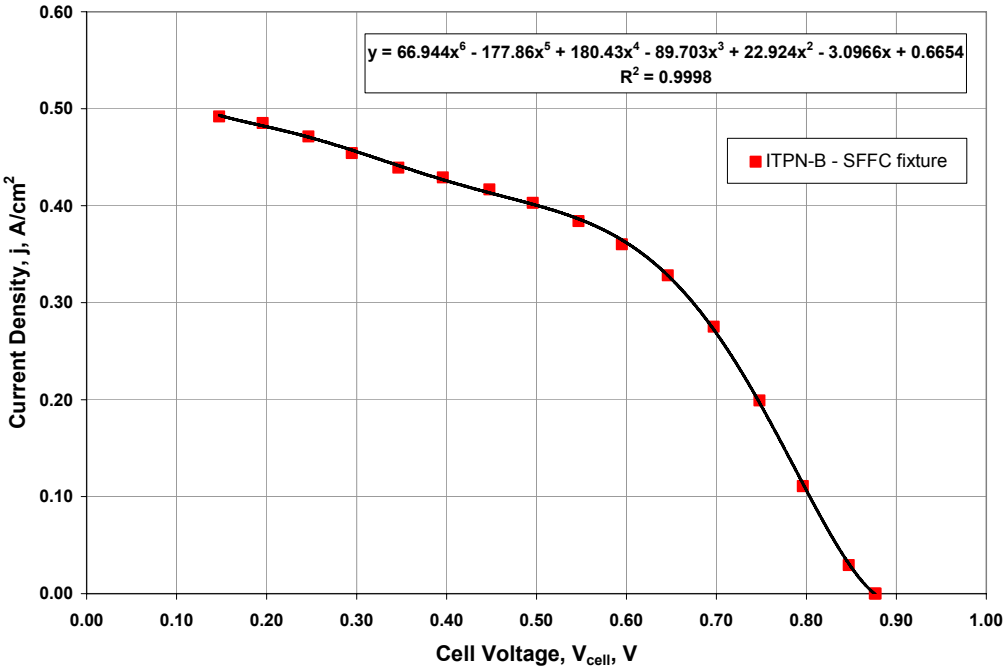

Figure 5.35 – Curve fit to characterize MEA performance when using ITPN-B.

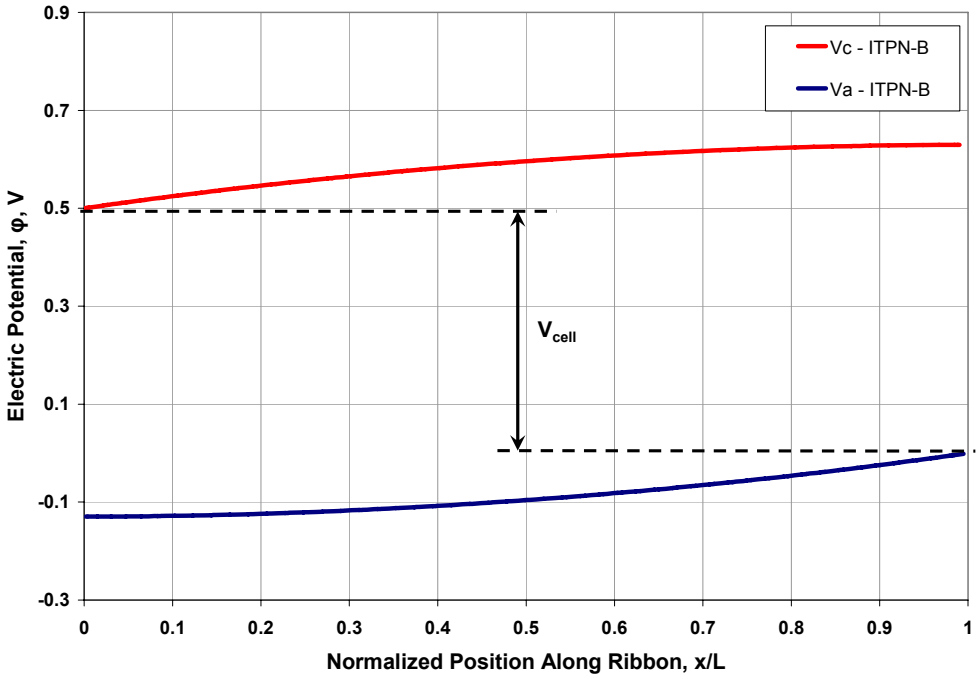

Figure 5.36 – Voltage variation for ITPN-B ribbon at 0.5 V.

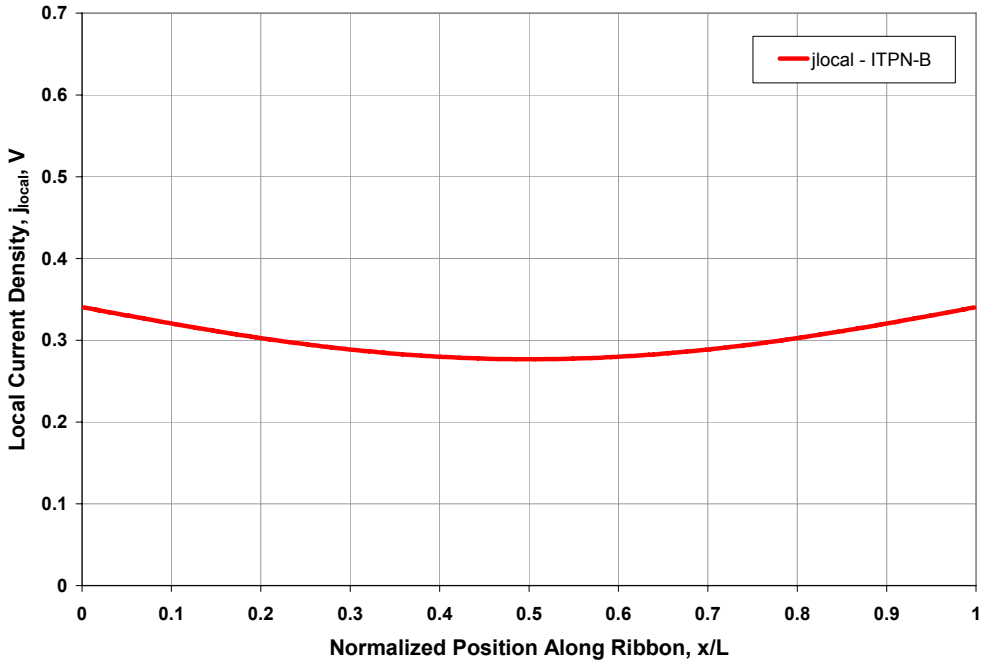

Figure 5.37 – Local current density variation for ITPN-B ribbon at 0.5 V.

The predicted polarization performance for the ribbon cell using ITPN-B diffusion layers (Figure 5.38) is significantly lower than the predicted performance of the ribbon cell using the ITPN-A diffusion layers. It may seem inconsistent that two material which exhibit nearly identical resistive properties could result in two different performance predictions. The reason for the difference is that although the added carbon black pore filler did improve the electrical properties, it also significantly reduced the ITPN-B material's ability to transport gases effectively. Therefore, the difference between the two materials is not captured in the materials themselves where only in-plane resistance is specified, but the difference is captured at the MEA interface where the conventional data is used to characterize the conventional V-I performance achieved at that interface. This result is indicative of the importance of characterizing the MEA performance in a conventional manner for each diffusion media prior to running the model.

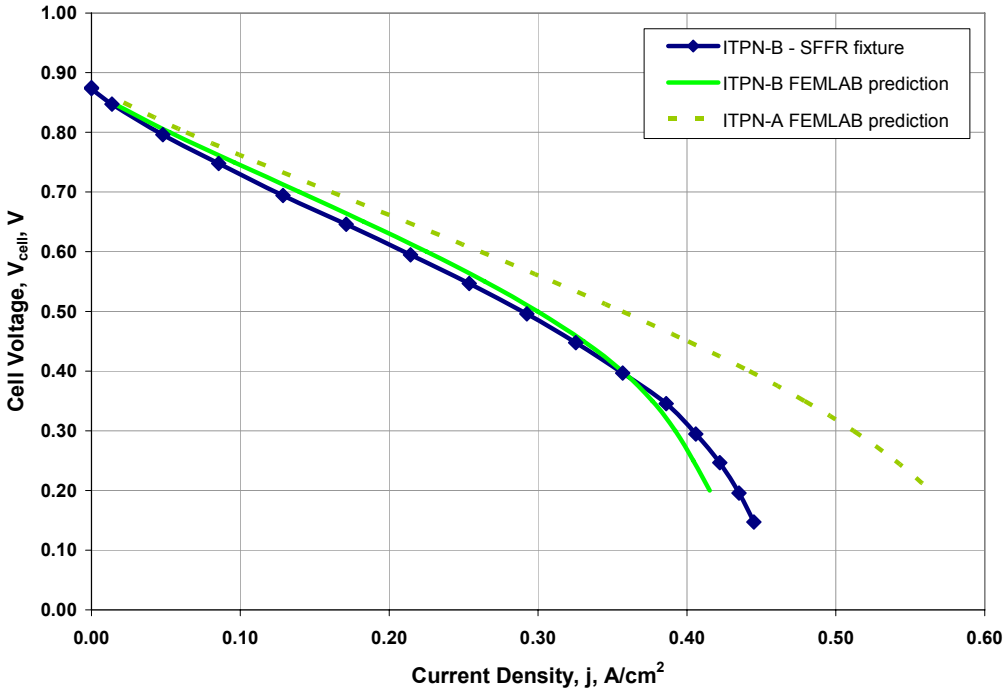

Figure 5.38 – Finite element results and experimental data for ITPN-B ribbon cell.

5.3.3 CWPT series diffusion media prediction

The curve used to represent the I-V characteristics of the MEA with the CWPT-A diffusion layer is presented in Figure 5.39. It can be seen in Figure 5.40 that the variation in voltage as a function of position is minimal due to the very low in-plane resistance of the CWPT-A material. The current density distribution along the MEA, shown in Figure 5.41, also indicates that the in-plane resistance is sufficiently small to allow for nearly uniform current generation along the length of the fuel cell ribbon using the CWPT-A material.

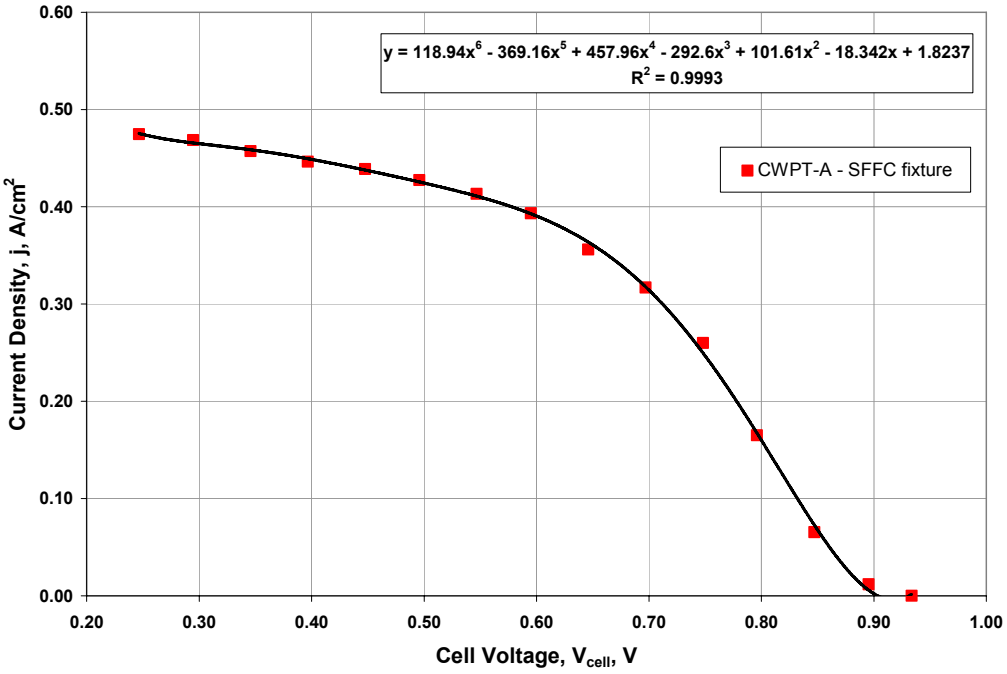

Figure 5.39 – Curve fit to characterize MEA performance when using CWPT-A.

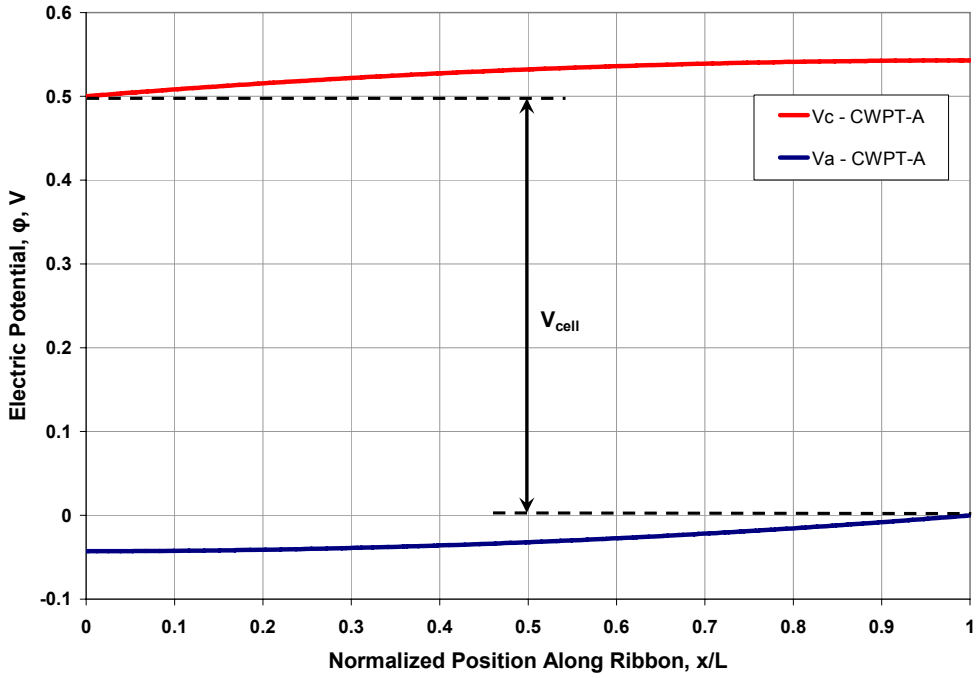

Figure 5.40 – Voltage variation for CWPT-A ribbon at 0.5 V.

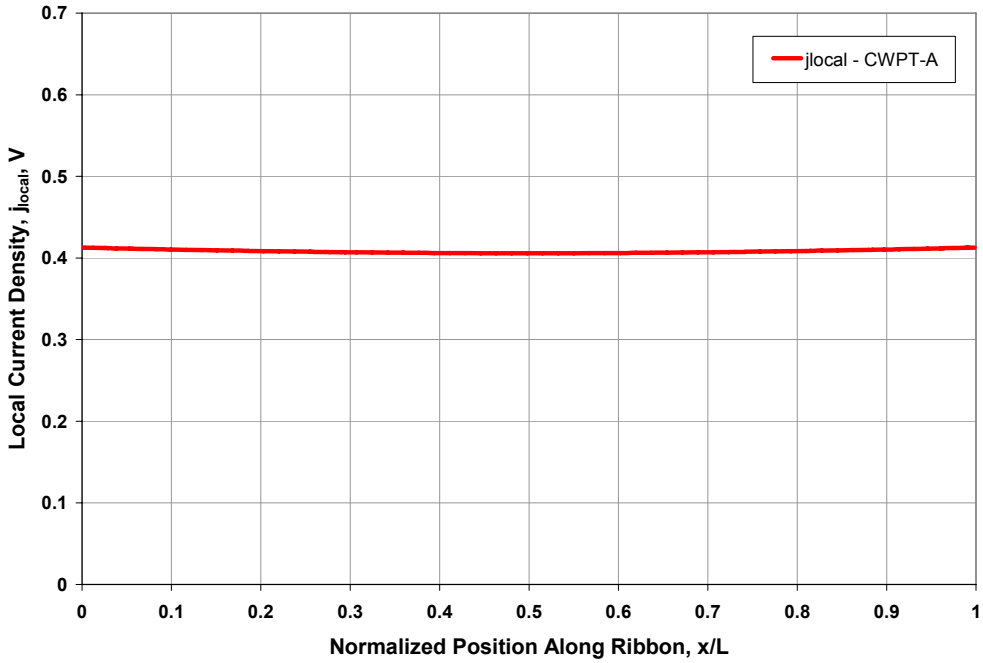

Figure 5.41 – Local current density variation for CWPT-A ribbon at 0.5 V.

It can be seen in Figure 5.42 that the finite element prediction was not as accurate as it was for the previously discussed materials. This behavior is expected at relatively high current densities because the ribbon cell using the CWPT-A GDL exhibits far greater mass diffusion limitations at current densities above 0.25 A/cm^2 than is observed for the ELAT and ITPN materials. Although the model partially includes diffusive losses as an through the I-V curve for the MEA, it lacks suitable characterization of the effect that liquid water can have within the porous structure of the catalyst layers and GDL.

In addition, the material specific MEA characterization of I-V performance includes the GDL-collector plate contact resistance associated with the SFFC fixture, rather than the GDL-collector plate contact resistance associated with the SFFR fixture. The GDL-collector plate contact resistance in the SFFR fixture is likely approximately three times the contact resistance encountered in the SFFC fixture due to the difference in contact area with the collector plates. The factor of three increase in GDL-collector plate contact resistance is not significant for finely woven smooth material that already exhibit minimal contact resistance due to their flat uniform surfaces. But, when the CWPT materials are considered, it is likely that the contact resistance is a major contributor to

the ohmic resistance encountered in the test fixture due to the coarsely woven nature of the material. Therefore, a factor of three increase in the GDL-collector plate contact resistance could significantly affect the finite element predictions. The polarization curve prediction presented in Figure 5.42 shows a fundamental difference in slope even at current densities less than 0.2 A/cm^2. This difference in slope is indicative of a misrepresentation of a purely ohmic (not electrochemical) loss such as contact resistance, in the CWPT-A fuel cell ribbon.

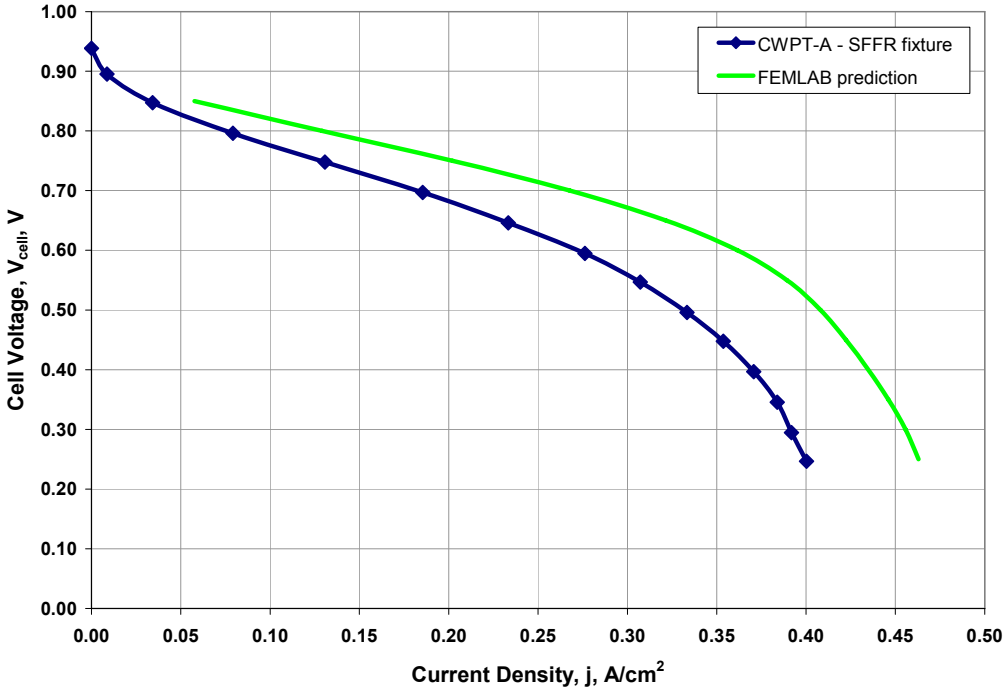

Figure 5.42 – Finite element results and experimental data for CWPT-A ribbon cell.

The MEA interface I-V characteristic curve for the CWPT-B test cell can be seen in Figure 5.43. Similar potential variation are observed in Figure 5.44 for the CWPT-B test cell being operated at a cell potential of 0.5 V, as were observed for the CWPT-A test cell. This result was expected due to the similar in-plane resistance measured for both materials. The current density distribution for the CWPT-B material is also similar to distribution for the CWPT-A material, and can be seen in Figure 5.45.

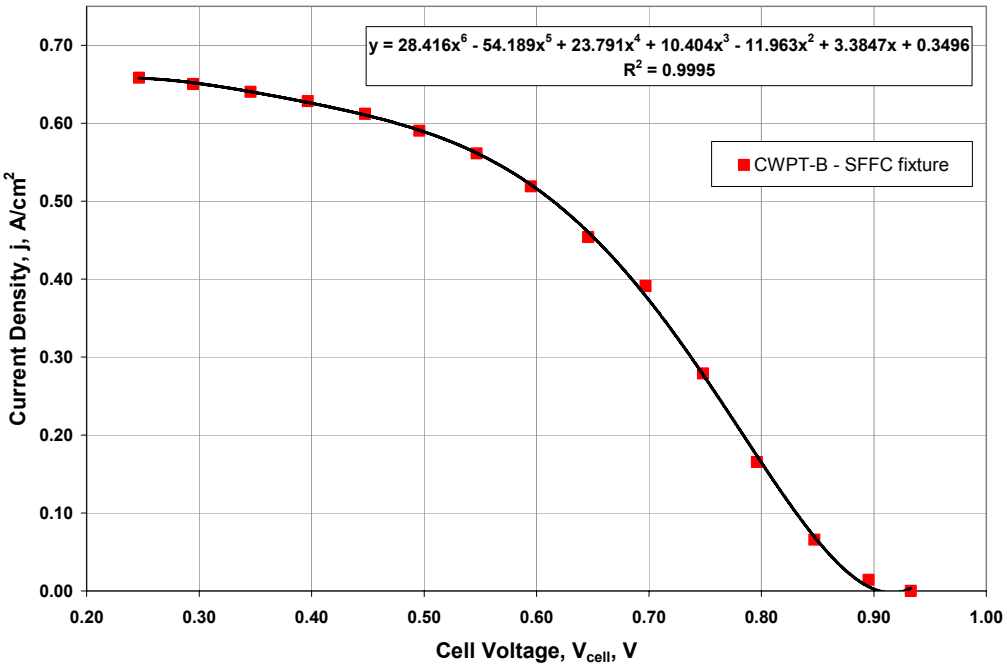

Figure 5.43 – Curve fit to characterize MEA performance when using CWPT-B.

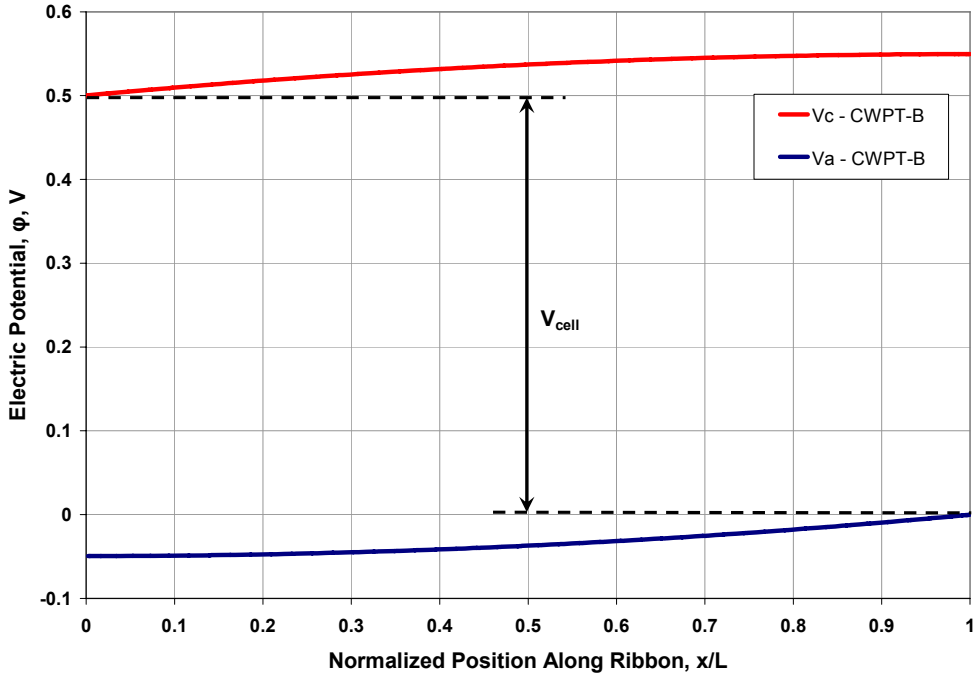

Figure 5.44 – Voltage variation for CWPT-B ribbon at 0.5 V.

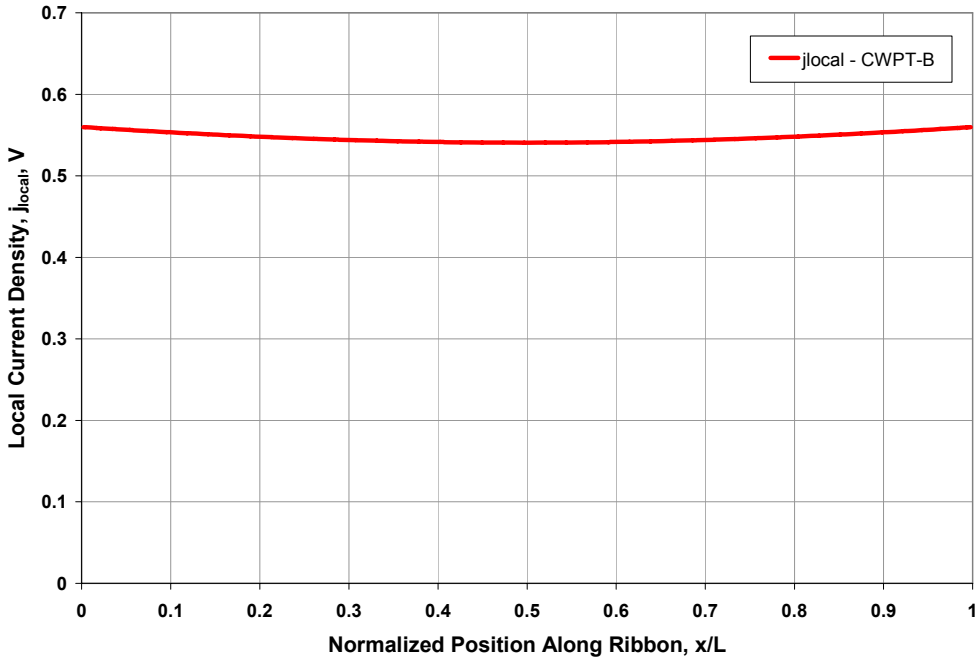

Figure 5.45 – Local current density variation for CWPT-B ribbon at 0.5 V.

The finite element polarization prediction for a ribbon fuel cell using the CWPT-B material as its gas diffusion layers can be seen in Figure 5.46. It can again be seen that the greatest deviation between the prediction and the experimental data occurs at the highest current densities where mass transport becomes the limiting factor. The improper representation of slope at low current densities observed for the CWPT-A cell is also prevalent for the cell using the CWPT-B GDL. It is again believed that the lack of slope agreement is due to the unaccounted for increase in contact resistance in the SFFR fixture versus the SFFC fixture. If, as suggested, the difference between the FEMLAB prediction and the actual data is due to contact resistance at the current collection point, then improving this contact area should lead to dramatic increases in performance. For example, if the current density at 0.5 V could be increased to the predicted value, the resulting current density of 0.55 A/cm^2 would be more than double the reported performance of any other fuel cell using in-plane current collection observed in the literature.

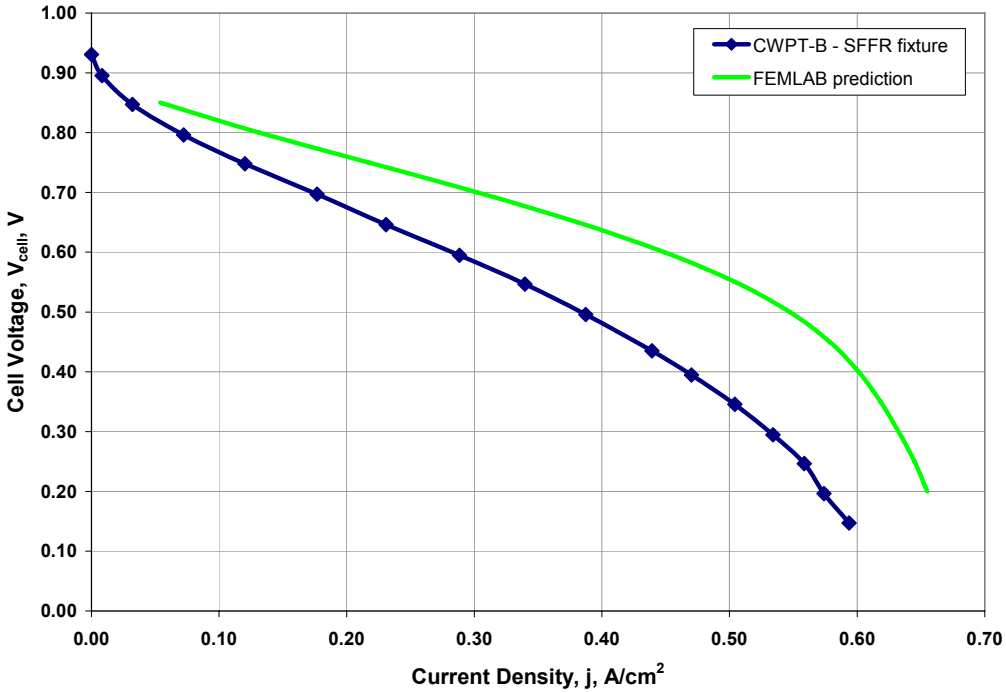

Figure 5.46 – Finite element results and experimental data for CWPT-B ribbon cell.

5.4 EXPLORATORY INVESTIGATION OF CWPT-B PERFORMANCE

Following the high current density achieved by the CWPT-B test cell when using 380 µm gaskets, an exploratory investigation of the potential performance of this test cell was performed. The first step taken was to determine the maximum possible performance attainable in the SFFR fixture when operating on air. In order to determine this, the cathode flow was doubled to a value of 1100 sccm (12 times stoichiometric flow at 1 A/cm^2) in order to provide a higher partial pressure of oxygen in the flow, and to aid in the removal of liquid water droplets from the GDL and gas channels. The resulting polarization curve is presented in Figure 5.47. It can be seen that the current density at 0.5 V increased from approximately 0.38 A/cm^2 at the low flow condition, up to approximately 0.44 A/cm^2 at the high flow condition. Since the stoichiometric ratio at the increased flow rate was so high it is unlikely that the improved performance seen in Figure 5.46 is due to reduced oxygen depletion in the fuel cell. However, it is believed that the increased velocity of air moving through the gas channels over the GDL

enhanced the removal rate of water from the cathode GDL. The more effective removal of water likely led to improved oxygen diffusion to the catalyst sites, thus improving performance.

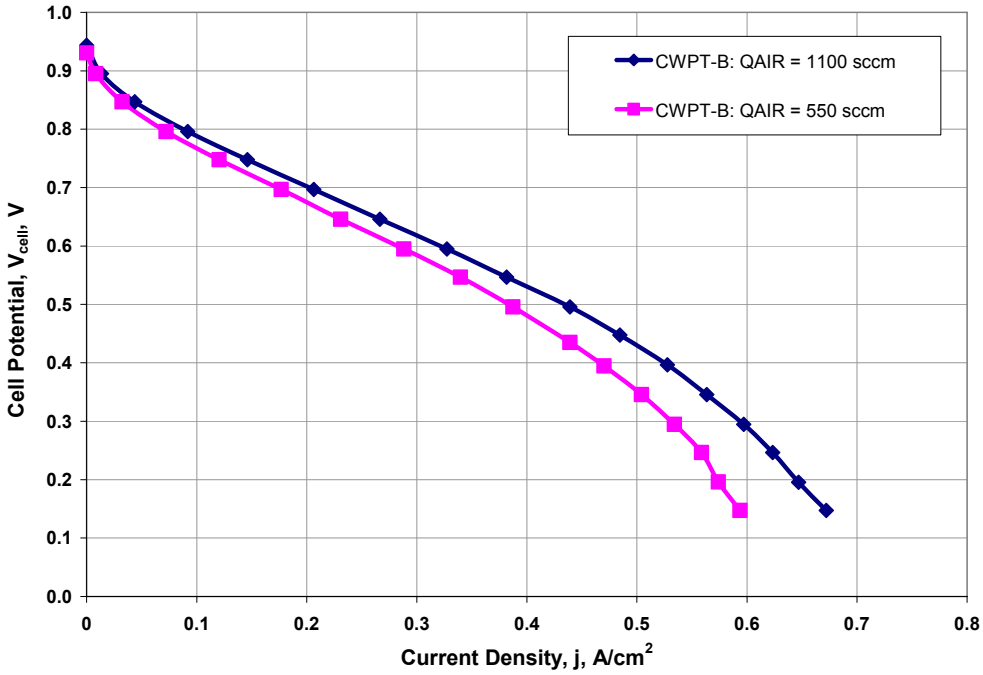

Figure 5.47 – CWPT-B performance in the SFFR fixture at high cathode flow.

The next step in the exploratory study of the CWPT-B material was to evaluate the quality of the adhesion between the CWPT-B GDL and the MEA. To do this, a series of tests were performed in the OFFR fixture. The first test in the OFFR fixture was simply an attempt to warm the cell up to 80°C and take a polarization curve. But, during the warm up process which can be seen in Figure 5.48, the current density at 0.5 V quickly rose to a value of 0.5 A/cm^2, then subsequently dropped significantly. One explanation for the high initial current density in the OFFR fixture is the lack of gas channel shoulders compressing the GDL. When gas channel shoulders compress the GDL, they cause reduced permeability, and thus lower current density below the shoulders. Therefore, if the shoulders are eliminated, a more even distribution of gas occurs over the entire surface of the electrode. Unfortunately, the high current density observed for the

CWPT-B material in the OFFR test fixture only survived for approximately 25 minutes after which the current density began to drop significantly.

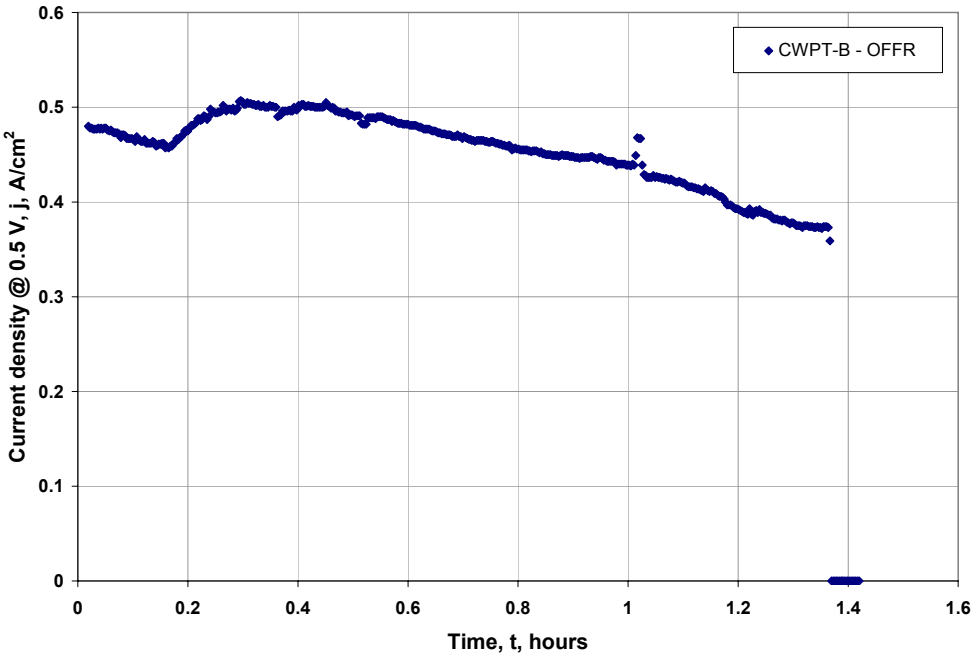

Figure 5.48 – CWPT-B performance during warm-up in the OFFR fixture at 0.5 V.

There are two possible causes for the significant drop in current density observed after 25 minutes in OFFR fixture. The first is that the initial high current density caused the electrode to flood due to increased water production. The second is that the adhesion between the GDL and the MEA began to fail. Failure of the adhesion between the GDL and MEA is a possibility in the OFFR fixture because there are no gas channel shoulders to apply pressure to the interface.

In order to determine which effect was the likely cause of the reduced performance, the cell was heated to the desired operating temperature of 80°C while producing no water. This was done by heating the cell while flowing humidified hydrogen on the anode, and humidified nitrogen on the cathode. By avoiding water production during the warm-up period, it was possible to avoid the formation of water condensate in the pores of the GDL. Ensuring that the GDL was not flooded during the

warm-up period was critical to diagnosing the source of the decreased performance over time observed in the OFFR fixture.

Once the cell reached 80°C, the cathode gas was switched to humidified air to allow the cell to produce current. The load was set to hold a constant current density (and consequently a constant rate of water production) of 0.1 A/cm^2. A plot of cell voltage and cell high frequency resistance (HFR), as a function of time can be seen in Figure 5.49. The HFR is a measure of the purely resistive component of the losses within the cell. Therefore, if water is being produced and no other source of ohmic resistance is introduced, then the HFR should never increase since the only effect that water production can have on HFR is to lower the ionic resistance of the membrane. But, it can be seen in Figure 5.49 that the HFR increases over time, thus indicating that a new source of ohmic resistance develops over time. The most likely source for this increasing ohmic resistance is the failure of the bond between the GDL and the MEA. This failure causes an increase in contact resistance at the GDL-MEA interface.

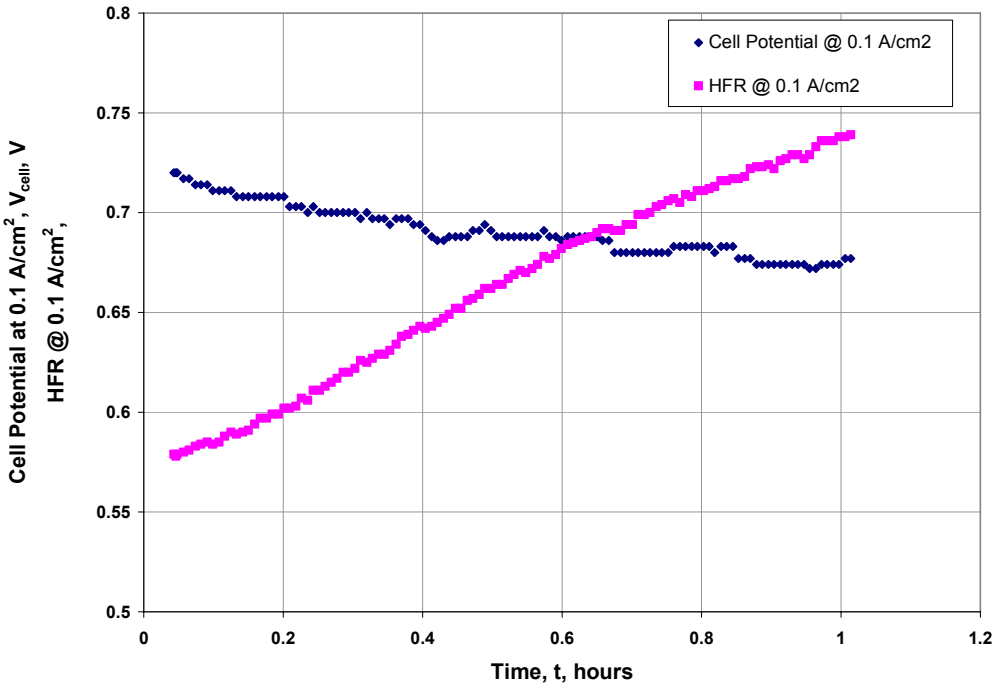

Figure 5.49 – Voltage and HFR trace of CWPT-B cell operating at constant current.

It is promising that the MEA with the CWPT-B GDL exhibited very high performance when it was first placed in the OFFR test fixture. The observed performance is approximately 25% higher than what has been observed in the SFFR fixture, and more than twice the current density reported in the literature for cells which use in-plane current collection. Unfortunately, the high performance was short lived. The time trace of HFR and cell voltage suggests that the GDL was delaminating from the MEA, thus causing a significant increase in the contact resistance at the MEA-GDL interface. This information will be very valuable for future development of the fuel cell ribbon concept.

6 CONCLUSIONS AND RECOMMENDATIONS

This work has presented an abundance of analytical and experimental results pertaining to the development of the fuel cell ribbon technology. Conclusions regarding these results, along with recommendations for future work based on these results will be presented in this chapter. In addition, a few closing remarks concerning the past, present, and future status of ribbon fuel cells will be made to conclude this work.

6.1 CONCLUSIONS

This work has yielded experimental procedures and analytical tools to support ribbon cell development. Experimental fixtures to characterize material properties critical to fuel cell ribbon performance were demonstrated. In addition, experimental fixtures were developed to evaluate diffusion media performance in conventional cells (SFFC), cells that utilize in-plane current collection and GDL compression (SFFR), and cells that utilize in-plane current collection and no GDL compression (OFFR). In addition, analytical tools to predict ribbon cell performance were developed and demonstrated to have reasonable accuracy. The experimental and analytical tools developed in the course of this research were demonstrated to be useful for guiding fuel cell ribbon development.

The results from the experimental work have identified critical material characteristics as well as treatments that can improve ribbon cell performance. Results from the resistance measurements indicate that pitch based carbon fiber materials provide significant reduction in in-plane resistance when compared to the more widely used PAN based materials. The reduced in-plane resistance of the pitch fiber based materials is ideal for fuel cell ribbon assemblies. In addition to reducing losses due to the in-plane current travel, low resistance pitch based materials may also provide benefits associated with more uniform current density. It is important to note that the corrosion resistance of pitch based diffusion media has not been characterized as completely as the corrosion resistance of PAN based diffusion media. Corrosion is a major concern in PEM fuel cells due to the possibility of reduced durability if corrosion takes place.

When the bulk treatments were compared, the material property characterization revealed that bulk Treatment B decreased in-plane and through-plane resistance at the expense of reduced permeability. However, the materials to which Treatment B was applied were still sufficiently permeable when compared to the commercially available ELAT diffusion media. Thus, treating the gas diffusion media with a PTFE and carbon emulsion appears to be a useful approach for improving ribbon cell performance. Future research related to the ratio of PTFE to carbon black used for treatment B could prove to be beneficial since significant reduction in resistance was observed for the single ratio of PTFE to carbon black investigated in this work.

The results from the analytical work have identified important observations about the local current density exhibited in ribbon cells and the accuracy of the finite element predictions. The *finite element predictions* presented in Chapter 5 show reasonable accuracy when compared to the experimental data. It is important to note that when the experimental polarization data was nearly linear (ELAT and ITPN series) that the model is extremely accurate since the model was designed with resistive losses in mind. Yet, when the experimental polarization curves exhibited a distinct change in slope due to mass transport limitations, the model tends over predicts the performance. This over prediction occurs because the mass diffusion limitations at each current density are not accounted for within the GDL domains of the model, but are only included implicitly at the MEA interface. The implicit inclusion of diffusive losses cannot sufficiently model the effects of local pore blockage in the GDL and catalyst layer. In spite of its limitations, the numerical model provided insights that could not have been obtained in other ways. For example, the relatively uniform local current density predicted by the model for ribbon cells using pitch based GDLs may provide enhanced durability in comparison to the PAN based materials. The wide variation in local current density predicted for the ELAT and ITPN materials would undoubtedly cause temperature gradients along the MEA which could cause a variety of problems to arise such as temperature induced stresses within the membrane. The minimal variation in local current density along the length of the fuel cell ribbon exhibited by the ribbons using the CWPT GDL's is another indication that pitch based materials are the prime candidates for fuel cell ribbon production.

The results of this work have also demonstrated the potential for fuel cell ribbon performance. The ribbon cells using pitch based diffusion layers demonstrated 67-78% of the current density achieved at 0.5 V when a conventional method of current collection is employed. In addition, a ribbon cell using a pitch fiber based GDL reached a current density at 0.5 V which was nearly twice the best value observed in literature in the SFFR test fixture. Even greater performance was achieved when the same cell was tested in the OFFR fixture, although this performance could not be sustained.

Overall, the objectives of this work, presented in Section 1.5, were met. Although the results of this work demonstrate the potential for fuel cell ribbon assemblies, several issues must still be addressed:

- Diffusion limitations seem to be a concern particularly in high current density regimes that are prone to flooding (as was achieved for the CWPT-B GDL). Therefore, coarse materials may not be amenable to good water transport.
- Some of the deviation between analytical and experimental results could be explained by significant contact resistance effects. The uneven surface of the coarsely woven pitch material is likely to exhibit large contact resistance. Approaches need to be identified to overcome this challenge.
- Preliminary results suggest that delamination of the GDL is a concern in the OFFR fixture. This concern needs to be addressed by a performing a more detailed study of the adhesion quality between the CWPT materials and a catalyzed membrane.

6.2 RECOMMENDATIONS FOR FUTURE WORK

This work addressed the fuel cell ribbon concept from an analytical and an experimental perspective. Based on the experience gained during this work, recommendations can be made for future work. These recommendations are presented as two lists; one for the continuation of the analytical efforts, and one for the continuation of the experimental efforts.

6.2.1 Recommendations for future analytical work

- *Replace the I-V curve fit at the MEA with a mathematical representation of the actual electrochemistry and transport phenomena taking place in the GDLs, catalyst layers, and membrane.* This will tie the effects of gas transport, proton transport, and electron transport together leading to a far more accurate representation of the interactions among these phenomena.
- *Include the effects of liquid water production, transport, and saturation in the GDL and catalyst layer of the 2-D model.* This will allow for diffusive losses within the ribbon cell to be more accurately modeled and will improve performance predictions.

6.2.2 Recommendations for future experimental work

- *Characterize and improve water transport within a diffusion material similar to the CWPT material.* This will enable understanding of the possible flooding which occurs in the CWPT materials and identify the key properties which can be tailored to improve water transport.
- *Improve the application of conductive filler, MPL, and adhesion to the MEA for a material similar to the CWPT material in order to improve the performance of fuel cells using the material as a GDL in a conventional and ribbon current collection scheme.* Optimizing the bulk treatments and adhesion characteristics of a high conductivity pitch based substrate could significantly improve the performance achieved in a ribbon configuration. The improved performance is expected to be within 15% of the performance observed for an MEA using commercially available GDLs in a conventional cell fixture.
- *Develop test fixtures for characterization of 3-cell fuel cell ribbon stacks to investigate varying methods of gas delivery.* Gas delivery is closely related to electrode flooding due to the importance of the gas streams removing water

droplets from the GDL surface. Additionally, a 3-cell ribbon assembly would be useful to identify potential challenges associated with additional cells.

- *Investigate the resistance to corrosion of pitch based diffusion media.* Since the corrosive properties of pitch based diffusion media in a PEM fuel cell environment is not well documented it is necessary to investigate this further to avoid durability issues in fuel cell ribbon assemblies.

6.3 CLOSING REMARKS

The development of the fuel cell ribbon concept is still in its early stages. The purpose of this work was to address the core issue of achieving suitable performance by means of applying a low in-plane resistivity material as a gas diffusion layer. Analytical results suggest that ribbon cells can yield current densities up to approximately 85% of that exhibited in conventional cells. Experimental results demonstrated a ribbon cell current density which was 79% of the current density achieved in a conventional cell at 0.5 V using first generation ribbon cell materials. These results suggest that the ribbon cell technology is very promising. The work presented here has laid the groundwork needed for further research aimed toward optimization and commercialization of fuel cell ribbon assemblies.

REFERENCES

[1] W. K. Lee, C. H. Ho, J. W. Van Zee, and M. Murthy, "The effects of compression and gas diffusion layers on the performance of a PEM fuel cell," *Journal of Power Sources*, 84:1 (1999), 45-51.

[2] X. Li and I. Sabir, "Review of Bipolar Plates in PEM Fuel Cells: Flow-field Designs," *International Journal of Hydrogen Energy*, 30:4 (2005), 359-371.

[3] DRI, "http://www.dri.edu/Projects/Energy/Fuelcells/img003.GIF," 12/12/2005,

[4] M. Ellis and D. Dillard, "*VTIP Disclosure No. 03.-129, "Novel PEM Fuel Cell Architectures"*," 2001.

[5] A. Heinzel, C. Hebling, M. Muller, M. Zedda, and C. Muller, "Fuel cells for low power applications," *Journal of Power Sources*, 105:2 (2002), 250-255.

[6] A. Heinzel, R. Nolte, K. Ledjeff-Hey, and M. Zedda, "Membrane fuel cells - concepts and system design," *Electrochimica Acta*, 43:24 (1998), 3817-3820.

[7] R. Z. Jiang and D. R. Chu, "Stack design and performance of polymer electrolyte membrane fuel cells," *Journal of Power Sources*, 93:1-2 (2001), 25-31.

[8] S. J. Lee, A. Chang-Chien, S. W. Cha, R. O'Hayre, Y. I. Park, Y. Saito, and F. B. Prinz, "Design and fabrication of a micro fuel cell array with "flip-flop" interconnection," *Journal of Power Sources*, 112:2 (2002), 410-418.

[9] J. M. Song, S. Y. Cha, and W. M. Lee, "Optimal composition of polymer electrolyte fuel cell electrodes determined by the AC impedance method," *Journal of Power Sources*, 94:1 (2001), 78-84.

[10] Detech, "www.detechinc.com/em/quad.htm," 12/13/2005,

[11] I. Bar-On, R. Kirchain, and R. Roth, "Technical cost analysis for PEM fuel cells," *Journal of Power Sources*, 109:1 (2002), 71-75.

[12] US-DOE, "http://www.eere.energy.gov/hydrogenandfuelcells/fuelcells/fc_challenges.html," 12/13/2005,

[13] E. Passalacqua, F. Lufrano, G. Squadrito, A. Patti, and L. Giorgi, "Influence of the structure in low-Pt loading electrodes for polymer electrolyte fuel cells," *Electrochimica Acta*, 43:24 (1998), 3665-3673.

[14] E. Passalacqua, F. Lufrano, G. Squadrito, A. Patti, and L. Giorgi, "Nafion content in the catalyst layer of polymer electrolyte fuel cells: effects on structure and performance," *Electrochimica Acta*, 46:6 (2001), 799-805.

[15] E. A. Ticianelli, C. R. Derouin, A. Redondo, and S. Srinivasan, "Methods to Advance Technology of Proton-Exchange Membrane Fuel-Cells," *Journal of the Electrochemical Society*, 135:9 (1988), 2209-2214.

[16] M. S. Wilson and S. Gottesfeld, "Thin-Film Catalyst Layers for Polymer Electrolyte Fuel-Cell Electrodes," *Journal of Applied Electrochemistry*, 22:1 (1992), 1-7.

[17] K. J. Green, R. Slee, and J. B. Lakeman, "The Development of Lightweight, Ambient Air Breathing, Tubular PEM Fuel Cell," *Journal of New Materials for Electrochemical Systems*, 5 (2002), 1-7.

[18] D. Chu, R. Jiang, and C. Walker, "Analysis of PEM fuel cell stacks using an empirical current-voltage equation," *Journal of Applied Electrochemistry*, 30:3 (2000), 365-370.

[19] D. Chu, R. Jiang, K. Gardner, R. Jacobs, J. Schmidt, T. Quakenbush, and J. Stephens, "Polymer electrolyte membrane fuel cells for communication applications," *Journal of Power Sources*, 96:1 (2001), 174-178.

[20] M. Mathias, J. Roth, J. Fleming, and W. Lehnert, "Chapter 46 - Diffusion media materials and characterisation," *Handbook of Fuel Cells: Volume 3 - Fuel Cell Technology and Applications* (W. Vielstich, H. Gasteiger and A. Lamm, eds.), John Wiley & Sons, Ltd, New York, 2003.

[21] Cytec, "http://www.cytec.com/business/EngineeredMaterials/Graphics/ThornelTP.pdf," 12/6/2005,

[22] C. Lim and C. Y. Wang, "Effects of hydrophobic polymer content in GDL on power performance of a PEM fuel cell," *Electrochimica Acta*, 49:24 (2004), 4149-4156.

[23] M. Prasanna, H. Y. Ha, E. A. Cho, S. A. Hong, and I. H. Oh, "Influence of cathode gas diffusion media on the performance of the PEMFCs," *Journal of Power Sources*, 131:1-2 (2004), 147-154.

[24] G. G. Park, Y. J. Sohn, T. H. Yang, Y. G. Yoon, W. Y. Lee, and C. S. Kim, "Effect of PTFE contents in the gas diffusion media on the performance of PEMFC," *Journal of Power Sources*, 131:1-2 (2004), 182-187.

[25] Z. G. Qi and A. Kaufman, "Improvement of water management by a microporous sublayer for PEM fuel cells," *Journal of Power Sources*, 109:1 (2002), 38-46.

[26] J. H. Nam and M. Kaviany, "Effective diffusivity and water-saturation distribution in single- and two-layer PEMFC diffusion medium," *International Journal of Heat and Mass Transfer*, 46:24 (2003), 4595-4611.

[27] U. Pasaogullari and C. Y. Wang, "Two-phase transport and the role of micro-porous layer in polymer electrolyte fuel cells," *Electrochimica Acta*, 49:25 (2004), 4359-4369.

[28] K. Henderson, Evaluation of the Effect of Microporous Sublayer Design and Fabrication on Performance and Adhesion in PEM Fuel Cell Assemblies, Virginia Polytechnic Institute and State University, 2005.

[29] V. A. Paganin, E. A. Ticianelli, and E. R. Gonzalez, "Development and electrochemical studies of gas diffusion electrodes for polymer electrolyte fuel cells," *Journal of Applied Electrochemistry*, 26:3 (1996), 297-304.

[30] L. Giorgi, E. Antolini, A. Pozio, and E. Passalacqua, "Influence of the PTFE content in the diffusion layer of low-Pt loading electrodes for polymer electrolyte fuel cells," *Electrochimica Acta*, 43:24 (1998), 3675-3680.

[31] L. R. Jordan, A. K. Shukla, T. Behrsing, N. R. Avery, B. C. Muddle, and M. Forsyth, "Diffusion layer parameters influencing optimal fuel cell performance," *Journal of Power Sources*, 86:1-2 (2000), 250-254.

[32] B. Chen, D. A. Dillard, J. G. Dillard, and R. L. Clark, "Crack path selection in adhesively bonded joints: the roles of external loads and speciment geometry," *International Journal of Fracture*, 114:2 (2002), 167-190.

[33] T. E. Springer, T. A. Zawodzinski, M. S. Wilson, and S. Gottesfeld, "Characterization of polymer electrolyte fuel cells using AC impedance spectroscopy," *Journal of the Electrochemical Society*, 143:2 (1996), 587-599.

[34] M. V. Williams, E. Begg, L. Bonville, H. R. Kunz, and J. M. Fenton, "Characterization of gas diffusion layers for PEMFC," *Journal of the Electrochemical Society*, 151:8 (2004), A1173-A1180.

[35] M. Coppo, N. P. Siegel, and M. R. vonSpakovsky, "On the Influence of Temperature on PEM Fuel Cell Operation," *Journal of Power Sources*, In Press (2005).

[36] N. P. Siegel, M. W. Ellis, D. J. Nelson, and M. R. von Spakovsky, "Single domain PEMFC model based on agglomerate catalyst geometry," *Journal of Power Sources*, 115:1 (2003), 81-89.

[37] W. R. Merida, G. McLean, and N. Djilali, "Non-planar architecture for proton exchange membrane fuel cells," *Journal of Power Sources*, 102:1-2 (2001), 178-185.

[38] "*Femlab 3.1i*," Comsol AB, Stockholm, Sweden, 2005.

[39] N. P. Siegel, M. W. Ellis, D. J. Nelson, and M. R. von Spakovsky, "A two-dimensional computational model of a PEMFC with liquid water transport," *Journal of Power Sources*, 128:2 (2004), 173-184.

[40] V. Mishra, F. Yang, and R. Pitchumani, "Measurement and Prediction of Electrical Contact Resistance Between Gas Diffusion Layers and Bipolar Plate for Applications to PEM Fuel Cells," *Journal of Fuel Cell Science and Technology*, 1 (2004), 2-9.

[41] H. K. Lee, J. H. Park, D. Y. Kim, and T. H. Lee, "A study on the characteristics of the diffusion layer thickness and porosity of the PEMFC," *Journal of Power Sources*, 131:1-2 (2004), 200-206.

[42] E. Passalacqua, G. Squadrito, F. Lufrano, A. Patti, and L. Giorgi, "Effects of the diffusion layer characteristics on the performance of polymer electrolyte fuel cell electrodes," *Journal of Applied Electrochemistry*, 31:4 (2001), 449-454.

[43] M. Kaviany, *Principles of Heat Transfer in Porous Media*, 2nd ed., Springer-Verlag, New York, NY, 1995.

[44] J. Larminie and A. Dicks, *Fuel Cell Systems Explained*, 2nd ed., John Wiley and Sons, West Sussex, England, 2003.

VITA

Joshua David Sole was born to Howard Brent and Susan Lee Sole on Saturday the eleventh day of April, in the year of our Lord nineteen hundred and eighty-one, and of the Independence of the United States of America the two hundred and fifth, in Moundsville, West Virginia. At the age of five Josh moved to Toms River, New Jersey where he remained until the age of seven. Upon his departure from New Jersey Josh relocated with his family to Damascus, Maryland where he remained until he received his High School Diploma from Damascus High School. In August of 1999 Josh departed Maryland to pursue an undergraduate degree in Mechanical Engineering at Virginia Polytechnic Institute and State University located in Blacksburg, Virginia. Josh earned the status of Bachelor of Science in Mechanical Engineering on May 10, 2003 granted by the Board of Visitors of the Virginia Polytechnic Institute and State University. Following graduation Josh chose to pursue a graduate level education at Virginia Tech where he remains to this day in pursuit of the status of Doctor of Philosophy.